SCUOLA DI DOTTORATO

UNIVERSITÀ DEGLI STUDI DI MILANO-BICOCCA

University of Milano-Bicocca
School of Medicine and Surgery

PhD program in
Translational and Molecular Medicine – DIMET
XXXI Cycle

Detection and characterization of extracellular vesicles of neural origin as possible tool for diagnosis and treatment of neurodegenerative diseases

Silvia PICCIOLINI
Matr.: 810078

Tutor: Prof. Massimo MASSERINI
Co-Tutor: Dr. Furio GRAMATICA

Coordinator: Prof. Andrea BIONDI

ACADEMIC YEAR 2017/2018

“‘Cause if you stay where you are
You'll never get burned.
And if you stay where you are
You'll never get hurt,
But if you stay where you are
You'll never know
Why you burn at all.”

Jacqui Treco

TABLE OF CONTENTS

CHAPTER 1

General introduction

1.1 Extracellular vesicles

Extracellular vesicles (EVs) are a heterogeneous group of particles defined by plasma membrane that are constitutively released by cells of diverse tissue origin. Despite controversies about their nomenclature, in the last years the scientific community found consensus defining EVs as the group of particles that could be broadly divided into two main categories: exosomes and microvesicles[1]. Particular attention has been given to these vesicles because of their emerging role, not only in paracrine intercellular communication, but also in the communication between tissues and organs due to body fluid transportation[2]. In biomedical research, EVs are becoming more interesting because of their proven involvement in several pathologies, encompassing cancer[3,4], neurodegenerative[5,6,7] and inflammatory diseases[8] and physiological adaptive mechanisms like tissue regeneration[9]. In particular, EVs are found in the majority of biological fluids such as blood, cerebrospinal fluid, breast milk, saliva, sperm, and urine, making them potential diagnostic markers for complex human diseases[10,11]. Moreover, EVs are stable under strenuous storage conditions since their lipid bilayer protects macromolecules on and inside EVs from degradation under non-physiological conditions which also qualifies them as potential diagnostic, prognostic and predictive biomarkers or drug delivery systems[12].

For these reasons, there has been a recent explosion of interest in the study of these vesicles: in 2006 there were only 183 EVs related publications which increased to 11200 as of today (data from PubMed.gov; keywords: Extracellular vesicles).

1.1.1 Biogenesis and dimensions

Exosomes and microvesicles are two distinct subsets of secreted membrane vesicles released from most body cells under both physiological and pathological conditions. They are different from each other because of their modes of biogenesis: microvesicles bud directly from the plasma membrane whereas exosomes originate from the endocytic pathway and from the fusion of multivesicular endosomes with the plasma membrane. Because of their origin, exosomes are enriched in proteins and lipids typically associated with lipid rafts, which are membrane microdomains that work as signalling platforms for multiple cellular functions[13].

Moreover, there is a lot of variation in the size of microvesicles and exosomes: microvesicles are bigger budding vesicles (up to 1 μm), whereas exosomes usually appear as vesicles with a diameter that varies from 40 to 150 nm, able to maintain their integrity in circulation for longer time[1].

It is important to note that, despite their different mechanism of biogenesis, exosomes and microvesicles display a similar morphology, sometimes overlapping in size and common composition as well; thereby challenging the current attempts to find a more precise nomenclature for EVs.

Besides, in addition to exosomes and microvesicles, there is discussion on additional EV subpopulations, that contribute to extend the heterogeneity making the need for a proper isolation and characterization methods more urgent.

1.1.2 Composition

EVs are bound by a lipid bi-layer; they contain specific lipid components, nucleic acids and cytosolic, membrane and transmembrane proteins, carrying with them the information of the cells of origin (Figure 1).

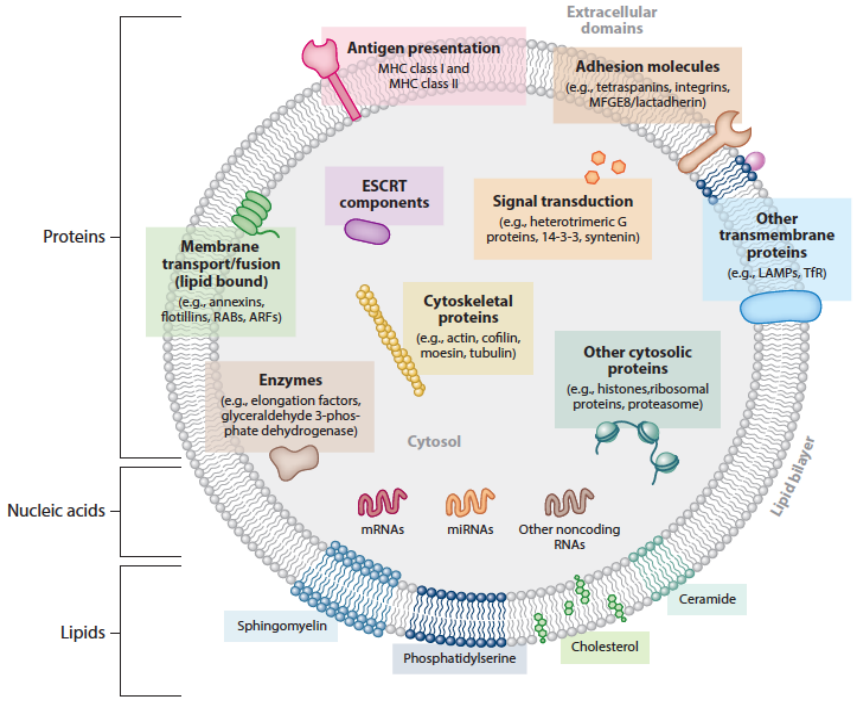

Figure 1. Overall composition of extracellular vesicles (Colombo, Raposo and Théry, Ann Rev Cell Dev Biol 2014).

EVs are enriched in sphingomyelin, gangliosides, and desaturated lipids, indicating an increased fraction of cholesterol in vesicles as compared to their respective cellular membranes[14]. Moreover, in contrast to cellular membranes, EVs, like must cell- and dendritic cell-

derived exosomes, contain more phosphatidylserine in the outer leaflet which may facilitate their internalization by recipient cells[15].

The protein content of different types of EVs includes adhesion molecules, membrane trafficking molecules, tetraspanins (such as CD9, CD81, CD63), cytoskeleton molecules, heat-shock proteins (such as HSP70), cytoplasmic enzymes, signal transduction proteins, cytokines, chemokines, proteinases and cell-specific antigens[16].

Regarding the nucleic acids, EVs contain messenger RNA (mRNAs) fragments, non-coding RNA (ncRNAs) including microRNAs (miRNAs) and extra-chromosomal DNA fragments. miRNAs are small RNAs (typically 17-24 nucleotides) which mediate post-transcriptional gene silencing usually by targeting the 3' region of mRNAs. Since the packing of extracellular miRNAs into exosomes or microvesicles protects miRNAs from degradation and guarantees their stability, the role of miRNAs in EVs is gaining an increasing interest. It is shown that they are not randomly incorporated into vesicles but a subset of miRNAs such as miR-150 and miR-142-3p preferentially enter the EVs[17]. As for mRNA, miRNAs profile in EVs reflect the cell of origin.

Therefore, considering their composition and their ability to cross biological barriers and move into the biological fluids, EVs are versatile carriers for proteins, lipids and oligonucleotides.

The biochemical composition of extracellular vesicles is finely controlled and strongly dependent on the type and the physiopathological conditions of the cell of origin both, for membrane and cytosolic molecules. For example, EV content is influenced by the whole body homeostasis, being related to inflammatory[18] or immune

activated state, by exogenous stress induced responses[19], together with disease conditions. In case of a pathological condition, the circulating EV populations may get influenced by the severity and duration of the pathology along with the organs involved in the disease, thereby changing their number, size, cargo and membrane composition[20].

In order to elucidate the molecular mechanisms and the pathophysiology underlying different disease conditions from which EVs are isolated, some free web-based platforms such as ExoCarta[21], EVpedia[22], and Vesiclepedia[23] were created as attempts for schematically report the main constituents of EVs, providing a kind of profile of their molecular cargo. However, these resources still cannot comprehensively describe the huge amount of molecules that characterize the different classes of EVs. Moreover, it is very challenging to sum up the vesicle features related to specific diseases because of the heterogeneity of the human or animal disease research models and the variability among patients due to age, sex, diet, and co-morbidity. These influencing parameters have to be considered together with the consistent methodological variability due to isolation and purification procedures that can introduce unpredictable variables in the analysis.

1.1.3 Functions

The first observations of EVs and their relevance occurred simultaneously in different physiological settings. In 1946, EVs were observed circulating in blood plasma as procoagulant particles derived from platelets[24]. Other studies demonstrated the release of EVs from rectal adenoma microvillus cells[25] and the presence of vesicles as

"virus-like" particles in human cell cultures and bovine serum[26,27]. In the 1980s Stahl and Johnstone described EVs as nano-sized vesicles involved in the process of reticulocyte maturation[28,29]. Although there was no clear evidence on the biological function of these new objects; in the first years of study on vesicles they were thought to be garbage bags eliminating unnecessary components from cellular cytoplasm[30]. The garbage-bag theory led to a lot of interest in the field which extended to studying the role of EVs in intercellular communication of information and compounds. However, the function as garbage bags remained associated only to one type of EVs called apoptotic bodies[31]. Since the discovery that EVs contain RNAs, they acquired a special status as mediators of cell-to-cell communication[32]. It's important to notice that EVs can be local messengers or they can travel through the systemic circulation to reach distant sites. The communication between cells could happen by following one of these pathways: (1) vesicles can be captured by neighboring cells by ligand-receptor interaction activating intracellular signaling; (2) vesicles can be internalized by phagocytosis or receptor-mediated endocytosis, releasing their content in the cytoplasm of the target cell; (3) vesicles may be directly taken up by membrane fusion, releasing their content in the cytoplasm[33]. The last one is a process that is currently poorly understood but it is the most efficient way for the delivery of intraluminal cargoes such as miRNA. Then, it is also possible that the plasma membrane of endocytosed vesicles could be recycled by the target cell[1] (Figure 2).

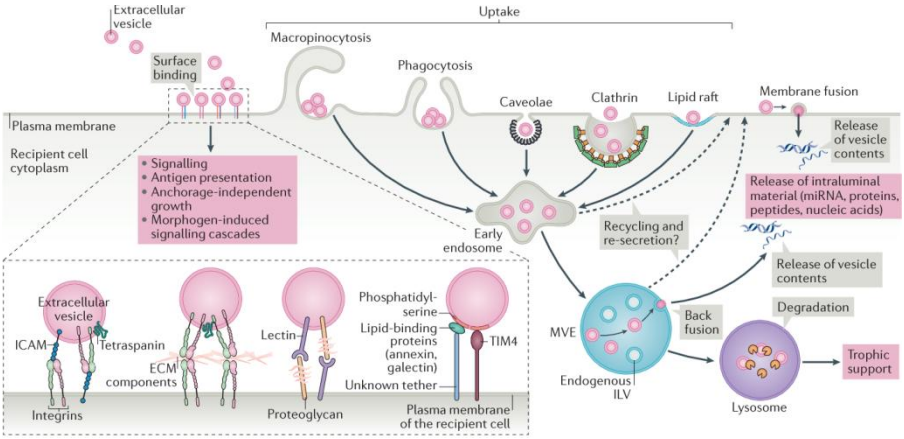

Figure 2. Fate of extracellular vesicles in recipient cells (Van Niel, D'Angelo, Raposo, Nature Reviews Molecular Cell Biology, 2018).

1.2 Study of EVs in translational medicine

EVs have potential in translational medicine since they can be used as diagnostic and prognostic biomarkers and as therapeutic tools for clinical applications[34]. Vesicles can be used as biomarkers, vaccines, therapeutic agents or drug delivery systems, due to their following properties: (1) they are sterilizable, (2) easy to handle; (3) not immunogenic/immunomodulators; (4) cross most of the biological barriers; (5) can travel via systemic therapy, both intravenous and intraperitoneal; (6) have a good therapeutic potential in regenerative medicine; (7) allow to reduce the risk of ectopic tissue formation; (8) activated EVs subset can *in vivo* deliver infinitesimal doses of miRNA cargo.

1.2.1 Biomarkers

One interesting and emerging clinical application of EVs is represented by their use as non-invasive diagnostic and prognostic biomarkers, that has lots of implications regarding personalized disease diagnosis and monitoring of the responsiveness to drug or rehabilitation protocols. Indeed EVs are easily accessible in biological fluids and reflect both the type and the status of the cells of origin. The possibility to identify EVs within body fluids related to a specific disease is very interesting for cancer, metabolomic, cardiovascular and neurodegenerative diseases and other disease syndromes. However, since biological fluids are complex samples it is important to define and adopt optimized standard operating procedures with the purpose to implement EV-based biomarkers into the clinics. In order to improve the transparency and compliance in reporting the details of

experimental protocols used for EV analysis, the EV-TRACK platform was recently created, contributing to increase the reproducibility of EV research.

Figure 3 summarises the main phases for the development of EVs as biomarker discovery and application with specific aims and the related problems that must be considered[35].

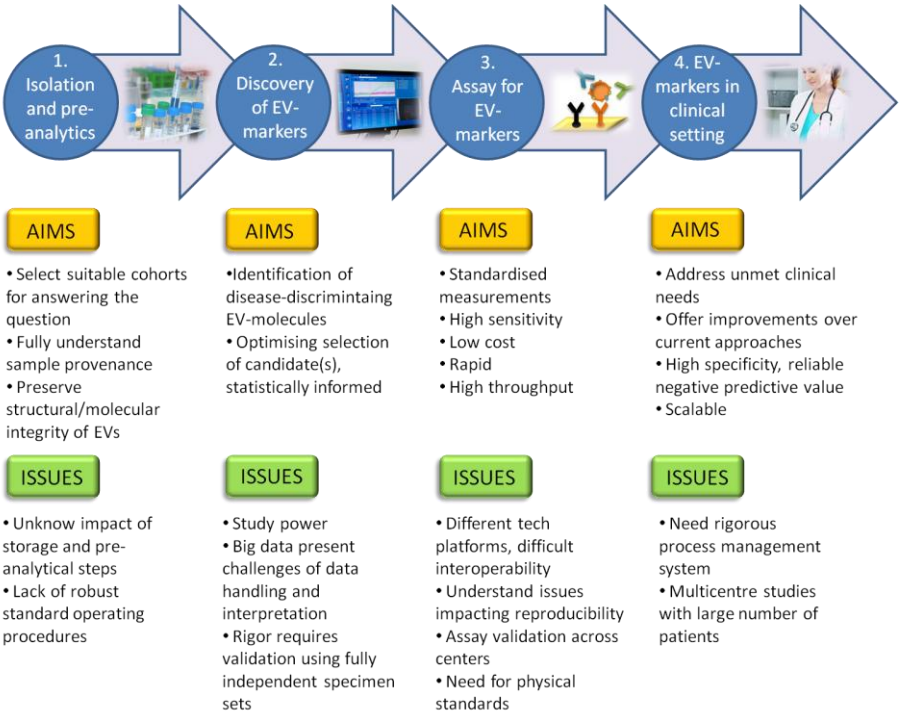

Figure 3. Phases for the study of EVs as biomarkers, with principal aims and related notable issues (adapted from Clayton A. et al, J. Extracell Vesicles, 2018).

One of the parameters indicative of a pathology is the *biochemical content* of vesicles isolated from a biological fluid or originating from one cell type. Particularly, the presence or the relative levels of specific proteins, lipids or miRNAs on the EVs could be related to a mechanism that leads to a specific disease or pathological status. For example, EVs derived from pancreatic cancer cells are enriched in a cell surface proteoglycan called glypican-1 (GPC1), that could be used as a highly specific biomarker of pancreatic cancer[36]. Another example is given by a recent study that showed that exosomal miRNA (miR-24-3p) present in saliva could be a potential marker of aging. Considering that saliva is a very accessible and noninvasive body fluid, the detection of salivary exosomal miRNAs represents a simple way for measuring and monitoring aging[37]. In another work, the lipid composition of urinary vesicles was demonstrated to be significantly different between patients with prostate cancer and matched healthy controls. In particular, the levels of phosphatidylserine 18:1/18:1 and lactosylceramide (d18:1/16:0) present in urinary exosomes allow to distinguished the two groups with high sensitivity and specificity, showing the potentiality of using exosomal lipid species in urine as prostate cancer biomarkers[38]. The analysis of the protein content of EVs as possible effective factor for the identification of a pathological process is applied in a lot of studies. For example, specific proteins, such as CD26, CD81, CD10 and Sic3A1, present in urinary vesicles have been identified as potential biomarkers for hepatic disease[39].

Moreover, the *concentration* of EVs is studied as another parameter able to indicate and reflect the presence and the evolution of diseases. Recently, a study showed that the levels of circulating Annexin V-

positive vesicles coming from different cell types (such as leukocytes or endothelium) increase or decrease according to the evolution of colorectal cancer, meaning that EV concentration could be used as a complex disease biomarker[40]. In another paper, circulating levels of vesicles were shown to be significantly higher ($p>0.0001$) in patients with non-small-cell lung cancer compared to healthy controls, providing new data on the prognostic value of vesicles present in the blood plasma[41].

1.2.2 Therapeutic use

EVs have been investigated as a therapeutic strategy with two different approaches: (1) by using vesicles as they are exploiting their native biological functions, for example the ability to mimic processes of repair; (2) by using vesicles as carriers of therapeutic agents in order to deliver them to the site of action[42].

The possibility of using EVs for therapeutic use has attracted wider attention as compared to conventional strategies because of the good biocompatibility and biodistribution of EVs. As mentioned before, EVs are well tolerate, have low immunogenicity, an innate stability and can bypass biological barriers such as blood-brain barrier (BBB)[43]. These features make them good candidates for providing an efficient drug delivery interface.

A recent study showed the capability of cell-derived EVs present in synovial fluid and cartilage extracellular matrix to restore joint homeostasis and promote articular tissue regeneration, demonstrating the good potentialities of “not-functionalized vesicles” once injected directly into the target site[44]. In general, it is shown that EVs derived

from stem cells could have different therapeutic effects including influencing growth of target cells or phenotype, promoting regeneration, anti-inflammatory or anti-fibrotic effects and immunomodulation[45].

Furthermore, regarding the use of EVs for drug delivery, it's interesting to note that lots of therapeutic molecules, such as proteins, miRNAs and siRNAs are more stable inside EVs; hence making vesicles an excellent vehicle to deliver them to their exact site of action. Nowadays, some synthetic alternatives, such as liposomal doxorubicin or daunorubicin, have been already developed and employed as drug carriers for decades, resulting in several approved liposomal nanomedicines used in the clinic, showing lots of benefits over the drug alone[46]. The development of a drug delivery system based on natural vesicles may provide unique advantages over other systems, including stability in the blood, limited immunogeneicity and possibly fewer off-target effects due to the natural tendency of EVs to act on specific target cells[47].

The direct loading of drugs into EVs can be done in different ways, for example by electroporation, sonication, or by extrusion of drug-loaded cells through a series of filters to generate mimetic vesicles. A freeze-thaw method has also been developed to create hybrid exosomes by the fusion of EVs and modified liposomes[48,49].

Even though there are currently no established clinical therapies based on the use of EVs as drug delivery systems, there are some EVs therapies that were clinically tested. For instance, Besse and co-workers showed the use of vesicles derived from pulsed dendritic cells

for promoting the immune cell response in non-small cell lung cancer immunotherapy[50].

In order to improve the specificity of the cell or tissue targeting, the specific target ligand could be anchored on the EV surface. For example, a study has functionalized the membrane of EVs with iRGD-Lamp2b as a targeting ligand, with the purpose to enhance the tumor-specific uptake of doxorubicin, loaded on EVs through electroporation[51].

EVs could be delivered systemically or locally depending on the target tissue or organ. They can be prepared in different formulations, like free suspensions or loaded into biomaterials, and administrated via intravenous, intraperitoneal, oral, intranasal or subcutaneous for their systemic distribution, allowing a rapid clearance from circulation into different organs. On the other hand, the choise to administer EVs locally is often supported by the evidence of reduction of side effects and the retention of higher EV doses at the target sites; for this reason it is preferred for anti-cancer treatment.

By adjusting EV formulation and their routes of administration it is possible to facilitate the delivery of EVs across the physiological barriers and obtain the desired therapeutic action[52].

1.3 Involvement of EVs in neurological diseases

The composition of EVs in healthy central nervous system (CNS) is different from that in CNS diseases. Each cell type, like neurons, oligodendrocytes, astrocytes and microglia, generates vesicles containing specific markers that can change qualitatively and quantitatively when a disease is occurring.

In particular, EVs released from healthy neurons are able to relay complex messages controlling mechanisms for local and systemic inter-neural transfer of information in the brain. Furthermore, the maintenance of axonal integrity and survival due to the process of myelination is controlled by the action of EVs released from oligodendrocytes. Indeed, these vesicles contain proteolipid protein (PLP) in the innermost layers of myelin in contact with axons during the process of myelination. It was shown in vitro that oligodendroglial EVs are able to improve the neuronal viability and contribute to the preservation of axonal health participating in a mode of bidirectional neuron-glia communication[53]. Oligodendroglia EVs have also a role in avoiding induction of the inflammatory response by being taken up by MHC-II negative microglia[15].

Also the functions of astrocytes take place via release of EVs. Astrocytes produce neural growth factors that are needed for neuronal growth and survival, together with angiogenic factors, mitochondria and excitatory amino acid transporters (EAAT)[54].

Finally, microglia-derived EVs promote neurotransmission stimulating excitatory transmission of neurons both *in vitro* and *in vivo*[55] (Figure 4).

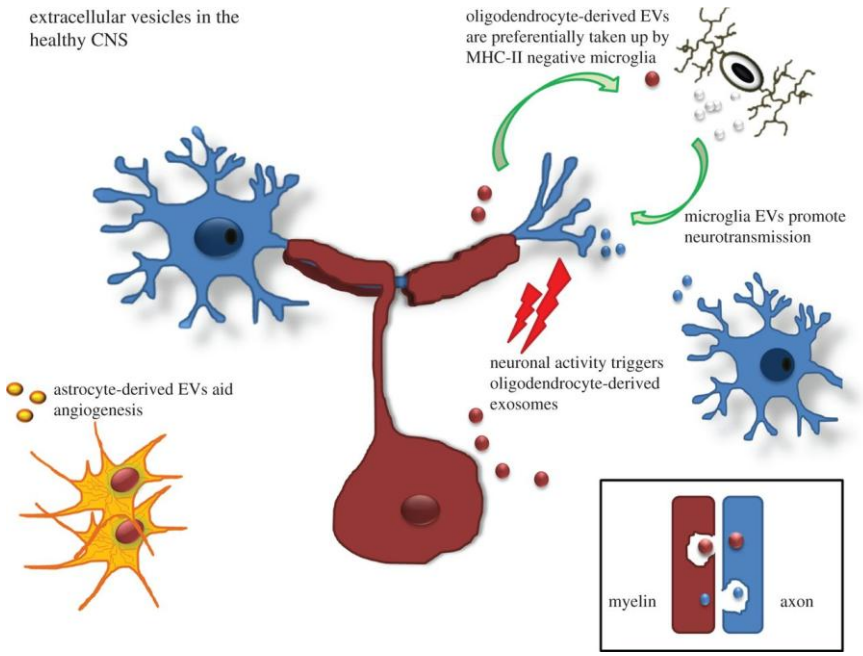

Figure 4. The role of EVs in the healthy central nervous system (Pegtel et al, Philos Trans R Soc Lond B Biol Sci, 2014).

While a CNS neurological disorder occur, the composition and the functions of the different EVs populations change; this fact has led to the study of the role of EVs in the development of several neurological diseases.

In neurodegenerative disorders, neurons can produce and release aggregated and pathogenic proteins such as amyloid precursor protein (APP), phosphorylated tau, α-synuclein or pathogenic PrPSc protein in case of prion disorders. The vesicles loaded with aggregated proteins could act as seeds that spread the damage throughout the brain[56] (Figure 5). Although a growing body of evidence has demonstrated the ability of EVs to spread misfolded proteins within and outside the brain, it remains still to be clarified whether there is an

active transport patway for these proteins, or whether they are simply a byproduct of disrupted cellular patways in the aging brain[57]. Indeed, in disease states, physiological lysosomal pathways for the destruction of unwanted proteins can be impaired, leading to a change in balance with a resulting increase in the release of vesicles loaded with unwanted protein products that can propagate the aggregation of proteins, like β-amyloid and α-synuclein, and the transmission of disease.

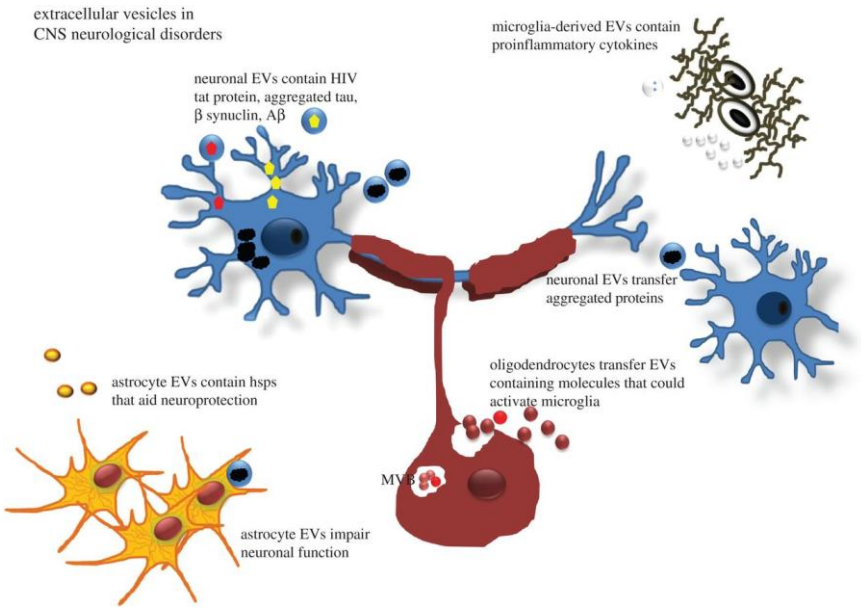

Figure 5. The role of EVs in central nervous system with neurological disorders (Pegtel et al, Philos Trans R Soc Lond B Biol Sci, 2014).

1.3.1 Circulating EVs as mirror of brain-derived EVs

The BBB is a highly selective and dynamic interface that controls the passage of substances between the peripheral vascular circulation and the brain. It is composed of brain microvascular endothelial cells surrounded by astrocytes, pericytes and endothelial basement membrane forming neurovascular unit. The BBB serves to protect the brain from harmful chemicals or toxins coming from the systemic circulation, thus also resulting in the inability of most therapeutic drugs to cross the BBB and reach the CNS. In particular, approximately 98% of small molecules and all large pharmaceutical molecules (including recombinant proteins, monoclonal antibodies, or gene-based medicines) are not able to cross the BBB[58,59], because of two main molecular properties of BBB: (1) the presence of tight junctions between endothelial cells; (2) the presence of selective influx and efflux transporters for the uptake of nutrients and molecules from blood and the elimination of toxins from the brain[60].

Although there are still some uncertainties about the mechanisms of how EVs may bypass the BBB, it is demonstrated that they can cross the intact BBB and can be detected in the peripheral blood, providing an interesting prerequisite to use a minimally invasive method for their detection, compared to liquid biopsies obtained from the cerebrospinal fluid.

Regarding the possible mechanisms of how EVs may bypass the BBB, it is reported that it could happen by their internalization by endothelial cells or by entering the brain via intercellular junctions of endothelial cells after the increment of the permeability of vascular

barriers[61]. However the exact mechanism remains elusive and might differ also depending on the particular EV type.

Besides, some studies reported that the composition of brain-derived vesicles detected in the peripheral blood is still related to the status of the brain even after the migration of the vesicles from the cerebrospinal fluid (CSF) to the blood, demonstrating the possibility to use them to detect the presence or absence of a neurological disorder or to monitor its progression and/or response to the therapy.

García-Romero and colleagues have proved that DNA sequences within glioma-derived EVs present in peripheral blood, isolated from a small cohort of brain tumor patients, correlate with the presence of molecular alterations, such as IDH1 that is an essential marker of human glioma[62]. This finding paves the way for improving diagnostics and prognostics of gliomas and potentially other neurological diseases by detecting and analysing circulating EVs as biomarkers of the CNS status.

Another work showed that the inflammasome protein levels in EVs released in serum of brain-injured patients are higher compared to healthy subjects, mirroring their levels in the CSF, thus indicating that this specific protein cargo of serum EVs may be used as biomarkers of CNS injuries[63].

These studies provided data regarding how circulating EVs could reflect the composition of brain-derived EVs, demonstrating similarities for specific cargo (e.g. proteins or nucleic acids). So, the analysis of circulating vesicles of neural origin could open new perspectives towards clinical applications for CNS diseases.

1.3.2 EVs as diagnostic tool for brain diseases

Because of their role as vehicles for atypical and pathological cargoes, some reports show promising results regarding the use of EVs as diagnostic tool for neurological diseases. The discovery that the EVs are able to cross most biological barriers, including the BBB, has opened new research avenues for developing diagnostic strategies, especially for neurological diseases. As mentioned before, the study of the amount and biochemical cargo of EVs that derived from the CNS and travel into the bloodstream is a promising approach for the discovery of the much needed peripheral biomarkers of neurodegenerative diseases. Considering the pathological heterogeneity of neurodegenerative disorders, peripheral biomarkers can be used to characterize an individual's underlying pathophysiology, to monitor the progression of the disease and define the optimal and personalized therapy. The development of these biomarkers will be critical for a broader characterization of the pathology and a precise identification of different patient sub-types based on the study of a biological phenomenon.

Saman et al showed that protein tau is secreted via exosomal release, influencing the unconventional secretion of other proteins (such as α-synuclein or β-amyloid) involved in neurodegenerative processes. In particular, they demonstrated an increased exosomal tau levels in CSF of patients with early-stage Alzheimer's disease (AD) which potentially could become a biomarker of the AD development in elderly people[64]. Similarly, blood EVs were reported to undergo proteomic modifications in patients with Parkinson's disease (PD)[65], being associated with α-synuclein, tau and LRRK2 and modify their

RNA profiling in relation to PD progression[66,67]. Changes in the number, phenotype and nucleic acid loading of microglia EVs were also demonstrated in multiple sclerosis patients, where the production of myeloid EVs dramatically increases under brain inflammation and correlates with bouts of clinical symptoms[68–70].

1.3.3 EVs as therapeutic tool for brain diseases

EVs are also extensively studied for drug delivery across the BBB, which represents a new strategy to face the actual difficulties in obtaining a safe and effective delivery of drugs to the brain. Tian et al developed exosomes conjugated with a specific peptide that was able to target a lesion area of an ischemic brain. They loaded that with curcumin, a natural polyphenol with anti-inflammatory activity, in order to deliver this drug to the brain after intravenous administration. They showed that this new exosomes-based drug delivery system provided benefits with strong suppression of the inflammatory response and cellular apoptosis in the lesion region, demonstrating its potentiality for the use as a new cerebral ischemia therapy[71].

Since EVs can be modified and loaded with different biomolecules to elicit a therapeutic response at the target site, this strategy could have application on different diseases. For instance, exosomes loaded with small interfering RNA (siRNA) for the knock-down of α-synuclein and engineered with a peptide that promotes the crossing of the BBB (rabbies virus glycoprotein), were used in a PD model, leading to a decrease in α-synuclein mRNA and protein levels throughout the brain[72].

Also unmodified EVs released from neural cells could be used as therapeutic tools for brain diseases, considering that they have beneficial effects over target cells and their use may be safer than the use of their progenitor cells. Figure 6 shows their potential therapeutic applications: (1) in ischemic conditions, mesenchymal stem cells (MSCs) produce EVs enriched in miRNA-133b able to stimulate neurovascular recovery in neurons and astrocytes[73]; (2) dendritic cells (DCs) stimulated by interferon gamma release EVs enriched in miRNA-219 that regulates oligodendrocyte remyelination and reduces oxidate stress, demonstrating their potential application in multiple sclerosis[74]; (3) EVs released during neuronal differentiation promote MSCs differentiation into neuron-like cells, useful for treatment of spinal cord injury and brain diseases that cause neuronal loss[75]; (4) EVs released by neuronal cells mediate the clearance of Aβ-peptides in AD[76].

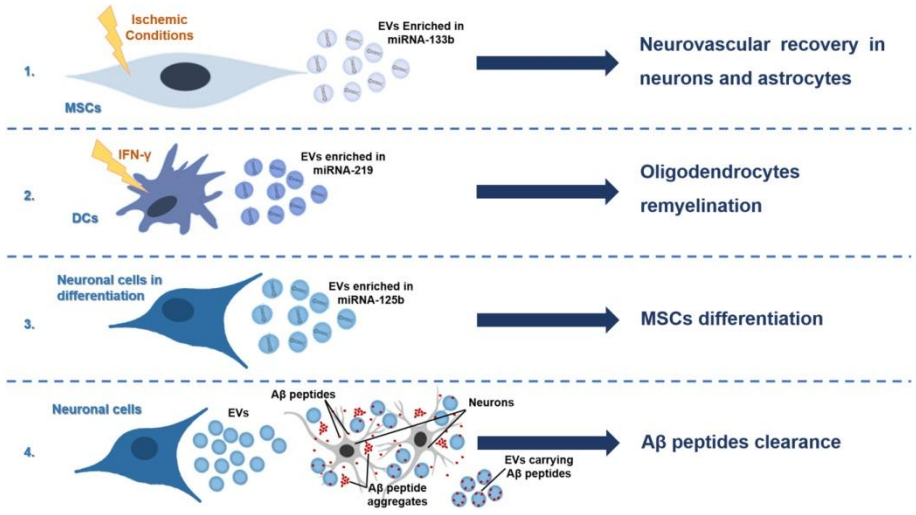

Figure 6. Representation of therapeutic applications of unmodified neural EVs (Rufino-Ramos D. et al, J Controlled Release, 2017)[77].

1.4 How to study EVs

One of the main hurdles in EVs research is the standardization of isolation and characterization methods. This needs to be urgently aligned among different research laboratories in order to make results comparable and data discussion more feasible. The International Society for Extracellular Vesicles (ISEV) has published the minimal experimental requirements that should be adopted by those who handle EVs to facilitate advancements in applied research and it is constantly working on updates[78,79].

1.4.1 Isolation methods

There are different isolation methods that could be used for obtaining EVs from body fluids or cell culture medium. It is worth noting that each of them have both advantages and limitations, sometimes causing confusion and contradicting results[80]. These methods can be used individually or in combination for the EVs isolation from diverse biological sources.

One of the first and most commonly used methods is the differential ultracentrifugation, both for cell culture supernatants and complex biofluids[81]. After removing whole cells and cell debris with one or more low force centrifugations (500-2000 x g), an ultracentrifugation step (10000-20000 x g for larger EVs, 100000-200000 x g for smaller EVs) is used to sediment the vesicles. The main limitation of this method is the contamination of the sample with protein aggregates and nucleosome fragments that can co-sediment in the pellet along with EVs. Moreover it is time-consuming and results in relatively low recovery[82].

Another method to isolate EVs is the density-gradient separation that allows to separate EVs according to their density. This method provides an increased sample purity because the protein and protein-RNA aggregates can be efficiently separated from the EVs. But, such isolation of EVs from serum or plasma samples will be contaminated with high-density lipoprotein (HDL), due to their similar density range as EVs[83].

Another technique that provides a high yield of EVs is the polymer-based precipitation method that commonly uses poly-ethylene glycol (PEG) as the water-excluding polymer that can alter the solubility or dispersibility of vesicles. However, this method too, results in aggregation of high portion of other contaminants, such as lipoproteins. Also, the presence of the polymer material in the sample could interfere with some analysis. Despite the limitations described here, some commercial kits based on this method were generated and used in laboratories, for example ExoQuick (System Biosciences, USA), that has the advantage of providing an easy and fast isolation of vesicles that can be still used to analyze the nucleic acid content of EVs[84].

The EV isolation can also be performed by using size-based isolation techniques, such as size-exclusion chromatography (SEC) and ultrafiltration. SEC uses a user defined porous column where smaller particles slow down in their passage, whereas the larger ones pass through the column quickly with the mobile phase. This method allows the isolation of high-purity and intact vesicles whose structure is not affected by shearing force compared to centrifugation methods. Currently, SEC is a widely accepted technique for the extraction of

EVs from blood and urine, sometimes combined with ultracentrifugation[85,86]. Ultrafiltration makes use of special membranes to separate vesicles from proteins or other macromolecules. During this process the vesicular populations are concentrated by the filtration membrane. Limitations of this method are due to the adhesion of EVs to filtration membranes and the application of additional force to pass through the membranes, that could potentially damage the structures of EVs.

EVs can be isolated also by using immuno-selection techniques. The sample is mixed with antibody, attached to magnetic beads, that are able to target known surface markers on EVs (for example CD9, CD63, CD81 or immune-regulator molecules) in order to isolate a purified population of EVs. Using this technique only those particles that express the specific surface markers can be successfully isolated. The capturing selectivity can be a limitation because some markers might not be expressed on all kinds of EVs; but it could be an advantage for those studies aimed to enrich a certain subpopulation of EVs[87].

It is important to understand that the choice of isolation method depends not only on the nature of the sample (cell culture media or a body fluid) from which the vesicles are isolated, but also on the downstream characterization needed for the study itself that could be different according to the medical application of interest.

1.4.2 Characterization methods

EVs characterization can be achieved through a range of methods.

For EVs biophysical characterization they are mainly analyzed with scanning and transmission electron microscopy (TEM), cryo-electron microscopy (cryo-TEM), atomic force microscopy (AFM) and nanoparticle tracking analysis (NTA). These techniques allow to measure size, distribution, concentration and morphologies of EVs. Figure 7 shows the morphology of EVs traditionally described as "typical cup-shaped" when visualized by TEM analysis, and a cryo-TEM image of a vesicle.

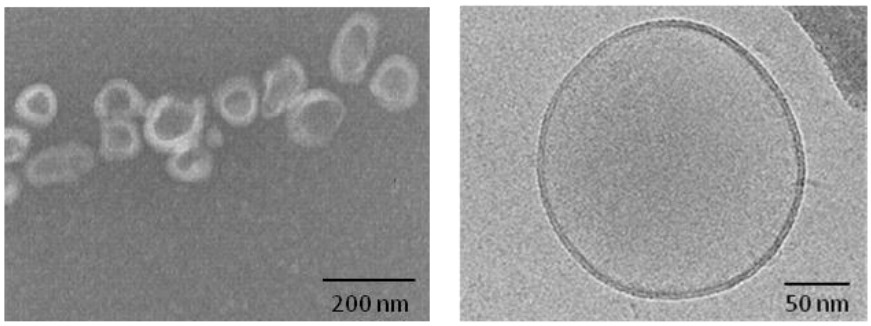

Figure 7. Transmission electron micrographs and cryo-TEM of EVs isolated by ultracentrifugation from plasma (Edwin van der Pol et al, Pharmacological Reviews, 2012; Huilin Shao et al, Chem Rev 2018).

While TEM analysis of EVs has some shortcomings related to dehydration, chemical fixation, and staining of the biological samples, cryo-TEM imaging can overcome these limitations because samples are directly applied onto a grid, vitrified and visualized, thus allowing the visualization of EVs near their native state[88].

AFM analysis of EVs allows to measure vesicle size distribution, map EV mechanical properties with nanometric precision and characterize the EV membrane protein content. Despite these properties, its used is still limited because of the strong effect of immobilization conditions on the measurement of their size[89].

NTA is a technique that enables characterisation of particles from 10–2000 nm in solution combines the properties of both laser light scattering microscopy and Brownian motion. The technique allows to obtain the size distributions of EVs and an estimation of their concentration, demonstrating to be more challenging than homogeneous particle preparations[90].

The biochemical characterization based on the measurement of the lipid and protein composition of isolated EVs, is mainly performed through western blotting, enzyme-linked immunosorbent assay (ELISA), mass spectrometry and flow cytometry.

Western blotting is commonly used for demonstrating the presence of specific proteins associated with EVs; it requires the separation of the proteins by electrophoresis before being transferred on a membrane for immunoblotting of protein targets. It is often limited by the amount of proteins required for the analysis and by the sensitivity of the visualization method, nonetheless it remains the most widely used characterization technique[81].

ELISA is another established technique used for protein identification and quantification. EVs could be captured on a solid support, that has been pre-treated with an immobilized antibody, and then exposed to another labeled antibody for their detection.

These first two approaches provide the quantification of specific and targeted proteins, whereas mass spectrometry is a technique able to provide high throughput peptide profiling, quantitative and comparative EV proteomic analyses. The experimental protocol provides that EVs undergo an enzymatic digestion and peptides separation; after that the sample is ionized and analyzed by mass spectrometry. The identification of proteins is performed by using the data of vesicular proteins that have been previously catalogued.

Flow cytometry is a well established method for the characterization of cells or particles with a diameter >500 nm based on light scattering and fluorescence. As EVs are smaller particles, they can be attached on beads of micrometer size in order to be analyzed by flow cytometry. The bound vesicles are stained with fluorescent antibodies and characterized for their protein markers.

However, these conventional analyses typically require a large sample volume and extensive processing of the sample, making them less suitable for clinical studies, especially if they involve a huge number of patients or the quantification of low levels of molecular markers[91,92].

Since EVs contain also different forms of DNA and RNA, some methods for the analysis of oligonucleotides are often applied to the study of EVs. Vesicular miRNAs are the most studied nucleic acids present in the EVs as they can regulate the translation of target mRNA in recipient cells. In particular, considering that the amount of nucleic acids inside the vesicles is low, the procedures to be adopted for their analysis need to be very efficient and sensitive[93]. The use and development of improved analytical approaches are very important

with the purpose of analyzing vesicular miRNAs as diagnostic or predictive markers of the progression of a disease, speeding up their introduction into clinical practice.

It is possible to use a phenol-chloroform based extraction where nucleic acids are able to partition into the aqueous phase and then are recovered through precipitation with ethanol. Another method takes advantage of spin columns covered with silica able to bind nucleic acids in the presence of chaotropic agents (for distrupting the structure of macromolecules). It is demonstrated to be a good approach to isolate pure RNA with high specificity for vesicular RNA. It was recently developed a kit utilizing this method for RNA extraction from plasma and serum vesicles, called "exoRNeasy Serum/Plasma Maxi Kit". Sometimes, the combination of spin columns and phenol-chloroform extraction is used to implement the yield of the detection[94].

Once being extracted, nucleic acids can be quantified with amplification and sequencing approaches like PCR and electrophoresis or real-time fluorescence measurements, allowing the quantification of known target sequences present in the vesicles. Other techniques are designed to provide a profiling analysis of vesicular RNA content characterizing the whole transcriptome[95,96].

However, in general, the platforms currently used for profiling and quantifying miRNAs are not always able to combine good analytical properties (like sensitivity, specificity and multiplexing capacity) with an high-throughput power, simplified workflows and cost-effectiveness[97].

So, the characterization of EVs regarding their protein, lipid and nucleic acid content needs to be improved by developing, using or combining other technologies. For instance, Raman spectroscopy (RS) and Surface Plasmon Resonance (SPR) are two biophotonics-based techniques that are recently proposed as label-free approaches for facilitating exosomes and microvesicles applied research. In fact, they can both overcome some limitations of the other techniques which require labeling of vesicles, consistent amount of vesicles and sometimes a laborious sample preparation, and improve the sensibility and specificity of the analysis.

1.5 Nanotechnology and Biophotonics for EVs analysis

Considering the remarkable potential of EVs in medicine, nanotechnologies and biophotonics seem to be an excellent candidate to speed up the from-bench-to-bed-side shift, with the aim of transferring the progresses of EV research to clinical practice.

The nanoscale dimensions of EVs allow an optimal interaction between vesicles and nanotechnology based approaches that include all those methods typically used in nanoparticle characterization. Moreover, biophotonics based techniques integrated with nanotechnology could be helpful in this field allowing the use of fully automated, high-throughput, multiplexing, and possibly label free technologies that can provide new perspectives in the study of EVs, for example for the identification of diagnostic relevant EVs. The use of innovative nanotechnologies is becoming a crucial step to unscramble the vesicle-enclosed information regarding the prognosis of a disease and the evaluation of the outcome of a therapy or of a rehabilitation process.

1.5.1 Surface Plasmon Resonance

SPR is a sensitive analytical technique able to detect variations in the mass adsorbed on top of a sensor chip without the need of any label. In particular, SPR is a phenomenon that occurs when polarized light, shone through a prism on a sensor chip with a thin metal film on top, is reflected by the metal film as a mirror. At the precise angle of incidence of the laser light that causes the minimum of the intensity of the reflected light, a wave of plasmons across the surface is generated. Indeed, photons of polarized light are able to interact with free

electrons of the metal layer, inducing a wave-like oscillation and thereby reducing the reflected light intensity. The angle at which the reflected light intensity reaches the minimum is called "resonance angle" or SPR angle. The SPR angle is dependent on the optical features of the system, like the refractive indices of the media, usually gold, and the refractive index in the immediate vicinity of the metal surface will change when accumulated mass adsorb on it[98].

In a typical SPR-based setup, ligands are immobilized onto the metal substrate and then brought into contact with an analyte. An optical reader shines laser light onto the substrate, and a detector collects the variations of the refracting index which are related to occurred binding between ligand and analyte (Figure 8)[99].

Figure 8 depicts the sensorgram related to SPR measurement: the angle at which the dip of the signal is observed vs time.

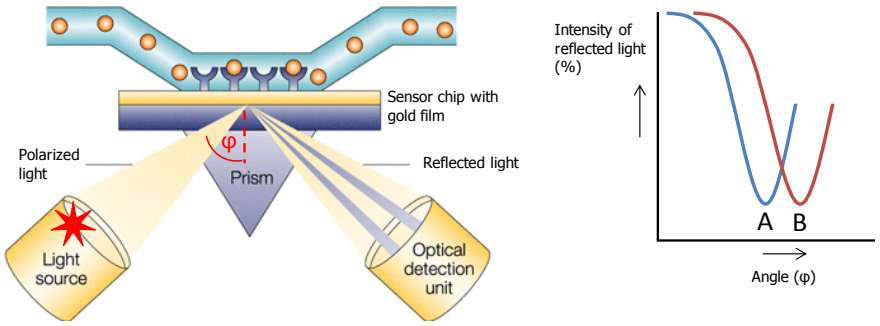

Figure 8. Schematic experimental set-up of surface plasmon resonance. A sensor chip coated with a gold film is placed on a prism. Polarized light shines from the light source (star) on the sensor chip. Reflected light intensity is measured in the detector. At a certain angle of incidence (φ), excitation of surface plasmons occurs, resulting in a dip in the intensity of the reflected light (A). A change in refractive index at the surface of the gold film will cause an angle shift from A to B. (adapted from Ref [97])

After the injection of the sample, biomolecules adsorb on the surface resulting in a change in the refractive index and a shift of the SPR angle shown by the increment of the SPR signal. The association step is followed by injection of buffer that causes the dissociation step; the last step consists in removing the bound species from the surface by injecting a suitable regeneration solution (Figure 9)[100]. The adsorption–desorption process can be followed in real time and the amount of adsorbed species can be determined.

Surface plasmon resonance is not only suited to measure the difference between these two states, but can also monitor the change in time, allowing to follow in time the shifts of the SPR angle. The shift of the SPR angle is suited to detect the presence of specific molecules, monitor and calculate affinity of interactions between biomolecules and provide information on the kinetics of molecules adsorption on the surface without the use of any other marker.

Surface Plasmon Resonance imaging (SPRi) is a development of the classical SPR biosensor able to monitor in real time the interactions across the entire chip surface of a large-format flow cell. It allows to visualize the whole surface of the chip with a video CCD camera; in this way it is possible to collect SPR signals simultaneously from every spots (that correspond to the active sites where ligands have been attached on the surface) and visualize the changes occurred on the surface while the analyte interacts with the ligand. Indeed, the SPRi equipment has a broad-beam monochromatic polarized light coming from a laser diode that illuminates the whole area of the chip. The high resolution CCD video camera provides real-time difference images capturing all of the local changes occurring at the surface of

the biochip. Each local change is related to molecular binding and biomolecular interactions. SPRi offers higher ligand throughput and flexibility in surface patterning.

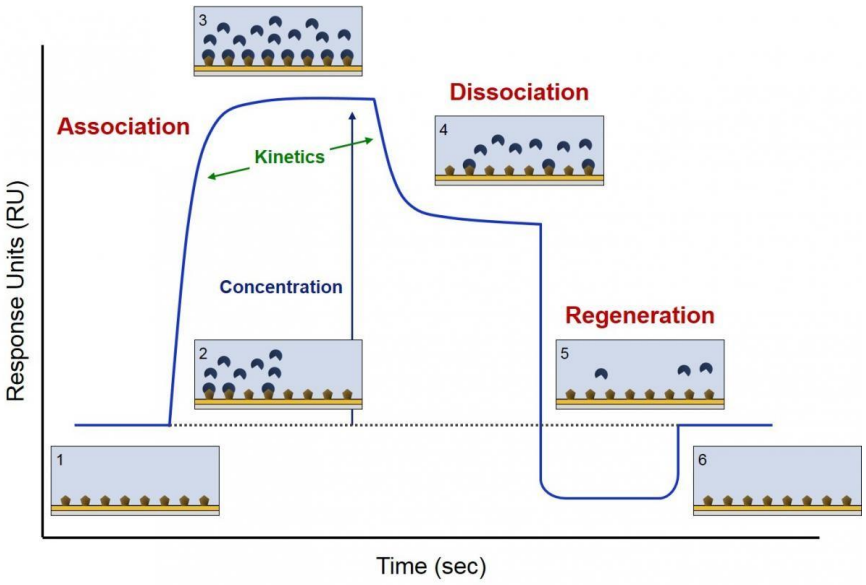

Figure 9. SPR Sensorgram: (1) Ligand immobilization; (2) analyte injection, complementary to the immobilized ligand giving a increment of the SPR response; (3) saturation; (4) dissociation of the analyte from the surface by replacing analyte injections with buffer; (5) removing of any remaining bound analyte by injection of a regeneration solution; (6) regeneration of the ligand-immobilized surface. (Adapted from Ref [98])

1.5.1.1 SPR surface chemistry for ligand immobilization

According to the ligand that needs to be immobilized on the sensor chip and to the analyte that is flowed over, a specific surface chemistry is adopted for the preparation of the SPR chip.

Typically, SPR sensor chip is made of glass and coated with a thin layer of a chemically inert metal (usually gold) that is functionalized for the ligand immobilization. There are different surface chemistries to enable ligand immobilization to the sensor chip.

One of the most common ways provides that a linking layer is deposited on the metal surface generating a self-assembled monolayer (SAM) with a high packing density. Indeed, the molecules organization into a densely packed layer is driven by van der Waals interactions between the chain, that usually take some hours to complete. This layer must has a thickness of 2-5 nm that is the good compromise in order to keep the chip sensitivity that decays exponentially with distance above the chip and to allow a uniform and stable coverage of the chip. A typical SAM consists of a three parts: a group for interaction with the surface (typically thiol groups for the interaction with gold), an alkyl chain and a tail group able to provide functionality to the SAM.

Sometimes, mixed monolayers are used to provide more stability and different surface engineering. In these cases, the molecules should be as similar as possible and preferably only differ in the tail group. For instance, a mixed SAM made of poly-ethylene glycol (PEG) functionalized with carboxyl groups and ethanolic groups has been used for some SPR biosensor preparations[101].

The carboxyl groups of the SAM are then used to immobilize ligands by amine coupling, where they form covalent amide bonds with primary amine groups of the ligands (for example, proteins, which contain several primary amines). To do this process, the activation of carboxyl groups is required and is often performed with a of N-Ethyl-

N'-(3-Dimethylaminopropyl) carbodiimide (EDC) and N-Hydroxy-succinimide (NHS). EDC reacts with the carboxyl group generating an unstable intermediate which is able to react with NHS to form an amine-reactive NHS ester. This compound can react with a primary amine group in the ligand thus forming a covalent bond, providing a direct conjugation of ligands on the surface (Figure 10).

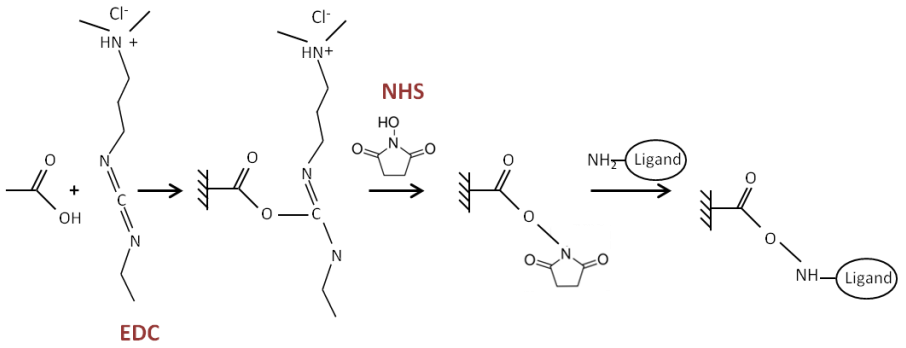

Figure 10. EDC/NHS activation of carboxyl groups for ligand immobilization by amine coupling.

After ligand immobilization, ethanolamine is used as a blocking reagent to deactivate excess NHS-activated carboxyl groups, in order to avoid aspecific binding on the surface.

Some not-direct ways to immobilize the ligand use the streptavidin-biotin or protein A-immunoglobulin interactions. After the activation with EDC/NHS, the immobilization of streptavidin or protein A on the sensor chip allows to capture biotinylated or non-modified ligands, respectively. The streptavidin-biotin is an established procedure, and makes use of the very high affinity of streptavidin to biotin, resulting in a stable surface. Protein A-IgG based capture method takes

advantage of their molecular affinity and the ease of eluting IgG ligand using lots of methods, which include low/high pH and competitive binding for chip regeneration.

Once the SPR chip is activated, the spotting procedure to immobilize the ligand can be performed through a contact printing by using an SPR-Arrayer. The SPRi-Arrayer of Horiba Scientific is an automatic benchtop instrument for printing microarrays of biological samples such as proteins and oligonucleotides, with a metal-ceramic capillary pin that can vary from 140 µm to 700 µm of diameter (Figure 11). The contact spotting procedure is very flexible, fast, versatile and requires low amount of samples and prints up to 400 samples on a SPRi biochip.

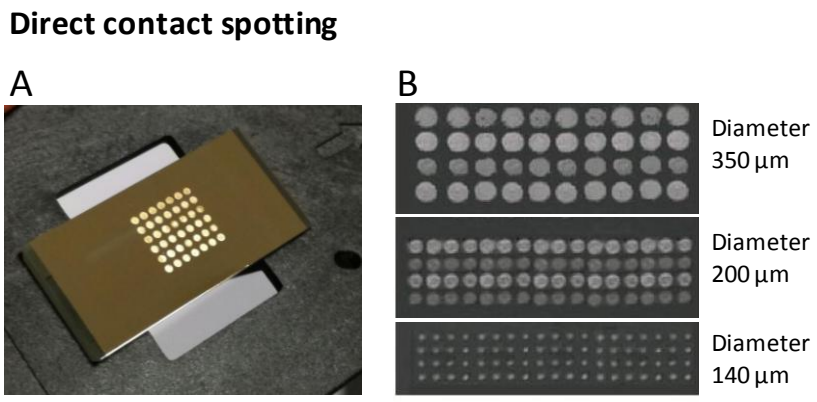

Figure 11. Spotting of SPRi biochip by direct contact spotting using SPRi-Arrayer of Horiba Scientific. A) Image of the chip with 48 printed spots (12 families of spots, 4 spots/family); B) CCD differential image (reflectivity variation) showing biomolecules spotted with different printing pins.

1.5.1.2 Applications

SPR is considered the gold standard for real time monitoring of molecular interactions able to determine specificity, affinity and kinetic parameters during the binding of macromolecules in many bonds types, such as protein-protein[102], protein-DNA[103], receptor-drug[104], lipid membrane-protein[105], complementary oligonucleotides[106,107]. Its extraordinary versatility makes it suitable for a broad range of biomedical applications, even in clinical laboratories, considering the high-throughput screening compatible with complex biological fluids analysis.

Above all, the use of SPR technology for biomedical purposes is very remarkable; for example it is an acceptable method for the development of a biosensor for the disease diagnosis and drug discovery[108]. The term "biosensor" indicates an analytical device comprised of a biological element and a transducer, able to detect the physico-chemical change due to specific interaction between the target analyte and the biological material. The transducer then yields an analog electronic signal proportional to the concentration of the specific analyte.

SPR could be used for creation of new diagnostic tools thanks to the ability of SPR-based sensors to detect low concentration of multiple biomarkers concomitantly and in a label-free manner. In particular, SPR technology is able to monitor, without the need of any label, multiple molecular interactions, such as protein binding and aggregation, occurring in a layer of about 200 nm from the surface[108]. The main advantages come from the ability to avoid the use of

fluorescent labels maintaining a high signal to noise ratio by means of its mass-sensitivity.

Moreover, the compatibility with microfluidic liquid handling and advanced chemical surface modifications makes it versatile, thus an attractive alternative to conventional assays with higher efficiency compared to classical ELISA immunoassay[109].

1.5.1.3 Advantages of using SPR for EVs analysis

Recent studies have shown the success of using plasmonic biosensors for the detection of vesicles from biological samples.

In particular, SPR is starting to emerge in EV research and it seems the ideal approach to study this target, thanks to the fact that the evanescent wave propagates for about 200 nm from the gold surface, and this range fits the dimension of vesicles.

SPR technology started to be used for obtaining a label-free profiling of the main proteins of EVs, analyzing samples from breast cancer, multiple myeloma and ovarian cancer[110–112]. In this latter case, an homemade SPR chip was developed for this specific purpose, otherwise commercially available instruments were used with these biomedical applications. The SPR based method for analysis of vesicles was improved by means of accurate surface modification strategies necessary to limit non specific binding and screen the presence of EVs and cancer specific biomarkers. In fact, most of the studies of the EVs characterization by using SPR are related to cancer research[113], and now the application field is expanding including coronary heart disease[114].

In these works, after EVs isolation by ultracentrifugation or size exclusion chromatography, vesicles are captured on the gold coated surface of the chip by means of specific antibodies and specific protocols to reduce the unspecific binding on the sensor surface. In this way, the ability of SPR to detect relative low concentration of EVs from cell supernatant or from plasma was assessed.

Considering that EVs are a very heterogeneous group of vesicles, advancement in SPR use were aimed to allow vesicle subtypes screening, developing a specific antibody microarray on the chip surface necessary to purify tissue-specific vesicles according to the presence of validated protein markers and performing the analysis by SPR imaging technique[115]. The SPRi method allows a multiplexing analysis and thus the phenotyping of vesicles, similarly to conventional microarrays that track multiple markers in parallel with limited amount of sample and reagents[116]. Moreover it allows to simultaneously quantify specific EVs subtypes, thus providing quantitative information thanks to the proportional relationship between SPR signal and the number of bound vesicles per area[117].

Considering the huge potentiality of this technique, what needs to be more examined and improved in this field is the application of such a methodology to complex biofluids, possibly without preliminary purification of vesicles, and the implementation of the technique to lower the detection limit that would allow the high-throughput investigation of disease related pattern of EVs in a highly reproducible manner.

1.5.1.4 Amplification of SPR signal

In order to enhance the biosensing capabilities of SPR, that sometimes could have some difficulties associated with detecting very low target concentration (< 1nm), some strategies based on the use of nanotechnology could be adopted. In particular, SPR chip characterized by nanostructured surfaces can be applied to exploit surface plasmonic effects for sensing biomolecular interactions. Moreover, metal nanoparticles with dimensions much smaller than the wavelength of the incident light and properly functionalized in order to bind the analyte, could significantly improve the surface plasmon effects. The increment of the SPR signal is due not only to the fact that metal particles can be exploited as intrinsic refractive index sensors, but also to the huge mass of the metal particles themselves able to strengthen the variation of the refractive index. Figure 12 shows a schematic representation of the strategies for enhancing the SPR signal.

A successful attempt to improve SPR sensitivity in exosomes detection is represented by the development of a nano-plasmonic sensor nPLEX[112]. The proposed sensor is made of a nanostructured chip where nanoholes of less than 200 nm match exosomes size range allowing improved sensitivity. Furthermore, the combination of nanostructures chip and gold nanoparticles (spherical and star shaped) proved to be an effective integration of nanotechnology approaches to increase the sensor sensitivity, a pivotal issue when handling with complex human fluids and heterogeneous vesicle populations.

In another study, He and colleagues demonstrated the nanoparticle-amplified SPR detection of DNA, by using DNA-modified

nanoparticles to achieve a detection limit of 10 pM in a sandwich assay format[118]. The intensity of SPR signals depends on nanoparticle size, shape and distance to the metal layer, and lots of groups has investigated all of these parameters, that has to be optimized according to specific application.

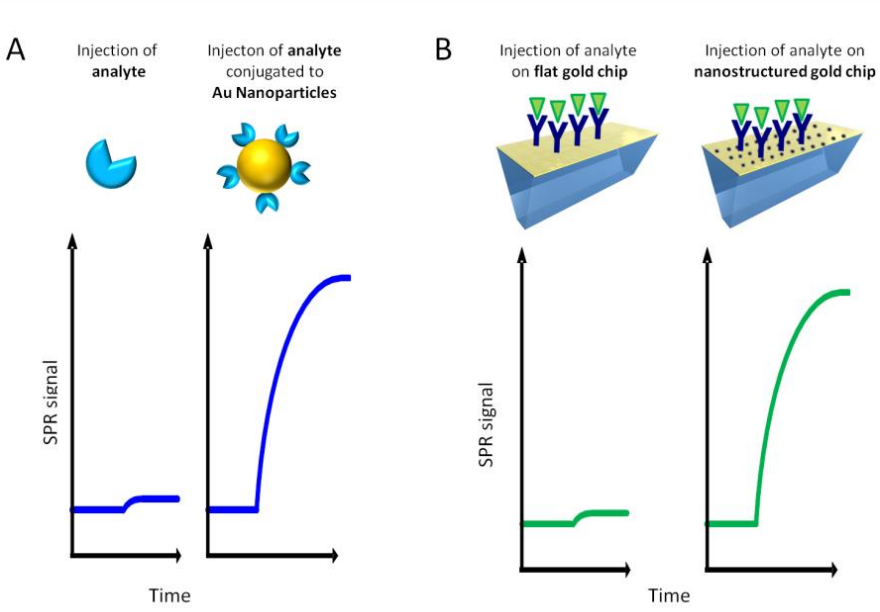

Figure 12. Schematic representation of the strategies for enhancing the SPR signal: (A) by conjugating the analyte to metal nanoparticles or (B) by using an SPR chip with nanostructured surface.

1.5.2 Raman Spectroscopy

Raman spectroscopy (RS) is a vibrational spectroscopy based on the use of a laser line to obtain information about the overall biochemical composition of a sample.

The theory of the Raman effect is based on the phenomenon of inelastic scattering of light. When light interacts with matter, the photons may be absorbed or scattered or may not interact and pass straight through it. In the scattering process the light is able to distort the cloud of electrons round the nuclei generating a not stable state, called "virtual state"; then the photons are re-radiated very quickly. Almost all of the scattering is an elastic process, called Rayleigh scattering: the scattered light has the same energy as the incident one, so there is no change in energy. However, a very small percentage of scattering is an inelastic process, called Raman scattering. In this case scattered light has different energy from incident light, because the cloud of electrons induces vibrational motions of the sample, like stretching or bending, capturing part of the incident energy. Raman scattering can occur in two different forms: when the scattered radiation has a lower energy than the incident one, it is called "Stokes"; whereas when the material loses energy and the scattered radiation has higher energy, it is called "Anti-Stokes" (Figure 13). Usually, in Raman analysis the Stokes scattering is collected.

In general, Raman scattering is an extremely weak process: it's able to collect only one in every 10^6 - 10^8 photons[119].

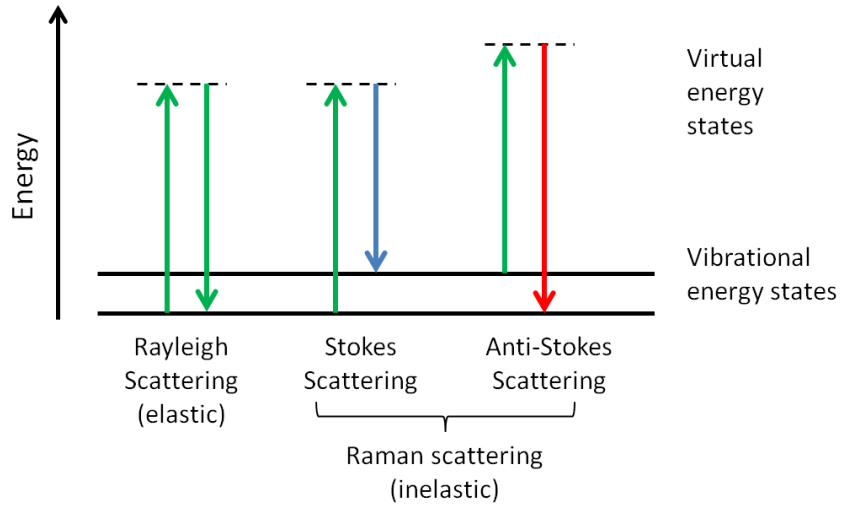

Figure 13. Schematic diagram of the Rayleigh and Raman scattering.

RS collects the inelastic scattering from a sample after the irradiation with a laser with a specific wavelength; the scattered light qualitatively and quantitatively describes the chemical moieties contained within the sample itself that are related to the biochemical composition of the sample. Raman signals arises from molecular vibrations causing a change in the polarizability, that typically occurs in symmetric vibrations able to induce a large distortion of the electron cloud around the molecule.

In a Raman spectrum, the intensity of scattered light is shown versus wavenumber, the reciprocal of wavelength called Raman shift (cm^{-1}); each peak is independent from the incident light and the energy is related to the vibrational status responsible for the scattering. Figure 14 shows an example of a Raman spectrum of a phospholipid. The major peaks have been associated to specific vibrational motions of the chemical bonds present in the molecule itself. As shown in the

figure, a single molecule can generate a complex signal in which every band is carefully assigned to a specific molecular vibration. To be able to carry out a complete and correct interpretation, the total Raman spectrum and the acquisition parameters (laser wavelength, laser power, time acquisition, etc) must be always considered.

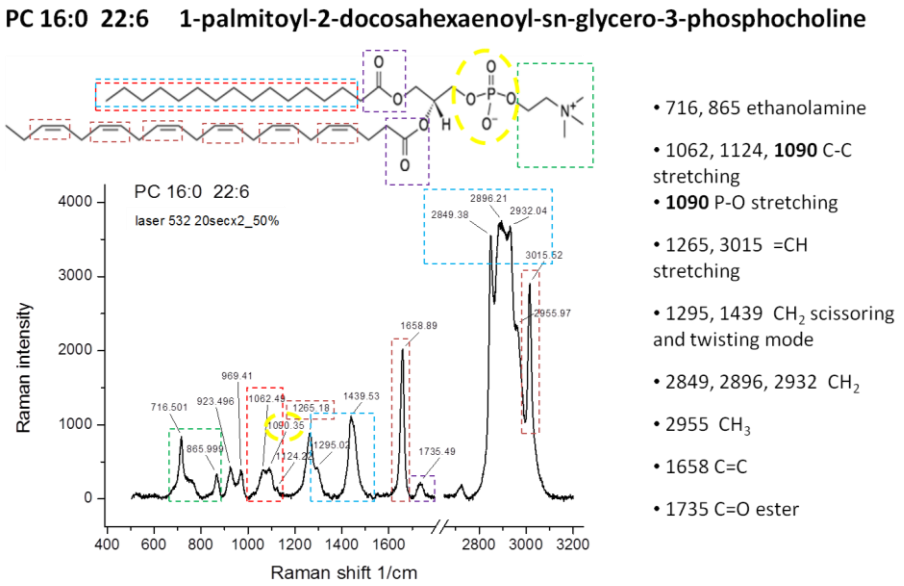

Figure 14. Raman spectrum of 1-palmitoyl-2-docosahexaenoyl-sn-glycero-3-phosphocholine on a CaF_2 slide. The spectrum is the average of 3 measures with substraction of the baseline. Parameters of acquisition: laser 532 nm, time 20 seconds, objective 50x.

The Raman spectra of biological samples contain contributions of all the biomolecules present, so that the interpretation could be hard. To avoid the complexity of the spectra, some works reported the use of surface enanched Raman spectroscopy (SERS) or resonance Raman (RR) spectroscopy, that could be adopted when only one or a limited number of molecules are of interest. However, to obtain information

about the entire composition of a biological sample, the Raman spectrum has to be compared with database of Raman spectra that serves as reference spectra of biomolecules. For example, an overview of Raman spectra of biomolecules present in a cell has been developed and consists in a database containing the most important building blocks of cellular molecules. It provides the basic information necessary to check the presence of specific molecules in biological materials, to monitor metabolism or to track changes induced by the environment[120].

1.5.2.1 Applications

RS is a non destructive, label-free, high specific and sensitive technique able to provide a characteristic fingerprint pattern of the analyzed sample. It is used in a variety of applications including the field of cultural heritage materials, semiconductors, geology and mineralogy, pharmaceuticals and cosmetics, life sciences, nanotechnology and biology on bacteria, cells or tissues.

For clinical applications, this technique is used to perform quantitative analysis of biomolecules, characterize complex biological sample, or identify unknown substances. In particular, RS has been explored as a powerful diagnostic tool for different pathologies, like cardiovascular diseases[121,122], acute nephrite[123] and cancers[124,125]. Some publications reported Raman analysis on cells and tissue for their characterization ex-vivo for purposes of basic research or as innovative alternative to classic and time-consuming diagnostic methods[126,127]. Indeed, the quantitative and qualitative assessment could allow to identify biochemical changes associated with a pathology. This is possible

because the majority of biological molecules are Raman active thus allowing to identify biochemical or molecular changes related to the onset of pathological processes.

1.5.2.2 Advantages of using RS for EVs analysis

The use of RS for the characterization of EVs both from cell culture supernatants and biological fluids was already proved to be effective. The advantages of applying this technique for EVs characterization include the fact that they don't have to be pre-processed or labeled and that RS analysis requires low amount of sample. Moreover, the measurement time is in the order of few hours.

The biochemical composition of EVs derived from different cell lines can be distinguished by a specific Raman fingerprint that shows peaks related to lipids, proteins and nucleic acids present in EVs.

Some Raman-based methods for EVs characterization have been developed, both for single-vesicle and in bulk analysis, from cell supernatants and biofluids[128–131].

Smith et al, for example, have used a Laser tweezers Raman spectroscopy (LTRS) to explore the chemical content of individual vesicle. They have demonstrated that exosomes derived from different cancerous cell lines can be distinguished from non-cancerous ones according to the expression of cholesterol and phospholipids[131]. This kind of analysis have shown an interesting diagnostic potential of EVs, that has still to be improved and strengthened.

However, regarding the use of EVs as therapeutic agents, RS appears to be a good technique that allows the rapid characterization of sample before its use *in vitro* or *in vivo*.

For instance, in the field of regenerative medicine, it is known that EVs from different mesenchymal stem cells have valuable therapeutic effects for tissue regeneration and immunomodulation, but their clinical applications have been limited by the lack of standardized and optimized procedures of EV isolation and characterization. RS can be used for routine bulk characterization of vesicles, identifying a specific fingerprint of the EV populations used for regenerative purposes. This approach can help to determine the best experimental settings and compare results from different cell sources thus promoting the translation of EV research to clinical practice.

1.6 Scope of the thesis

The scope of the thesis is to detect and characterize EVs as complex biomarkers involved in neurodegenerative diseases and as potential therapeutic agents by means of label-free biophotonics techniques: Surface Plasmon Resonance imaging (SPRi) and Raman Spectroscopy (RS).

SPRi was used with the aim to analyze EVs as clinical minimally invasive **biomarkers** for the diagnosis, the monitoring of the disease progression, and the assessment of the response to treatments with the vision of precision medicine. Indeed, SPRi allows to detect not only intact vesicles but also multiple miRNAs, that represent an important class of molecules present inside the EVs.

RS was used for providing a routine quality check of EVs before their use as **therapeutic agents.** In particular, the bulk characterization of the chemical content of EVs can be determined in a label- and sample processing- free way thus allowing the transferability into laboratory practice.

The circulating brain-derived EVs were the populations of interest in the work reported in chapter 2, and they were detected on a SPRi-based biosensor by creating a microarray of antibodies that were chosen in order to recognize specific classes of vesicles. The SPRi technology was exploited for the identification of populations of vesicles according to the presence of specific membrane molecules and for the concomitant evaluation of the presence of other molecules potentially involved in pathological mechanisms of neurodegenerative diseases. The optimized SPRi biosensor represents a promising

platform for the characterization of vesicles involved in neurodegenerative diseases and for their possible use as peripheral biomarkers.

Furthermore, in order to implement the characterization of vesicles not only by analyzing membrane molecules but also their internal cargo, SPRi is an appropriate method as it allows the detection of miRNAs with a good specificity and sensibility. A proof of concept (chapter 3) was performed by developing a biosensor based on the use of a nanostructured enhancer of SPRi for the detection of multiple miRNAs related to multiple sclerosis.

In parallel, a method based on RS was developed for the overall biochemical characterization of EVs. Our first application of this method (chapter 4) was demonstrated in the study of stem cell phenotype. Indeed, the biological and functional features that can help to distinct between bone marrow and adipose tissue mesenchymal stem cells are usually difficult to be obtained. However, RS has shown to be able to clearly distinguish EVs with different cell origin identifying tissue-specific features of vesicles with a good accuracy.

1.7 References

(1) van Niel, G.; D'Angelo, G.; Raposo, G. Shedding Light on the Cell Biology of Extracellular Vesicles. *Nat. Rev. Mol. Cell Biol.* **2018**, *19* (4), 213–228.

(2) Camussi, G.; Deregibus, M. C.; Bruno, S.; Cantaluppi, V.; Biancone, L. Exosomes/Microvesicles as a Mechanism of Cell-to-Cell Communication. *Kidney Int.* **2010**, *78* (9), 838–848.

(3) Yang, C.; Robbins, P. D. The Roles of Tumor-Derived Exosomes in Cancer Pathogenesis. *Clin. Dev. Immunol.* **2011**, *2011*, 842849.

(4) Tickner, J. A.; Urquhart, A. J.; Stephenson, S.-A.; Richard, D. J.; O'Byrne, K. J. Functions and Therapeutic Roles of Exosomes in Cancer. *Front. Oncol.* **2014**, *4*, 127.

(5) Quek, C.; Hill, A. F. The Role of Extracellular Vesicles in Neurodegenerative Diseases. *Biochem. Biophys. Res. Commun.* **2017**, *483* (4), 1178–1186.

(6) Lim, Y.-J.; Lee, S.-J. Are Exosomes the Vehicle for Protein Aggregate Propagation in Neurodegenerative Diseases? *Acta Neuropathol. Commun.* **2017**, *5* (1), 64.

(7) Soria, F. N.; Pampliega, O.; Bourdenx, M.; Meissner, W. G.; Bezard, E.; Dehay, B. Exosomes, an Unmasked Culprit in Neurodegenerative Diseases. *Front. Neurosci.* **2017**, *11*, 26.

(8) György, B.; Szabó, T. G.; Pásztói, M.; Pál, Z.; Misják, P.; Aradi, B.; László, V.; Pállinger, E.; Pap, E.; Kittel, A.; et al. Membrane Vesicles, Current State-of-the-Art: Emerging Role

of Extracellular Vesicles. *Cell. Mol. Life Sci. CMLS* **2011**, *68* (16), 2667–2688.

(9) Cobelli, N. J.; Leong, D. J.; Sun, H. B. Exosomes: Biology, Therapeutic Potential, and Emerging Role in Musculoskeletal Repair and Regeneration. *Ann. N. Y. Acad. Sci.* **2017**, *1410* (1), 57–67.

(10) Whiteside, T. L. Extracellular Vesicles Isolation and Their Biomarker Potential: Are We Ready for Testing? *Ann. Transl. Med.* **2017**, *5* (3).

(11) Ramirez, S. H.; Andrews, A. M.; Paul, D.; Pachter, J. S. Extracellular Vesicles: Mediators and Biomarkers of Pathology along CNS Barriers. *Fluids Barriers CNS* **2018**, *15* (1), 19.

(12) Xu, R.; Greening, D. W.; Zhu, H.-J.; Takahashi, N.; Simpson, R. J. Extracellular Vesicle Isolation and Characterization: Toward Clinical Application. *J. Clin. Invest.* **2016**, *126* (4), 1152–1162.

(13) Raposo, G.; Stoorvogel, W. Extracellular Vesicles: Exosomes, Microvesicles, and Friends. *J. Cell Biol.* **2013**, *200* (4), 373–383.

(14) Llorente, A.; Skotland, T.; Sylvänne, T.; Kauhanen, D.; Róg, T.; Orłowski, A.; Vattulainen, I.; Ekroos, K.; Sandvig, K. Molecular Lipidomics of Exosomes Released by PC-3 Prostate Cancer Cells. *Biochim. Biophys. Acta* **2013**, *1831* (7), 1302–1309.

(15) Fitzner, D.; Schnaars, M.; van Rossum, D.; Krishnamoorthy, G.; Dibaj, P.; Bakhti, M.; Regen, T.; Hanisch, U.-K.; Simons,

M. Selective Transfer of Exosomes from Oligodendrocytes to Microglia by Macropinocytosis. *J. Cell Sci.* **2011**, *124* (Pt 3), 447–458.

(16) Robbins, P. D.; Morelli, A. E. Regulation of Immune Responses by Extracellular Vesicles. *Nat. Rev. Immunol.* **2014**, *14* (3), 195–208.

(17) Guduric-Fuchs, J.; O'Connor, A.; Camp, B.; O'Neill, C. L.; Medina, R. J.; Simpson, D. A. Selective Extracellular Vesicle-Mediated Export of an Overlapping Set of MicroRNAs from Multiple Cell Types. *BMC Genomics* **2012**, *13* (1), 357.

(18) Lee, H.; Abston, E.; Zhang, D.; Rai, A.; Jin, Y. Extracellular Vesicle: An Emerging Mediator of Intercellular Crosstalk in Lung Inflammation and Injury. *Front. Immunol.* **2018**, *9*.

(19) Colombo, M.; Raposo, G.; Théry, C. Biogenesis, Secretion, and Intercellular Interactions of Exosomes and Other Extracellular Vesicles. *Annu. Rev. Cell Dev. Biol.* **2014**, *30*, 255–289.

(20) Isola, A. L.; Chen, S. Exosomes: The Messengers of Health and Disease. *Curr. Neuropharmacol.* **2017**, *15* (1), 157–165.

(21) Keerthikumar, S.; Chisanga, D.; Ariyaratne, D.; Al Saffar, H.; Anand, S.; Zhao, K.; Samuel, M.; Pathan, M.; Jois, M.; Chilamkurti, N.; et al. ExoCarta: A Web-Based Compendium of Exosomal Cargo. *J. Mol. Biol.* **2016**, *428* (4), 688–692.

(22) Kim, D.-K.; Lee, J.; Simpson, R. J.; Lötvall, J.; Gho, Y. S. EVpedia: A Community Web Resource for Prokaryotic and Eukaryotic Extracellular Vesicles Research. *Semin. Cell Dev. Biol.* **2015**, *40*, 4–7.

(23) Kalra, H.; Simpson, R. J.; Ji, H.; Aikawa, E.; Altevogt, P.; Askenase, P.; Bond, V. C.; Borràs, F. E.; Breakefield, X.; Budnik, V.; et al. Vesiclepedia: A Compendium for Extracellular Vesicles with Continuous Community Annotation. *PLoS Biol.* **2012**, *10* (12), e1001450.

(24) Chargaff, E.; West, R. The Biological Significance of the Thromboplastic Protein of Blood. *J. Biol. Chem.* **1946**, *166* (1), 189–197.

(25) De Broe, M.; Wieme, R.; Roels, F. Letter: Membrane Fragments with Koinozymic Properties Released from Villous Adenoma of the Rectum. *Lancet Lond. Engl.* **1975**, *2* (7946), 1214–1215.

(26) Benz, E. W.; Moses, H. L. Small, Virus-like Particles Detected in Bovine Sera by Electron Microscopy. *J. Natl. Cancer Inst.* **1974**, *52* (6), 1931–1934.

(27) Dalton, A. J. Microvesicles and Vesicles of Multivesicular Bodies versus "Virus-like" Particles. *J. Natl. Cancer Inst.* **1975**, *54* (5), 1137–1148.

(28) Harding, C.; Heuser, J.; Stahl, P. Receptor-Mediated Endocytosis of Transferrin and Recycling of the Transferrin Receptor in Rat Reticulocytes. *J. Cell Biol.* **1983**, *97* (2), 329–339.

(29) Pan, B. T.; Teng, K.; Wu, C.; Adam, M.; Johnstone, R. M. Electron Microscopic Evidence for Externalization of the Transferrin Receptor in Vesicular Form in Sheep Reticulocytes. *J. Cell Biol.* **1985**, *101* (3), 942–948.

(30) Johnstone, R. M.; Adam, M.; Hammond, J. R.; Orr, L.; Turbide, C. Vesicle Formation during Reticulocyte Maturation. Association of Plasma Membrane Activities with Released Vesicles (Exosomes). *J. Biol. Chem.* **1987**, *262* (19), 9412–9420.

(31) Kalra, H.; Drummen, G. P. C.; Mathivanan, S. Focus on Extracellular Vesicles: Introducing the Next Small Big Thing. *Int. J. Mol. Sci.* **2016**, *17* (2).

(32) Valadi, H.; Ekström, K.; Bossios, A.; Sjöstrand, M.; Lee, J. J.; Lötvall, J. O. Exosome-Mediated Transfer of MRNAs and MicroRNAs Is a Novel Mechanism of Genetic Exchange between Cells. *Nat. Cell Biol.* **2007**, *9* (6), 654–659.

(33) Maia, J.; Caja, S.; Strano Moraes, M. C.; Couto, N.; Costa-Silva, B. Exosome-Based Cell-Cell Communication in the Tumor Microenvironment. *Front. Cell Dev. Biol.* **2018**, *6*.

(34) He, C.; Zheng, S.; Luo, Y.; Wang, B. Exosome Theranostics: Biology and Translational Medicine. *Theranostics* **2018**, *8* (1), 237–255.

(35) Clayton, A.; Buschmann, D.; Byrd, J. B.; Carter, D. R. F.; Cheng, L.; Compton, C.; Daaboul, G.; Devitt, A.; Falcon-Perez, J. M.; Gardiner, C.; et al. Summary of the ISEV Workshop on Extracellular Vesicles as Disease Biomarkers, Held in Birmingham, UK, during December 2017. *J. Extracell. Vesicles* **2018**, *7* (1).

(36) Melo, S. A.; Luecke, L. B.; Kahlert, C.; Fernandez, A. F.; Gammon, S. T.; Kaye, J.; LeBleu, V. S.; Mittendorf, E. A.; Weitz, J.; Rahbari, N.; et al. Glypican-1 Identifies Cancer

Exosomes and Detects Early Pancreatic Cancer. *Nature* **2015**, *523* (7559), 177–182.

(37) Machida, T.; Tomofuji, T.; Ekuni, D.; Maruyama, T.; Yoneda, T.; Kawabata, Y.; Mizuno, H.; Miyai, H.; Kunitomo, M.; Morita, M. MicroRNAs in Salivary Exosome as Potential Biomarkers of Aging. *Int. J. Mol. Sci.* **2015**, *16* (9), 21294–21309.

(38) Skotland, T.; Ekroos, K.; Kauhanen, D.; Simolin, H.; Seierstad, T.; Berge, V.; Sandvig, K.; Llorente, A. Molecular Lipid Species in Urinary Exosomes as Potential Prostate Cancer Biomarkers. *Eur. J. Cancer Oxf. Engl. 1990* **2017**, *70*, 122–132.

(39) Conde-Vancells, J.; Rodriguez-Suarez, E.; Gonzalez, E.; Berisa, A.; Gil, D.; Embade, N.; Valle, M.; Luka, Z.; Elortza, F.; Wagner, C.; et al. Candidate Biomarkers in Exosome-like Vesicles Purified from Rat and Mouse Urine Samples. *Proteomics Clin. Appl.* **2010**, *4* (4), 416–425.

(40) Mege, D.; Panicot-Dubois, L.; Ouaissi, M.; Robert, S.; Sielezneff, I.; Sastre, B.; Dignat-George, F.; Dubois, C. The Origin and Concentration of Circulating Microparticles Differ According to Cancer Type and Evolution: A Prospective Single-Center Study. *Int. J. Cancer* **2016**, *138* (4), 939–948.

(41) Fleitas, T.; Martínez-Sales, V.; Vila, V.; Reganon, E.; Mesado, D.; Martín, M.; Gómez-Codina, J.; Montalar, J.; Reynés, G. Circulating Endothelial Cells and Microparticles as Prognostic Markers in Advanced Non-Small Cell Lung Cancer. *PLOS ONE* **2012**, *7* (10), e47365.

(42) Armstrong, J. P. K.; Stevens, M. M. Strategic Design of Extracellular Vesicle Drug Delivery Systems. *Adv. Drug Deliv. Rev.* **2018**, *130*, 12–16.

(43) Tominaga, N.; Kosaka, N.; Ono, M.; Katsuda, T.; Yoshioka, Y.; Tamura, K.; Lötvall, J.; Nakagama, H.; Ochiya, T. Brain Metastatic Cancer Cells Release MicroRNA-181c-Containing Extracellular Vesicles Capable of Destructing Blood-Brain Barrier. *Nat. Commun.* **2015**, *6*, 6716.

(44) Malda, J.; Boere, J.; van de Lest, C. H. A.; van Weeren, P. R.; Wauben, M. H. M. Extracellular Vesicles — New Tool for Joint Repair and Regeneration. *Nat. Rev. Rheumatol.* **2016**, *12* (4), 243–249.

(45) ltd, R. and M. The Market for Stem Cell Exosomes - Research and Markets https://www.researchandmarkets.com/reports/4437322/the-market-for-stem-cell-exosomes.

(46) van der Meel, R.; Fens, M. H. A. M.; Vader, P.; van Solinge, W. W.; Eniola-Adefeso, O.; Schiffelers, R. M. Extracellular Vesicles as Drug Delivery Systems: Lessons from the Liposome Field. *J. Control. Release Off. J. Control. Release Soc.* **2014**, *195*, 72–85.

(47) Kooijmans, S. A. A.; Vader, P.; van Dommelen, S. M.; van Solinge, W. W.; Schiffelers, R. M. Exosome Mimetics: A Novel Class of Drug Delivery Systems. *Int. J. Nanomedicine* **2012**, *7*, 1525–1541.

(48) Armstrong, J. P. K.; Holme, M. N.; Stevens, M. M. Re-Engineering Extracellular Vesicles as Smart Nanoscale Therapeutics. *ACS Nano* **2017**, *11* (1), 69–83.

(49) Fuhrmann, G.; Serio, A.; Mazo, M.; Nair, R.; Stevens, M. M. Active Loading into Extracellular Vesicles Significantly Improves the Cellular Uptake and Photodynamic Effect of Porphyrins. *J. Control. Release Off. J. Control. Release Soc.* **2015**, *205*, 35–44.

(50) Besse, B.; Charrier, M.; Lapierre, V.; Dansin, E.; Lantz, O.; Planchard, D.; Chevalier, T. L.; Livartoski, A.; Barlesi, F.; Laplanche, A.; et al. Dendritic Cell-Derived Exosomes as Maintenance Immunotherapy after First Line Chemotherapy in NSCLC. *OncoImmunology* **2016**, *5* (4), e1071008.

(51) Tian, Y.; Li, S.; Song, J.; Ji, T.; Zhu, M.; Anderson, G. J.; Wei, J.; Nie, G. A Doxorubicin Delivery Platform Using Engineered Natural Membrane Vesicle Exosomes for Targeted Tumor Therapy. *Biomaterials* **2014**, *35* (7), 2383–2390.

(52) Pinheiro, A.; Silva, A. M.; Teixeira, J. H.; Gonçalves, R. M.; Almeida, M. I.; Barbosa, M. A.; Santos, S. G. Extracellular Vesicles: Intelligent Delivery Strategies for Therapeutic Applications. *J. Control. Release Off. J. Control. Release Soc.* **2018**, *289*, 56–69.

(53) Frühbeis, C.; Fröhlich, D.; Kuo, W. P.; Amphornrat, J.; Thilemann, S.; Saab, A. S.; Kirchhoff, F.; Möbius, W.; Goebbels, S.; Nave, K.-A.; et al. Neurotransmitter-Triggered Transfer of Exosomes Mediates Oligodendrocyte–Neuron Communication. *PLOS Biol.* **2013**, *11* (7), e1001604.

(54) Guescini, M.; Genedani, S.; Stocchi, V.; Agnati, L. F. Astrocytes and Glioblastoma Cells Release Exosomes Carrying MtDNA. *J. Neural Transm. Vienna Austria 1996* **2010**, *117* (1), 1–4.

(55) Antonucci, F.; Turola, E.; Riganti, L.; Caleo, M.; Gabrielli, M.; Perrotta, C.; Novellino, L.; Clementi, E.; Giussani, P.; Viani, P.; et al. Microvesicles Released from Microglia Stimulate Synaptic Activity via Enhanced Sphingolipid Metabolism. *EMBO J.* **2012**, *31* (5), 1231–1240.

(56) Pegtel, D. M.; Peferoen, L.; Amor, S. Extracellular Vesicles as Modulators of Cell-to-Cell Communication in the Healthy and Diseased Brain. *Philos. Trans. R. Soc. Lond. B. Biol. Sci.* **2014**, *369* (1652).

(57) Howitt, J.; Hill, A. F. Exosomes in the Pathology of Neurodegenerative Diseases. *J. Biol. Chem.* **2016**, jbc.R116.757955.

(58) Pardridge, W. M. The Blood-Brain Barrier: Bottleneck in Brain Drug Development. *NeuroRx J. Am. Soc. Exp. Neurother.* **2005**, *2* (1), 3–14.

(59) Pardridge, W. M. Drug Transport across the Blood-Brain Barrier. *J. Cereb. Blood Flow Metab. Off. J. Int. Soc. Cereb. Blood Flow Metab.* **2012**, *32* (11), 1959–1972.

(60) Chow, B. W.; Gu, C. The Molecular Constituents of the Blood-Brain Barrier. *Trends Neurosci.* **2015**, *38* (10), 598–608.

(61) Jarmalavičiūtė, A.; Pivoriūnas, A. Exosomes as a Potential Novel Therapeutic Tools against Neurodegenerative Diseases. *Pharmacol. Res.* **2016**, *113* (Pt B), 816–822.

(62) García-Romero, N.; Carrión-Navarro, J.; Esteban-Rubio, S.; Lázaro-Ibáñez, E.; Peris-Celda, M.; Alonso, M. M.; Guzmán-De-Villoria, J.; Fernández-Carballal, C.; de Mendivil, A. O.; García-Duque, S.; et al. DNA Sequences within Glioma-Derived Extracellular Vesicles Can Cross the Intact Blood-Brain Barrier and Be Detected in Peripheral Blood of Patients. *Oncotarget* **2016**, *8* (1), 1416–1428.

(63) Kerr, N.; García-Contreras, M.; Abbassi, S.; Mejias, N. H.; Desousa, B. R.; Ricordi, C.; Dietrich, W. D.; Keane, R. W.; de Rivero Vaccari, J. P. Inflammasome Proteins in Serum and Serum-Derived Extracellular Vesicles as Biomarkers of Stroke. *Front. Mol. Neurosci.* **2018**, *11*, 309.

(64) Saman, S.; Kim, W.; Raya, M.; Visnick, Y.; Miro, S.; Saman, S.; Jackson, B.; McKee, A. C.; Alvarez, V. E.; Lee, N. C. Y.; et al. Exosome-Associated Tau Is Secreted in Tauopathy Models and Is Selectively Phosphorylated in Cerebrospinal Fluid in Early Alzheimer Disease. *J. Biol. Chem.* **2012**, *287* (6), 3842–3849.

(65) Tomlinson, P. R.; Zheng, Y.; Fischer, R.; Heidasch, R.; Gardiner, C.; Evetts, S.; Hu, M.; Wade-Martins, R.; Turner, M. R.; Morris, J.; et al. Identification of Distinct Circulating Exosomes in Parkinson's Disease. *Ann. Clin. Transl. Neurol.* **2015**, *2* (4), 353–361.

(66) Matsumoto, J.; Stewart, T.; Sheng, L.; Li, N.; Bullock, K.; Song, N.; Shi, M.; Banks, W. A.; Zhang, J. Transmission of α-Synuclein-Containing Erythrocyte-Derived Extracellular Vesicles across the Blood-Brain Barrier via Adsorptive Mediated Transcytosis: Another Mechanism for Initiation and Progression of Parkinson's Disease? *Acta Neuropathol. Commun.* **2017**, *5* (1), 71.

(67) Tofaris, G. K. A Critical Assessment of Exosomes in the Pathogenesis and Stratification of Parkinson's Disease. *J. Park. Dis.* **2017**, *7* (4), 569–576.

(68) Verderio, C.; Muzio, L.; Turola, E.; Bergami, A.; Novellino, L.; Ruffini, F.; Riganti, L.; Corradini, I.; Francolini, M.; Garzetti, L.; et al. Myeloid Microvesicles Are a Marker and Therapeutic Target for Neuroinflammation. *Ann. Neurol.* **2012**, *72* (4), 610–624.

(69) Drago, F.; Lombardi, M.; Prada, I.; Gabrielli, M.; Joshi, P.; Cojoc, D.; Franck, J.; Fournier, I.; Vizioli, J.; Verderio, C. ATP Modifies the Proteome of Extracellular Vesicles Released by Microglia and Influences Their Action on Astrocytes. *Front. Pharmacol.* **2017**, *8*, 910.

(70) Colombo, F.; Bastoni, M.; Nigro, A.; Podini, P.; Finardi, A.; Casella, G.; Ramesh, M.; Farina, C.; Verderio, C.; Furlan, R. Cytokines Stimulate the Release of Microvesicles from Myeloid Cells Independently from the P2X7 Receptor/Acid Sphingomyelinase Pathway. *Front. Immunol.* **2018**, *9*, 204.

(71) Tian, T.; Zhang, H.-X.; He, C.-P.; Fan, S.; Zhu, Y.-L.; Qi, C.; Huang, N.-P.; Xiao, Z.-D.; Lu, Z.-H.; Tannous, B. A.; et al.

Surface Functionalized Exosomes as Targeted Drug Delivery Vehicles for Cerebral Ischemia Therapy. *Biomaterials* **2018**, *150*, 137–149.

(72) Cooper, J. M.; Wiklander, P. B. O.; Nordin, J. Z.; Al-Shawi, R.; Wood, M. J.; Vithlani, M.; Schapira, A. H. V.; Simons, J. P.; El-Andaloussi, S.; Alvarez-Erviti, L. Systemic Exosomal SiRNA Delivery Reduced Alpha-Synuclein Aggregates in Brains of Transgenic Mice. *Mov. Disord. Off. J. Mov. Disord. Soc.* **2014**, *29* (12), 1476–1485.

(73) Xin, H.; Li, Y.; Cui, Y.; Yang, J. J.; Zhang, Z. G.; Chopp, M. Systemic Administration of Exosomes Released from Mesenchymal Stromal Cells Promote Functional Recovery and Neurovascular Plasticity After Stroke in Rats. *J. Cereb. Blood Flow Metab.* **2013**, *33* (11), 1711–1715.

(74) Pusic, A. D.; Pusic, K. M.; Clayton, B. L. L.; Kraig, R. P. IFNγ-Stimulated Dendritic Cell Exosomes as a Potential Therapeutic for Remyelination. *J. Neuroimmunol.* **2014**, *266* (1), 12–23.

(75) Takeda, Y. S.; Xu, Q. Neuronal Differentiation of Human Mesenchymal Stem Cells Using Exosomes Derived from Differentiating Neuronal Cells. *PLOS ONE* **2015**, *10* (8), e0135111.

(76) Yuyama, K.; Sun, H.; Mitsutake, S.; Igarashi, Y. Sphingolipid-Modulated Exosome Secretion Promotes Clearance of Amyloid-β by Microglia. *J. Biol. Chem.* **2012**, *287* (14), 10977–10989.

(77) Rufino-Ramos, D.; Albuquerque, P. R.; Carmona, V.; Perfeito, R.; Nobre, R. J.; Pereira de Almeida, L. Extracellular Vesicles: Novel Promising Delivery Systems for Therapy of Brain Diseases. *J. Controlled Release* **2017**, *262*, 247–258.

(78) Lötvall, J.; Hill, A. F.; Hochberg, F.; Buzás, E. I.; Di Vizio, D.; Gardiner, C.; Gho, Y. S.; Kurochkin, I. V.; Mathivanan, S.; Quesenberry, P.; et al. Minimal Experimental Requirements for Definition of Extracellular Vesicles and Their Functions: A Position Statement from the International Society for Extracellular Vesicles. *J. Extracell. Vesicles* **2014**, *3*, 26913.

(79) Witwer, K. W.; Soekmadji, C.; Hill, A. F.; Wauben, M. H.; Buzás, E. I.; Di Vizio, D.; Falcon-Perez, J. M.; Gardiner, C.; Hochberg, F.; Kurochkin, I. V.; et al. Updating the MISEV Minimal Requirements for Extracellular Vesicle Studies: Building Bridges to Reproducibility. *J. Extracell. Vesicles* **2017**, *6* (1), 1396823.

(80) Tauro, B. J.; Greening, D. W.; Mathias, R. A.; Ji, H.; Mathivanan, S.; Scott, A. M.; Simpson, R. J. Comparison of Ultracentrifugation, Density Gradient Separation, and Immunoaffinity Capture Methods for Isolating Human Colon Cancer Cell Line LIM1863-Derived Exosomes. *Methods San Diego Calif* **2012**, *56* (2), 293–304.

(81) Gardiner, C.; Vizio, D. D.; Sahoo, S.; Théry, C.; Witwer, K. W.; Wauben, M.; Hill, A. F. Techniques Used for the Isolation and Characterization of Extracellular Vesicles: Results of a Worldwide Survey. *J. Extracell. Vesicles* **2016**, *5* (1), 32945.

(82) Momen-Heravi, F.; Balaj, L.; Alian, S.; Mantel, P.-Y.; Halleck, A. E.; Trachtenberg, A. J.; Soria, C. E.; Oquin, S.; Bonebreak, C. M.; Saracoglu, E.; et al. Current Methods for the Isolation of Extracellular Vesicles. *Biol. Chem.* **2013**, *394* (10), 1253–1262.

(83) Yuana, Y.; Levels, J.; Grootemaat, A.; Sturk, A.; Nieuwland, R. Co-Isolation of Extracellular Vesicles and High-Density Lipoproteins Using Density Gradient Ultracentrifugation. *J. Extracell. Vesicles* **2014**, *3*.

(84) Laurent, L. C.; Alexander, R. P. Exosome Isolation from Plasma Using ExoQuick Reagent. **2015**.

(85) Lozano-Ramos, I.; Bancu, I.; Oliveira-Tercero, A.; Armengol, M. P.; Menezes-Neto, A.; Del Portillo, H. A.; Lauzurica-Valdemoros, R.; Borràs, F. E. Size-Exclusion Chromatography-Based Enrichment of Extracellular Vesicles from Urine Samples. *J. Extracell. Vesicles* **2015**, *4*, 27369.

(86) An, M.; Wu, J.; Zhu, J.; Lubman, D. M. A Comparison of an Optimized Ultracentrifugation Method versus Size-Exclusion Chromatography for Isolation of Exosomes from Human Serum. *J. Proteome Res.* **2018**.

(87) Bukong, T. N.; Momen-Heravi, F.; Kodys, K.; Bala, S.; Szabo, G. Exosomes from Hepatitis C Infected Patients Transmit HCV Infection and Contain Replication Competent Viral RNA in Complex with Ago2-MiR122-HSP90. *PLOS Pathog.* **2014**, *10* (10), e1004424.

(88) Cizmar, P.; Yuana, Y. Detection and Characterization of Extracellular Vesicles by Transmission and Cryo-

Transmission Electron Microscopy. *Methods Mol. Biol. Clifton NJ* **2017**, *1660*, 221–232.

(89) Parisse, P.; Rago, I.; Ulloa Severino, L.; Perissinotto, F.; Ambrosetti, E.; Paoletti, P.; Ricci, M.; Beltrami, A. P.; Cesselli, D.; Casalis, L. Atomic Force Microscopy Analysis of Extracellular Vesicles. *Eur. Biophys. J.* **2017**, *46* (8), 813–820.

(90) Vestad, B.; Llorente, A.; Neurauter, A.; Phuyal, S.; Kierulf, B.; Kierulf, P.; Skotland, T.; Sandvig, K.; Haug, K. B. F.; Øvstebø, R. Size and Concentration Analyses of Extracellular Vesicles by Nanoparticle Tracking Analysis: A Variation Study. *J. Extracell. Vesicles* **2017**, *6* (1).

(91) Witwer, K. W.; Buzás, E. I.; Bemis, L. T.; Bora, A.; Lässer, C.; Lötvall, J.; Nolte-'t Hoen, E. N.; Piper, M. G.; Sivaraman, S.; Skog, J.; et al. Standardization of Sample Collection, Isolation and Analysis Methods in Extracellular Vesicle Research. *J. Extracell. Vesicles* **2013**, *2*.

(92) Shao, H.; Im, H.; Castro, C. M.; Breakefield, X.; Weissleder, R.; Lee, H. New Technologies for Analysis of Extracellular Vesicles. *Chem. Rev.* **2018**, *118* (4), 1917–1950.

(93) Mateescu, B.; Kowal, E. J. K.; van Balkom, B. W. M.; Bartel, S.; Bhattacharyya, S. N.; Buzás, E. I.; Buck, A. H.; de Candia, P.; Chow, F. W. N.; Das, S.; et al. Obstacles and Opportunities in the Functional Analysis of Extracellular Vesicle RNA - an ISEV Position Paper. *J. Extracell. Vesicles* **2017**, *6* (1), 1286095.

(94) Enderle, D.; Spiel, A.; Coticchia, C. M.; Berghoff, E.; Mueller, R.; Schlumpberger, M.; Sprenger-Haussels, M.;

Shaffer, J. M.; Lader, E.; Skog, J.; et al. Characterization of RNA from Exosomes and Other Extracellular Vesicles Isolated by a Novel Spin Column-Based Method. *PloS One* **2015**, *10* (8), e0136133.

(95) Huang, X.; Yuan, T.; Tschannen, M.; Sun, Z.; Jacob, H.; Du, M.; Liang, M.; Dittmar, R. L.; Liu, Y.; Liang, M.; et al. Characterization of Human Plasma-Derived Exosomal RNAs by Deep Sequencing. *BMC Genomics* **2013**, *14*, 319.

(96) Conley, A.; Minciacchi, V. R.; Lee, D. H.; Knudsen, B. S.; Karlan, B. Y.; Citrigno, L.; Viglietto, G.; Tewari, M.; Freeman, M. R.; Demichelis, F.; et al. High-Throughput Sequencing of Two Populations of Extracellular Vesicles Provides an MRNA Signature That Can Be Detected in the Circulation of Breast Cancer Patients. *RNA Biol.* **2017**, *14* (3), 305–316.

(97) Graybill, R. M.; Bailey, R. C. Emerging Biosensing Approaches for MicroRNA Analysis. *Anal. Chem.* **2016**, *88* (1), 431–450.

(98) Schasfoort, R. B. M. *Handbook of Surface Plasmon Resonance: 2nd Edition*; Royal Society of Chemistry, **2017**.

(99) MagHelix™ Surface Plasmon Resonance (SPR) - Creative Biostructure https://www.creative-biostructure.com/maghelix%E2%84%A2-surface-plasmon-resonance-spr-12.htm

(100) DHVI BIA Core | Shared Resources for Duke Human Vaccine Institute https://shared-resources.dhvi.duke.edu/dhvi-core-facilities/dhvi-bia-core

(101) Subramanian, A.; Irudayaraj, J.; Ryan, T. A Mixed Self-Assembled Monolayer-Based Surface Plasmon Immunosensor for Detection of E. Coli O157:H7. *Biosens. Bioelectron.* **2006**, *21* (7), 998–1006.

(102) Kim, M.; Park, K.; Jeong, E.-J.; Shin, Y.-B.; Chung, B. H. Surface Plasmon Resonance Imaging Analysis of Protein-Protein Interactions Using on-Chip-Expressed Capture Protein. *Anal. Biochem.* **2006**, *351* (2), 298–304.

(103) Majka, J.; Speck, C. Analysis of Protein-DNA Interactions Using Surface Plasmon Resonance. *Adv. Biochem. Eng. Biotechnol.* **2007**, *104*, 13–36.

(104) Rich, R. L.; Hoth, L. R.; Geoghegan, K. F.; Brown, T. A.; LeMotte, P. K.; Simons, S. P.; Hensley, P.; Myszka, D. G. Kinetic Analysis of Estrogen Receptor/Ligand Interactions. *Proc. Natl. Acad. Sci. U. S. A.* **2002**, *99* (13), 8562–8567.

(105) Baron, O.; Pauron, D. Protein-Lipid Interaction Analysis by Surface Plasmon Resonance (SPR). *BIO-Protoc.* **2014**, *4* (18).

(106) Wolf, L. K.; Fullenkamp, D. E.; Georgiadis, R. M. Quantitative Angle-Resolved SPR Imaging of DNA-DNA and DNA-Drug Kinetics. *J. Am. Chem. Soc.* **2005**, *127* (49), 17453–17459.

(107) Lao, A. I. K.; Su, X.; Aung, K. M. M. SPR Study of DNA Hybridization with DNA and PNA Probes under Stringent Conditions. *Biosens. Bioelectron.* **2009**, *24* (6), 1717–1722.

(108) Homola, J. Present and Future of Surface Plasmon Resonance Biosensors. *Anal. Bioanal. Chem.* **2003**, *377* (3), 528–539.

(109) Rupert, D. L. M.; Lässer, C.; Eldh, M.; Block, S.; Zhdanov, V. P.; Lotvall, J. O.; Bally, M.; Höök, F. Determination of Exosome Concentration in Solution Using Surface Plasmon Resonance Spectroscopy. *Anal. Chem*. **2014**, *86* (12), 5929–5936.

(110) Grasso, L.; Wyss, R.; Weidenauer, L.; Thampi, A.; Demurtas, D.; Prudent, M.; Lion, N.; Vogel, H. Molecular Screening of Cancer-Derived Exosomes by Surface Plasmon Resonance Spectroscopy. *Anal. Bioanal. Chem*. **2015**, *407* (18), 5425–5432.

(111) Di Noto, G.; Bugatti, A.; Zendrini, A.; Mazzoldi, E. L.; Montanelli, A.; Caimi, L.; Rusnati, M.; Ricotta, D.; Bergese, P. Merging Colloidal Nanoplasmonics and Surface Plasmon Resonance Spectroscopy for Enhanced Profiling of Multiple Myeloma-Derived Exosomes. *Biosens. Bioelectron*. **2016**, *77*, 518–524.

(112) Im, H.; Shao, H.; Park, Y. I.; Peterson, V. M.; Castro, C. M.; Weissleder, R.; Lee, H. Label-Free Detection and Molecular Profiling of Exosomes with a Nano-Plasmonic Sensor. *Nat. Biotechnol*. **2014**, *32* (5), 490–495.

(113) Im, H.; Shao, H.; Weissleder, R.; Castro, C. M.; Lee, H. Nano-Plasmonic Exosome Diagnostics. *Expert Rev. Mol. Diagn*. **2015**, *15* (6), 725–733.

(114) Hosseinkhani, B.; van den Akker, N.; D'Haen, J.; Gagliardi, M.; Struys, T.; Lambrichts, I.; Waltenberger, J.; Nelissen, I.; Hooyberghs, J.; Molin, D. G. M.; et al. Direct Detection of Nano-Scale Extracellular Vesicles Derived from

Inflammation-Triggered Endothelial Cells Using Surface Plasmon Resonance. *Nanomedicine Nanotechnol. Biol. Med.* **2017**, *13* (5), 1663–1671.

(115) Zhu, L.; Wang, K.; Cui, J.; Liu, H.; Bu, X.; Ma, H.; Wang, W.; Gong, H.; Lausted, C.; Hood, L.; et al. Label-Free Quantitative Detection of Tumor-Derived Exosomes through Surface Plasmon Resonance Imaging. *Anal. Chem.* **2014**, *86* (17), 8857–8864.

(116) Jørgensen, M.; Bæk, R.; Pedersen, S.; Søndergaard, E. K. L.; Kristensen, S. R.; Varming, K. Extracellular Vesicle (EV) Array: Microarray Capturing of Exosomes and Other Extracellular Vesicles for Multiplexed Phenotyping. *J. Extracell. Vesicles* **2013**, *2*.

(117) Jung, L. S.; Shumaker-Parry, J. S.; Campbell, C. T.; Yee, S. S.; Gelb, M. H. Quantification of Tight Binding to Surface-Immobilized Phospholipid Vesicles Using Surface Plasmon Resonance: Binding Constant of Phospholipase A $_2$. *J. Am. Chem. Soc.* **2000**, *122* (17), 4177–4184.

(118) He, L.; Musick, M. D.; Nicewarner, S. R.; Salinas, F. G.; Benkovic, S. J.; Natan, M. J.; Keating, C. D. Colloidal Au-Enhanced Surface Plasmon Resonance for Ultrasensitive Detection of DNA Hybridization. *J. Am. Chem. Soc.* **2000**, *122* (38), 9071–9077.

(119) Introduction, Basic Theory and Principles. In *Modern Raman Spectroscopy – A Practical Approach*; Wiley-Blackwell, **2005**; pp 1–21.

(120) Gelder, J. D.; Gussem, K. D.; Vandenabeele, P.; Moens, L. Reference Database of Raman Spectra of Biological Molecules. *J. Raman Spectrosc.* **2007**, *38* (9), 1133–1147.

(121) Yang, H.; Zhao, C.; Li, R.; Shen, C.; Cai, X.; Sun, L.; Luo, C.; Yin, Y. Noninvasive and Prospective Diagnosis of Coronary Heart Disease with Urine Using Surface-Enhanced Raman Spectroscopy. *The Analyst* **2018**, *143* (10), 2235–2242.

(122) van de Poll, S. W. E.; Römer, T. J.; Puppels, G. J.; van der Laarse, A. Raman Spectroscopy of Atherosclerosis. *J. Cardiovasc. Risk* **2002**, *9* (5), 255–261.

(123) Li, J.; Du, Y.; Qi, J.; Sneha, R.; Chang, A.; Mohan, C.; Shih, W.-C. Raman Spectroscopy as a Diagnostic Tool for Monitoring Acute Nephritis. *J. Biophotonics* **2016**, *9* (3), 260–269.

(124) Austin, L. A.; Osseiran, S.; Evans, C. L. Raman Technologies in Cancer Diagnostics. *Analyst* **2016**, *141* (2), 476–503.

(125) Vanna, R.; Ronchi, P.; Lenferink, A. T. M.; Tresoldi, C.; Morasso, C.; Mehn, D.; Bedoni, M.; Picciolini, S.; Terstappen, L. W. M. M.; Ciceri, F.; et al. Label-Free Imaging and Identification of Typical Cells of Acute Myeloid Leukaemia and Myelodysplastic Syndrome by Raman Microspectroscopy. *The Analyst* **2015**, *140* (4), 1054–1064.

(126) Wachsmann-Hogiu, S.; Weeks, T.; Huser, T. Chemical Analysis in Vivo and in Vitro by Raman Spectroscopy—from Single Cells to Humans. *Curr. Opin. Biotechnol.* **2009**, *20* (1), 63–73.

(127) Krafft, C.; Popp, J. The Many Facets of Raman Spectroscopy for Biomedical Analysis. *Anal. Bioanal. Chem.* **2015**, *407* (3), 699–717.

(128) Tatischeff, I.; Larquet, E.; Falcón-Pérez, J. M.; Turpin, P.-Y.; Kruglik, S. G. Fast Characterisation of Cell-Derived Extracellular Vesicles by Nanoparticles Tracking Analysis, Cryo-Electron Microscopy, and Raman Tweezers Microspectroscopy. *J. Extracell. Vesicles* **2012**, *1*.

(129) Krafft, C.; Wilhelm, K.; Eremin, A.; Nestel, S.; von Bubnoff, N.; Schultze-Seemann, W.; Popp, J.; Nazarenko, I. A Specific Spectral Signature of Serum and Plasma-Derived Extracellular Vesicles for Cancer Screening. *Nanomedicine Nanotechnol. Biol. Med.* **2017**, *13* (3), 835–841.

(130) Carney, R. P.; Hazari, S.; Colquhoun, M.; Tran, D.; Hwang, B.; Mulligan, M. S.; Bryers, J. D.; Girda, E.; Leiserowitz, G. S.; Smith, Z. J.; et al. Multispectral Optical Tweezers for Biochemical Fingerprinting of CD9-Positive Exosome Subpopulations. *Anal. Chem.* **2017**, *89* (10), 5357–5363.

(131) Smith, Z. J.; Lee, C.; Rojalin, T.; Carney, R. P.; Hazari, S.; Knudson, A.; Lam, K.; Saari, H.; Ibañez, E. L.; Viitala, T.; et al. Single Exosome Study Reveals Subpopulations Distributed among Cell Lines with Variability Related to Membrane Content. *J. Extracell. Vesicles* **2015**, *4* (1), 28533.

CHAPTER 2

Detection and Characterization of Different Brain-Derived Subpopulations of Plasma Exosomes by Surface Plasmon Resonance Imaging

Silvia Picciolini, Alice Gualerzi, Renzo Vanna, Andrea Sguassero, Furio Gramatica, Marzia Bedoni, Massimo Masserini, Carlo Morasso

Analytical Chemistry, 2018; 90(15):8873-8880
Doi: 10.1021/acs.analchem.8b00941

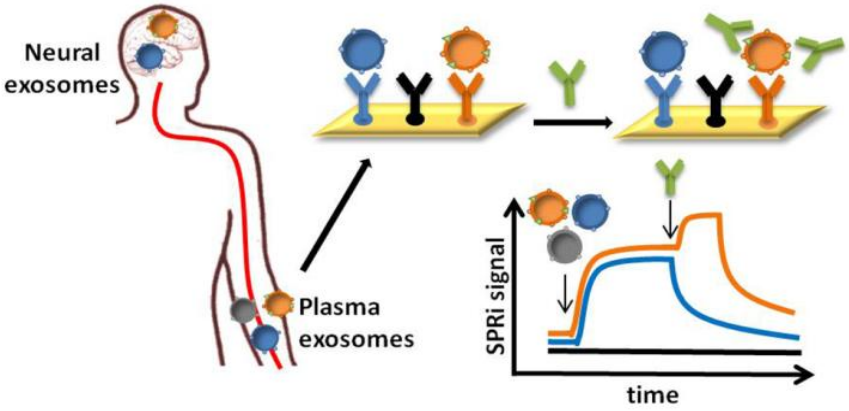

Abstract

The use of exosomes for diagnostic and disease monitoring purposes is becoming particularly appealing in biomedical research because of the possibility to study directly in biological fluids some of the features related to the organs from which exosomes originate. A paradigmatic example are brain-derived exosomes that can be found in plasma and used as a direct read-out of the status of the central nervous system (CNS). Inspired by recent remarkable development of plasmonic biosensors, we have designed a surface plasmon resonance imaging (SPRi) assay that, taking advantage of the fact that exosome size perfectly fits within the surface plasmon wave depth, allows the detection of multiple exosome subpopulations of neural origin directly in blood. By use of an array of antibodies, exosomes derived from neurons and oligodendrocytes were isolated and detected with good sensitivity. Subsequently, by injecting a second antibody on the immobilized vesicles, we were able to quantify the amount of CD81 and GM1, membrane components of exosomes, on each subpopulation. In this way, we have been able to demonstrate that they are not homogeneously expressed but exhibit a variable abundance according to the exosome cellular origin. These results confirm the extreme variability of exosome composition and demonstrate how SPRi can provide an effective tool for their characterization. Besides, our work paves the road toward more precise clinical studies on the use of exosomes as potential biomarkers of neurodegenerative diseases.

2.1 Introduction

Exosomes (EXOs) are a group of secreted membrane vesicles characterized by nanoscale dimensions and a complex chemical composition made up of proteins, lipids, and nucleic acids.[1,2] While all EXOs share a common set of components, their biochemical composition is strongly dependent on the cell or tissue of origin and on its physiopathological condition.[3,4]

First studied because of their role in paracrine intercellular communication, they were then proven to be involved in the communication between tissues and organs thanks to body fluid transportation.[5,6] Evidence about their involvement in several pathologies (i.e., cancer[7,8] and neurodegenerative[9−11] and inflammatory diseases[12]) and physiological adaptive mechanisms like tissue regeneration[13,14] has led to the hypothesis that EXOs might also play an active role in the propagation or resolution of a specific disease.

One of the most exiting findings about EXOs is that they were demonstrated to cross most biological barriers, including the blood−brain barrier (BBB).[15] This latter observation has recently opened new research challenges in the rapidly expanding field of drug delivery across the BBB and of the elusive biochemical processes occurring within the central nervous system (CNS).[16−18] The study of proteins and lipids present on EXOs derived from CNS and traveling in the bloodstream is a promising approach for the discovery of much needed biomarkers of neurodegeneration in Alzheimer's disease (AD), Parkinson's disease (PD), and multiple sclerosis (MS). In particular, EXOs have been found associated with pathogenic proteins like α-synuclein and β-amyloid (Aβ) in PD and AD, respectively.[19,20]

Fiandaca et al. reported that the concentration of Aβ peptides associated with EXOs in the blood of AD patients is statistically different when compared with a cohort of healthy subjects,[21] whereas glial EXOs were proposed as mediators of neuroinflammation in MS.[22] On the other hand, promising results obtained from in vitro and in vivo experiments, have faced difficulties once applied to human samples because of a lack of standardized preanalytical procedures and reproducible methodologies.[23] The heterogeneity of the experimental settings together with the laborious and various proposed procedures for EXO isolation introduce great variability, making our current knowledge about EXOs still incomplete.[24]

Recent studies have shown the success of using plasmonic biosensors for the detection of EXOs from biological samples. In particular, surface plasmon resonance imaging (SPRi) is a surface based technique that allows one to monitor, in real time and without the need for any label, variations in the molecular mass adsorbed on top of a gold layer, thanks to an evanescent wave that propagates for about 200 nm from the gold surface. As this range closely matches the dimension of EXOs, SPRi seems the ideal approach to study this target.

SPRi has been previously presented as an effective method for the label-free profiling of the main membrane proteins of EXOs.[25,26] Commercially available SPR instruments were used to profile EXOs in breast cancer or in multiple myeloma.[27,28] In addition, in a landmark paper from Im and co-workers, a homemade SPRi chip was used for the study of EXOs related to ovarian cancer.[29] However, except for a recent study focused on coronary heart disease,[30] most SPR-based

research studies are aimed at the characterization of EXOs related to cancer, whereas to the best of our knowledge no study has been published about the use of SPRi for the detection and characterization of brain-derived EXOs.

Nevertheless, in previous studies EXOs were considered as a single population, while as already noticed, they are a very heterogeneous group of vesicles. In clinical samples (i.e., plasma or urine), this diversity is pushed to its limit, because EXOs released by the different tissues and cell types are collected and mixed together. In order to find robust vesicle associated biomarkers in clinical samples, it is thus necessary to purify tissue-specific EXOs according to the presence of validated protein markers. Thanks to its multiplexing capabilities, SPRi seems particularly well suited for this task. An SPRi chip can be spotted at separate positions with antibodies (Abs) specific for the subtypes of interest allowing the simultaneous detection of multiple subpopulations of EXOs and avoiding the use of immunoaffinity beads that are difficult to removed and could interfere with the subsequent analysis. Moreover, in this study, we demonstrate that it is also possible to study the amount of a specific protein or lipid present on the membrane of each subpopulation by injecting a second Ab. As SPRi is not only able to separate the different EXOs but also to quantify the adsorbed amount, the results are more reliable than those obtained with other approaches: it is possible to use the value relative to the EXO detection to normalize the final result avoiding uncertainties due to the amount of extracted EXOs (a task notoriously difficult and characterized by low reproducibility).[31,32]

In the present work, we focused our attention on circulating EXOs derived from the cells of the CNS, which can provide an overview of the physiopathological condition related to the CNS directly from an easily accessible fluid. EXOs were initially prepurified from human plasma samples by using size exclusion chromatography (SEC) columns. This approach is much more rapid and easily applicable to clinical practice compared with ultracentrifugation.33−35 An array of Abs was then used to separate the subpopulations of vesicles of different neural origin on distinct positions of the chip surface. Abs targeting markers of neuronal and glial EXOs were used, as well as Abs targeting markers considered widespread on EXOs and thus commonly used as general references. The relative amount of CD81 and GM1 was subsequently measured on the membrane of immobilized EXOs, providing evidence of their heterogeneous distribution. The robustness of the whole protocol was then tested by the analysis of a small number of plasma samples from healthy volunteers demonstrating the overall feasibility of this approach for further clinical studies.

2.2 Experimental section

We have submitted all relevant data of our experiments to the EV-TRACK knowledgebase (EV-TRACK ID: EV180004).[36]

Sample Collection. Human peripheral blood was collected from five healthy volunteers in EDTA-treated tubes (BD Vacutainer, Becton Dickinson). Subjects (<40 years old, 3 females and 2 males) were enrolled at IRCCS Fondazione Don Carlo Gnocchi Onlus, after approval by the institutional Ethics Committee. Written informed consent was obtained from the volunteers in accordance with the ethical principles of the Declaration of Helsinki. All of the samples were anonymized, and no information or image could lead to identification of a study participant. Plasma was obtained after a 10 min centrifugation at 1300g for removing cells and a second 10 min centrifugation at 1800g for the depletion of platelets. Plasma samples were apportioned in aliquots and stored at −80 °C until further use.

Exosome Extraction and Characterization. EXOs were isolated from plasma by SEC using qEV Columns (IZON, qEVoriginal) following the manufacturer's instructions (see Supporting Information for further details). To verify the isolation yield and repeatability of the qEV columns, protein absorbance at 280 nm and total protein content were measured. Morphology, physical, and molecular characterization were performed as described in the Supporting Information.

SPRi Chip Preparation. In SPRi chip preparation and experiments, all reagents were purchased from Merck KGaA (Darmstadt, Germany)

and used without any further purification, if not stated otherwise. SPRi bare gold chips were purchased from Horiba Scientific SAS (SPRi-Biochip, Palaiseau, France). An array of Abs was conjugated on top of the SPRi gold chips by using an SPRi-arrayer (Horiba Scientific SAS).

Prior to the Ab conjugation, the chip surface was cleaned with piranha solution and rinsed with ultrapure water and ethanol. The surface was then coated with a self-assembled monolayer (SAM) using ethanolic solutions of thiolated PEG molecules (ProChimia Surfaces). The SAM was obtained by using a mixture of HS-C11-EG2-OH (TH 001-m11.n2) and HS-C11-EG6-COOH (TH 003-m11.n6) in specific percentages (see Results and Discussion). After 24 h of incubation in the ethanolic solution of PEGs, the chip was washed with ethanol, and the carboxylic groups were activated by incubation with an aqueous solution of EDC 0.2 M and NHS 0.05 M for 15 min.

The spotting procedure for the immobilization of the Abs was done at about 70% relative humidity at room temperature with a capillary pin of 0.7 mm spot diameter. The pin was automatically washed with 5 wash cycles of ethanol 10% and air-dried after each spotting step. Each Ab family was represented by four spots, with 0.9 mm distance between spots; 6 families of Abs were spotted on the same chip with the anti-rat IgG used as negative control (Table 1). The blocking of the chip was done by dipping the surface in a solution of ethanolamine 1 M, pH 9, for 30 min. Finally, the chip was washed with water, and if not immediately used in SPRi instrument, it was stored at 4 °C with a layer of StabilCoat Immunoassay stabilizer for the preservation of the activity.

Antibody	Manufacturer	Clone	pH for spotting
Anti-CD9	Affymetrix	eBioSN4(SN4 C3-3A2)	5.0
Anti-CD81	R&D	454720	7.4
Anti-CD171	Affymetrix	eBio5G3 (5G3)	7.4
Anti-ephrinB	HansaBioMed	Polyclonal	7.4
Anti-PLP1	HansaBioMed	Polyclonal	7.4
Anti-rat IgG	Biolegend	MRG1-58	7.2
Anti alpha Lactalbumin	GeneTex	GTX77275	7.4

Table 1. Details about antibodies used for the SPRi array

SPRi Measurements and Data Analysis. SPRi measurements were performed using XelPleX instrument (Horiba Scientific SAS). Before every experiment, the instrument was calibrated with the injection of 200 µL of sucrose (3 mg/mL) at 50 µL/min flow rate. Experiments were performed using HBS-ET as running buffer (1.5 M NaCl, 100 mM HEPES, 30 mM EDTA, Tween 0.5%, pH 7.4). To test the functionality of the chip, the specific interaction between α-lactalbumin and its Ab was assessed before each EXO study.

EXO aliquots of 500 µL were then injected in the SPRi flow chamber with a flow rate of 10 µL/min and by adding one recycling step (i.e., additional and consecutive injection of the same injected volume in the flow cell). Finally, 200 µL of 200 nM solution of secondary Abs (anti-CD81 and anti-ganglioside GM1, AbCam), were injected at 25

μL/min (with 2 recycling steps) to characterize the surface of the immobilized EXOs. The SPRi signals of each injection were collected and analyzed by using EzSuite software and OriginLab. Sensorgrams were corrected by subtracting the signal related to anti-rat IgG Abs spotted in parallel on the surface.

2.3 Results and discussion

Isolation and Characterization of Exosomes. Human EXOs were preisolated from plasma to reduce the risk of protein complex formation and vesicle aggregation during SPRi experiments. Among the different approaches that could be used for the isolation of EXOs, SEC was chosen to obtain vesicles in a rapid and reproducible way from a limited amount of plasma (500 μL). Moreover, this approach avoids the use of purification reagents (i.e., PEGs or other polymers) present in the most common extraction kits thus limiting contaminations or artifacts.[37,38] Thanks to this approach, we managed to reduce the sample preparation time to about 30 min, a time that is compatible with the clinical workflow. On the other hand, the main limitations of SEC approaches can be the copurification of a small amount of free proteins in the sample and the relatively low yield. The first limitation is here negligible due to the specificity of the SPRi Ab-based approach for the recognition and immobilization of EXOs. On the contrary, the selection of just a small portion of the total number of plasma EXOs could introduce a sampling issue in the analysis that would result in inaccurate biological results. SEC fractions were analyzed by UV−vis spectroscopy and BCA assay in order to select the largest and cleanest possible amount of EXOs from the clinical samples. According to the results of these experiments (Figure S-1A,B,C), fractions from 7 to 11 were selected and used for the following EXO characterization steps and SPRi analyses.

EXOs were characterized according to ISEV guidelines for the minimal experimental requirements for definition of extracellular vesicles.[39] TEM images acquired on the fractions of our interest

confirmed the presence of vesicles with EXO typical morphology and size range (Figure 1A). Dimensions and concentration of the purified EXOs were tested by nanoparticle tracking analysis (NanoSight). Results were in accordance with previous reports from literature with a mean size of about 150 nm and a concentration of approximately 1.5 × 10^9 particles/mL (Figure 1B).[40,41] Western blot analysis was used to demonstrate the presence of some of the main markers of EXOs such as flotillin-1 and CD81 in our samples (Figure 1C).

Moreover, the purity of EXOs was determined by using a recently developed nanoplasmonic assay based on the use of gold nanoparticles.[42] Our results (Figure S-2) confirmed that plasmatic EXOs obtained by SEC are almost as pure as the commercially available ones that were used as reference, with an aggregation index AI% (AI = A520/A650) of 13.1% (calculated with regard to the peak of water dispersed nanoparticles), which is indicative of a good level of purity of the sample.

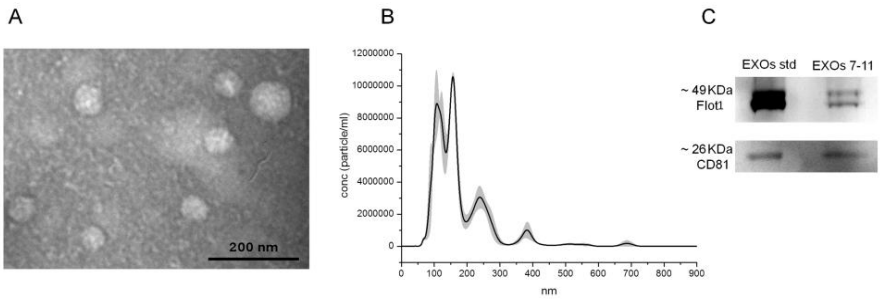

Figure 1. EXO characterization by transmission electron microscopy (TEM), Nanoparticle tracking analysis (NTA), and Western blot. (A) TEM image of EXOs collected from fractions 7 to 11 in PBS. Bar = 200 nm; (B) size distribution of EXOs as measured by NTA (mean size = 150 nm); (C) immunoblotting with Abs against exosomal proteins flotillin-1 (Flot 1) and CD81. EXOs purchased from HansaBioMed (EXO std) were used as positive control.

Surface Chemistry and Antibody Conjugation. The reliable detection of EXOs by SPRi is subsequent to the careful preparation of an appropriate surface chemistry that makes it possible (i) to stably immobilize active Abs in a repeatable way on the surface and (ii) to reduce the unspecific binding of the vesicles on the gold layer. A mixed layer of PEG molecules was used to cover the gold surface. Thence, to find the best Ab conjugation protocol, the anti-CD171 Ab was immobilized on the chip surface by different approaches: (1) streptavidin conjugation by using biotinylated anti-CD171; (2) protein-A oriented conjugation; (3) EDC/NHS coupling. As summarized in Figure 2A, the EDC/NHS coupling gave the best results.

The streptavidin-based approach produced scarce signal and unspecific adsorption of EXOs on the chip. Both EDC coupling and protein-A approaches are characterized by good specificity, but EDC coupling provides higher SPRi signal, probably due to a higher amount of Ab on the surface, as suggested by the difference shown in the plasmonic curves after the spotting procedures (Figure S-3).

Once EDC/NHS coupling was chosen, other parameters such as the density and the length of the carboxylated PEGs in the mixed monolayers were tested. We found that the signal increased with the density of the carboxylated PEG used, from 5% to 20% (Figure 2B). The use of a long carboxylated PEG, in contrast, affects negatively the performance of the assay (Figure 2C). To prepare the array of Abs targeting general exosomal makers (anti-CD9 and anti-CD81) as well as markers of EXOs released by cell types present in the CNS (anti-CD171 and anti-ephrinB specific for neurons,[43−45] anti-PLP1 specific

for oligodendrocytes[46]), a screening of several clones was performed (data not shown), and we studied also the best pH to be used in the spotting procedure (Figure S-4). Table 1 summarizes the Abs that were finally selected for the study and the pH used for spotting.

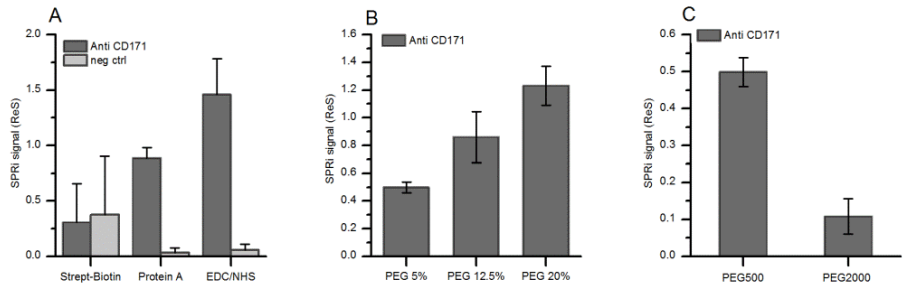

Figure 2. Intensities of SPRi signals at the end of EXO injection (340 µL of 15 µg/mL protein content, 10 µL/min) measured for the anti-CD171 family (A) on different SPRi chips prepared with streptavidin−biotin chemistry, protein A chemistry, or direct conjugation, which is here called EDC/NHS, using 20% of the carboxylated PEG of MW 500 (error bars indicate standard deviation of 2 chips for each strategy adopted), (B) on three different SPRi chips prepared with direct conjugation using 5%, 12.5%, or 20% of the carboxylated PEG of MW 500 (error bars indicate standard deviation of four spots on the same chip) and (C) on 2 different SPRi chips prepared with direct conjugation using carboxylated PEG of MW 500 (PEG500) or MW 2000 (PEG2000) both at 5% (the error bars indicate standard deviation of four spots on the same chip).

Specific Detection of Multiple Subpopulations of Plasma Exosomes. EXOs extracted from plasma contain a mixture of vesicles coming from virtually any cell present in the organism. The SPRi chip was used to simultaneously detect multiple subpopulations of EXOs dispersed in plasma with a special focus on the vesicles released by the CNS. Before the injection, EXOs were diluted in HSB-ET buffer used as running buffer in all experiments. Sensorgrams reported in Figure 3 show the signals related to the adsorption of EXOs in

correspondence to three Abs chosen to select different membrane biomarkers (anti-CD9, anti-CD171, and anti-CD81). In contrast, no signal comes from the respective negative controls, as demonstrated also by the corresponding chip CCD differential images. Differences in the signals are related to the amount of EXOs in the sample but also to the association and dissociation rates of the selected Abs and to their density on the chip surface.

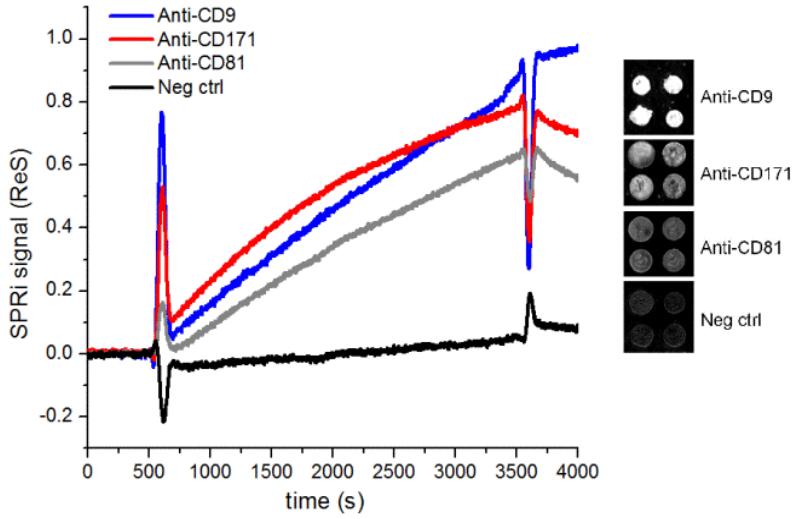

Figure 3. SPRi sensorgram of injection of 500 µL of EXOs (15 µg/mL of total protein content) at 10 µL/min with 1 recycling step. The signal of each family is the average of four spots after the subtraction of the signals from a family of negative control (IgG) spotted in parallel on the same chip. The SPRi signal on a second family of the same IgG is shown in black. The CCD differential image (reflectivity variation) of the SPRi chip acquired during the EXO detection phase at equilibrium is shown beside the sensorgram.

The sensitivity of the assay was tested by injecting progressively increasing concentrations of EXOs diluted in running buffer. The resulting calibration curve shown in Figure 4A demonstrates a

detection limit of around 1 μg/mL of the total amount of protein measured by BCA assay, which is in line with the best ELISA based approaches available on the market.[47] While it is not immediately possible to translate the sensitivity of this kind of assay to the amount of the target protein, it is worth noting that the detection of molecules present on EXO membranes can be achieved thanks to the enhancement of the signal due to the relative high molecular weight of the whole vesicles. In fact, SPRi signals are proportional to the adsorbed amount of material during the measurement; the EXO membrane effectively increases the local molecular mass adsorbed on the chip. This means that the presence of unbound proteins contaminating the sample does not affect the analysis, as their molecular mass is vastly lower. This intrinsic enhancing mechanism gives SPRi a higher specificity in the detection of EXOs toward other immune based approaches.

To demonstrate that the signal observed was due to the detection of EXOs and not of solubilized membrane molecules, we injected a sample of lysed EXOs, prepared as for the immunoblotting experiments, where their typical structure was destroyed. Figure 4B shows the intensity of the signal collected on the anti-CD9 spots after the injection of either the lysed or the intact vesicles. This demonstrates that proteins alone are not able to produce a relevant SPRi signal.

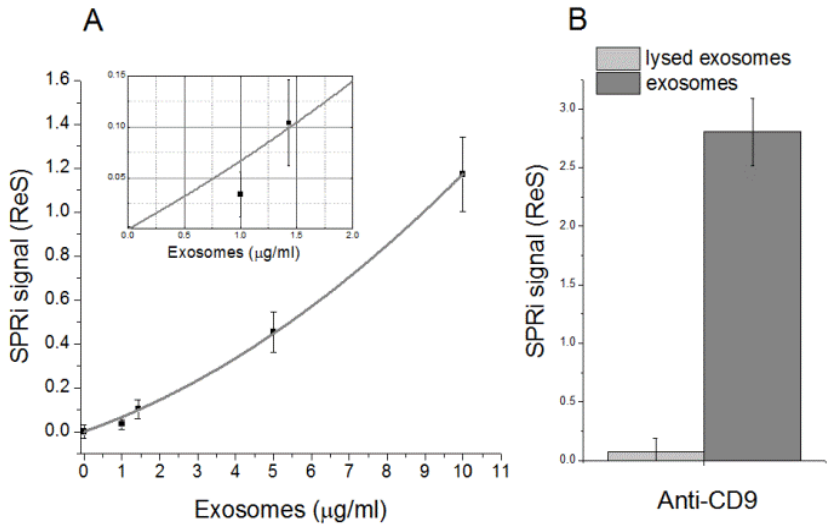

Figure 4. (A) Calibration curve obtained by injecting different amounts of EXOs. The SPRi signal corresponds to the signal related to anti-CD9 Abs corrected using the signal related to the negative control. The amount expressed in µg/mL is the total protein content measure by BCA assay. (B) Comparison between the intensities of SPRi signal after the injection of lysed EXOs and the injection of intact EXOs, collected on anti-CD9 Abs. Error bars indicate standard deviations of four spots on the same chip.

Multiplexing Identification of Membrane Specific Molecules on CNS-Derived Exosomes. The label-free detection of EXOs by SPRi allows the use of a single Ab conjugated on the surface of the chip and does not require the typical sandwich configuration of other ELISA assays. This feature leaves much of the surface of vesicles available for their further characterization. Hence, the relative abundance of a membrane component can be simultaneously evaluated on different EXO subpopulations taking into account the amount of captured EXOs on the different positions of the chip.

To confirm that what stops on spotted Abs after the injection of SEC eluted fractions were EXOs and to verify the possibility to

characterize them once immobilized on the chip with a second Ab, we injected an unconjugated monoclonal Ab specific for a typical exosomal transmembrane marker, CD81. The spots where EXOs were supposed to be present revealed a further increase in the SPRi signal.

Figure 5 shows the adsorption of plasma EXOs onto anti-CD171 spotted on the chip surface and the consecutive interaction of injected anti-CD81 Ab on the membrane of immobilized vesicles. This result confirmed the feasibility of SPRi to study interactions between EXOs and other molecules thanks to vesicle dimensions (40−150 nm) that remain within the range scanned by the instrument. From the biological point of view, this graph confirmed that the materials absorbed on the anti-CD171 Abs are EXOs as they carry the CD81 marker.

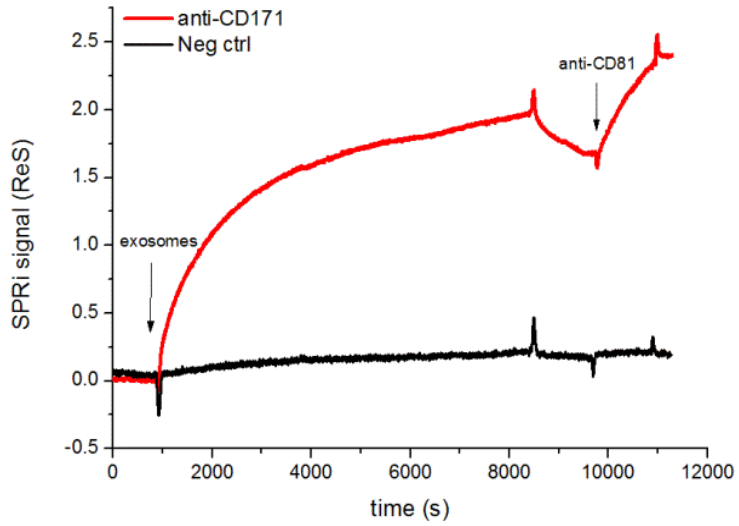

Figure 5. SPRi signal collected on anti-CD171 Ab during the injection of 500 µL of EXOs (20 µg/mL of total protein content at 10 µL/min) and 200 µL of anti-CD81 (200 nM at 25 µL/min). The signal is the average of four spots after the subtraction of the signals from the negative control (IgG) spotted in parallel on the same chip. The SPRi signal on another IgG is shown in black.

One of the main advantages of the SPRi-based biosensor is the opportunity to perform simultaneously the detection and characterization of multiple markers (and thus subpopulations of EXOs) vastly reducing the amount of sample and the time required for the analysis.

We thus evaluated the feasibility of performing a multiplexing experiment using an Ab-array specific for CNS related markers (CD171, EphrinB, PLP1). Our data demonstrate that the brain-derived EXO subpopulations circulating in the bloodstream, in particular those from neurons and oligodendrocytes, can be successfully isolated on distinct spots on the surface (Figure 6A). The specificity of the biomarkers chosen to detect the neural EXOs was verified by injecting the corresponding Abs after the EXO suspension and analyzing the SPRi signals related to the possible interaction of the injected antibodies with the EXOs adsorbed on the chip (Figure S-5). In addition, we were able to further characterize immobilized vesicles by means of the injection of an Ab targeting CD81 and of an Ab against ganglioside GM1, performed in sequence. Figure S-6 shows the sensorgrams of this experiment for each Ab family analyzed. As expected, SPRi was able to quantify the relative amounts of CD81 and GM1 showing that EXOs have a different composition according to their cellular origin (Figure 6B,D). Moreover, the possibility to quantify the amount of EXOs captured on the surface also allows a normalization of the data allowing a more precise profiling of the subpopulations (Figure 6C,E). For this purpose, the signal related to the injection of anti-CD81 or anti-GM1 is divided by the signal

intensity related to the amount of EXOs previously immobilized on the surface (Figure S-6), allowing comparison of all subpopulations.

Our multiplexing approach allowed analysis of the relative presence of CD81 on each family of EXOs detected. Interestingly, even if CD81 is commonly considered a general marker of EXOs, we demonstrated that it is not homogeneously expressed in CD9, CD171, PLP1, and ephrinB positive vesicles, as shown in Figure 6C. EXOs expressing CD171 are richer in CD81 on their membranes than CD9-positive vesicles. Indeed, although some proteins were conventionally identified as useful general markers for EXO definition, recent studies have exposed the fact that these markers can exhibit diverse abundance according to their originating cell type.[48]

Similarly, our results showed that GM1 was more abundant on the membrane of CD171 and PLP1 positive EXOs, reflecting their neuronal and oligodendrocyte origin, respectively. More precisely, normalized data clearly show that PLP1 positive EXOs are richer in the amount of ganglioside GM1 in comparison with the generic EXOs (CD9 positive) and also with the neuronal ones selected with anti-CD171 and antiephrinB (Figure 6E). Although both anti-CD171 and anti-ephrinB were chosen for the selection of neuronal EXOs, our SPRi array was not able to capture a relevant amount of ephrinB-positive EXOs, as is visible also in Figure S-6. Our data are in line with the current controversy about a valid and shared marker for neuronal EXOs.[43] Indeed, several studies have addressed the aim of identifying a robust marker for EXOs released by neurons; still no consensus has been found. CD171 is one of the most commonly used neuronal markers for EXOs, studied in both in vitro and in vivo

studies like those devoted to the investigation of AD, PD, and MS pathogenesis. [21,43,49] However, its concomitant expression on the membrane of cells from other organs (i.e., kidney,[50] immune system,[51,52] and epithelial cells of the urogenital tract and intestine[51]) might explain its higher binding to EXOs in our SPRi approach compared to ephrinB. In contrast, the latter is a neuronal marker expressed on the membranes of excitatory or inhibitory neurons in the neocortex able to regulate cell migration,[53] and its higher specificity may account for the smaller proportion of ephrinB-positive EXOs detected on the SPRi array compared to CD171 positive ones.

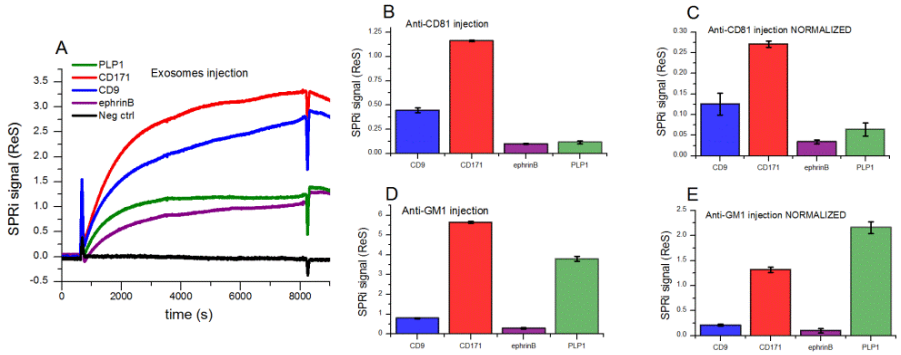

Figure 6. (A) Sensorgram related to the injection of 500 µL of EXOs (20 µg/mL of total protein content) at 10 µL/min on a SPRi chip with spots of anti-PLP1 (marker of oligodendrocytes), anti-CD171 and anti-ephrinB (neuronal markers), and anti-CD9 (marker of generic EXOs). Each curve represents the average of four spots after the subtraction of the signals from a family of negative control (IgG) spotted in parallel on the same chip. The SPRi signal on a second family of the same IgG is shown in black. (B, C) Intensity of SPRi signal after the injection of anti-CD81 (200 µL, 25 µL/min) before and after being normalized for the amount of EXOs detected on each family of Ab. (D, E) Intensity of SPRi signal after the injection of anti-GM1 before and after being normalized for the amount of EXOs detected on each family of Ab. The values of intensities were calculated by performing a linear or polynomial fitting of the curves in order to consider the dissociation rate of each interaction. Error bars indicate standard deviations of four spots on the same chip.

Beyond this, our data related to the other spotted Abs are in agreement with the well-known presence of the phospholipid family of glycosphingolipids in neuronal and glial membranes, which have been proposed to have a biological role in the pathogenesis of neurodegenerative diseases. For example, GM1 was shown to favor the aggregation of Aβ in AD.[54,55] In particular GM1 was the first ganglioside to be found directly and tightly bound to Aβ peptides[56] and from that discovery on, several studies confirmed the involvement of GM1 in Aβ aggregation.[57] In the study of the pathogenesis of PD, gangliosides were found to be able to accelerate the process of α-synuclein aggregation in neurons contributing to the spread of the disease.[19] Moreover, in MS lesions the ganglioside expression on oligodendrocytes and in general on glial cell subpopulations is higher than in normal CNS, showing their involvement in this demyelinating disease.[58]

Repeatability of the SPRi Approach on Exosomes from Different Plasma Samples. In order to evaluate the efficacy of the SPRi biosensor for EXO detection and characterization and the potential for use in clinical studies, we tested the repeatability of our method by analyzing vesicles extracted from five young healthy subjects with five distinct SPRi chips prepared in the same way. The analysis of this little and homogeneous cohort was intended to verify the efficacy of the proposed method, from the preparation of the sample to the data analysis, and the possibility to detect all the EXO subfamilies in all of the samples. We determined that the normalized intensities of the SPRi signals related to the injections of anti-CD81 and anti-GM1 are

in the same order of magnitude for all of the subjects (Figure 7). Our experiments confirm that EXOs can be detected and characterized by a SPRi approach, creating solid foundations for a following comparative analysis between healthy donors and selected patients.

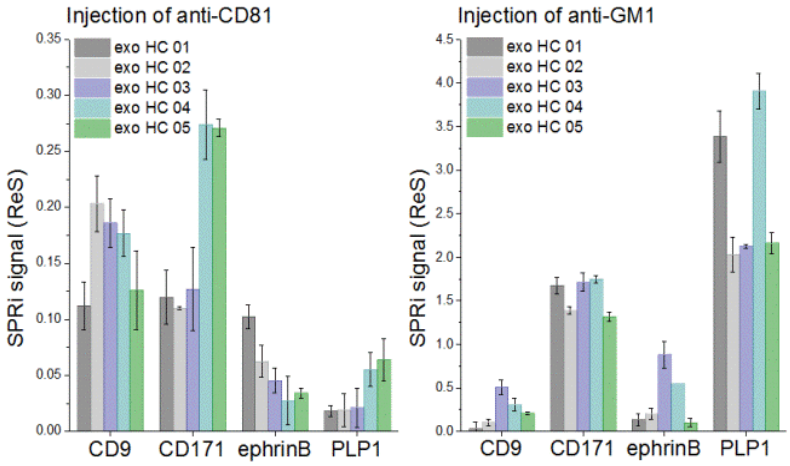

Figure 7. SPRi intensities related to the injections of 200 µL of anti-CD81 and 200 µL of anti-GM1 in sequence (normalized for the amount of EXOs previously detected on the chip) for EXOs derived from blood plasma of five healthy subjects. Error bars indicate standard deviations of four spots on the same chip.

2.4 Conclusion

In this work, we developed an Ab-array based on SPRi for the isolation and in situ characterization of multiple EXO subpopulations of neural origin directly from plasma. We demonstrated that this label-free technology is a suitable method for clinical studies, as it can precisely quantify multiple membrane components of EXOs starting from a limited amount of human plasma (500 μL) and by using commercially available reagents and instrumentation. The array preparation was optimized for the identification of circulating EXOs released from neurons and oligodendrocytes, reaching a level of sensitivity and specificity matching the traditionally used ELISA method but with the inherent possibility to simultaneously analyze multiple subpopulations.

The herein reported SPRi-based biosensor represents an innovative and practical approach that allows the assessment of different amounts of specific membrane markers by simply injecting the Abs of interest in sequence on multiple EXO subpopulations. Indeed, the discrimination and the characterization of different brain-derived EXOs directly from human plasma represent an important step toward the use of circulating EXOs for the noninvasive diagnosis and monitoring of neurodegenerative and other CNS diseases. Considering that the SPRi assay could be created by spotting all kinds of Abs, this approach can be optimized and adapted for the characterization of EXOs derived from other somatic cell types, including astrocytes and microglia. Future studies will be focused on the analysis of other clinically relevant molecules present on or interacting with the EXO membranes that could be involved in specific pathological processes.

ASSOCIATED CONTENT

Supporting Information

The Supporting Information is available free of charge on the ACS Publications website at DOI: 10.1021/acs.analchem. 8b00941.

Experimental protocols used for EXO isolation and characterization by transmission electron microscopy, nanoparticle tracking analysis, and Western blot and by using the colorimetric test for EXO purity, measurements of total protein content of EXO fractions by absorbance at 280 nm and BCA assay, colorimetric test for EXO purity, plasmonic curves of SPRi chip after Ab conjugation, SPRi signals on Abs spotted at different pH, SPRi signal intensity for evaluation of the specificity of antibodies, and sensorgrams of the injections of EXOs, anti-CD81, and anti-GM1 in sequence.

ACKNOWLEDGMENTS

The work was supported by Italian Ministry of Health (Ricerca Corrente 2017, IRCCS Fondazione Don Carlo Gnocchi ONLUS).

2.5 Supporting Information

Abstract

In this supporting information we provide the description of the protocols of the EXOs isolation and characterization by Transmission Electron Microscopy, Nanoparticle Tracking Analysis, western blot and by using the colorimetric test for exosomes purity.

Then, we provide the data regarding the EXOs characterization in terms of the total protein content (absorbance at 280 nm and BCA assay, Figure S-1) and in terms of sample purity (by using the nanoplasmonic assay, Figure S-2). In these experiments we have to consider that during SEC isolation, proteins start being collected only after that most vesicles have already been eluted, since the EXOs elution under these experimental conditions occurs from fraction 7, as reported by Böing et al (J. Extracell. Vesicles, 2014). From these data we were able to select the largest and cleanest possible amount of EXOs from the clinical sample.

Moreover, we show the plasmonic curves of SPRi chips obtained after the immobilization of anti-CD171 antibody (Figure S-3) and the comparison between SPRi signals collected by using different pH for the solution of the antibodies to be spotted (Figure S-4); these are supporting data that we considered for the optimization of the preparation of the SPRi array of antibodies of our interest. We also verified a good level of specificity of anti-CD171 and anti-PLP1 antibodies as markers of CNS cell types (Figure S-5).

In the end, the whole sensograms related to the injections of exosomes, anti-CD81 and anti-GM1 in sequence are here reported for

each exosome subpopulations immobilized on the same SPRi chip (Figure S-6).

2.5.1 Experimental section

EXOs isolation and characterization:

EXOs isolation. Prior to isolating vesicles, plasma samples were thawed and centrifuged at 10,000g for 10 minutes at 4°C to remove any free-thaw aggregates. Subsequently, EXOs were isolated by SEC using qEV Columns (IZON, qEVoriginal) following the manufacturer's instructions. Briefly, columns were firstly rinsed with 10 ml of freshly prepared phosphate-buffered saline (PBS) solution filtered through a 0.22 µm filter. Afterwards, 500 µl of clarified plasma were loaded onto the column and PBS was added as the eluent. Twenty-three fractions of 500 µl were collected.

To verify the isolation yield and repeatability of the qEV columns, protein absorbance at 280 nm (NanoDrop 2000c, Thermo Scientific) was measured on all the collected fractions, and the total protein content was more precisely quantified for the fractions containing EXOs (from 7 to 11) by BCA protein assay kit (Pierce BCA assay kit, Thermo Scientific, Waltham, MA, USA).

Transmission electron microscopy (TEM). The morphology of the isolated vesicles was assessed by TEM analysis. 5 µl of freshly isolated EXOs were absorbed on Formvar carbon-coated grids for 10 minutes and then negatively stained with 2% uranyl acetate in aqueous suspension for 10 minutes. Filter paper was used to remove the excess of uranyl. After having dried the grids, the sample was analyzed with

a transmission electron microscope (Leo 812AB, Zeiss, Oberkochen, Germany) at 80 kV.

Nanoparticle Tracking Analysis (NTA). The size and concentration of the isolated EXOs were measured by Nanoparticle Tracking Analysis using a NanoSight NS300 Instrument (Malvern) with flow-cell top-plate. The sample solution was homogenized by vortexing and followed by serial dilutions to a final of 1:5,000. The analysis was conducted for 60 seconds in triplicate.

Western Blot. For immunoblotting experiments, the samples were lysed in RIPA buffer in the presence of protease inhibitors, sonicated in a water bath 3 times for 5 minutes and centrifuged for 20 minutes at 12,000g, following the protocol of Lässer et al (J. Vis. Exp. JoVE, 2012). Lysed EXOs were treated with SDS-PAGE Sample Prep Kit (Thermo Scientific) to remove eventual interfering chemicals. Proteins (15 µg per well) were separated by gel electrophoresis and transferred on a nitrocellulose membrane. Immunoblotting was performed at 4°C overnight using anti-flotillin-1 (BD Transduction Laboratories™, San Jose, CA, USA) and anti-CD81 (clone 1.3.3.22, Thermo Scientific) Abs. The secondary HRP conjugated Ab used was goat anti-mouse (Thermo Scientific). EXOs standards purchased by HansaBioMed (HBM-PES-100/4) were used as control in all experiments.

Colorimetric test of exosomes purity. The purity of the fractions containing EXOs was determined through a colorimetric nanoplasmonic assay developed by Maiolo and co-workers (Anal. Chem., 2015). Briefly, EXOs were incubated with gold spherical

nanoparticles (6 nM) for 30 minutes; the solution color changes and the calculated aggregation index (ratio between the LSPR absorption peak at 520 and 650 nm) are indicative of the purity level of the sample.

2.5.2 Figures

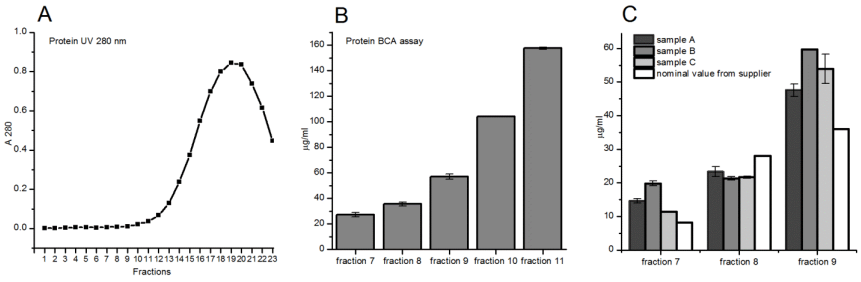

Figure S-1. (A) Absorbance at 280 nm of each fraction (from 1st to 23rd) collected by size-exclusion chromatography with an Izon qEV column. The volume of each fraction is about 500 µl. Results showed that the elution of contaminant proteins is slow and starts predominantly just after the 12-13th fraction. (B) Quantification of total protein content for fractions 7, 8, 9, 10 and 11 by using the BCA assay. Error bars indicate standard deviation of two different replicates. This accurate quantification showed that fractions 7 to 9 contain very little amount of proteins, with just a small increment in fractions 10 and 11 (Figure S-1B). (C) The reproducibility and the yield of the isolation were verified by the quantification of the total protein content measured by BCA assay of fractions 7, 8 and 9 obtained from three different plasma samples in comparison to the nominal value from the qEV column supplier (Figure S-1C).

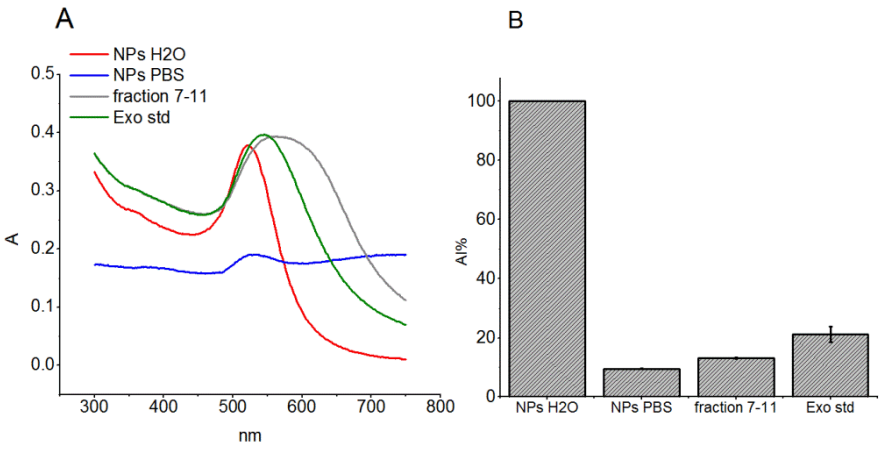

Figure S-2. Nanoplasmonic and colorimetric assay of fractions 7-11 and exosomes purchased from HansaBioMed (Exo std). (A) UV spectra of aqueous dispersion of nanoparticles 6nM (red), nanoparticles dispersed in 10 mM PBS (blue), nanoparticles with plasmatic exosomes obtained from SEC - fractions from 7 to 11 - (gray) and nanoparticles with exosomes from HansaBioMed (green). (B) Aggregation index (AI%) of each sample. Error bars indicate standard deviation of two different replicates.

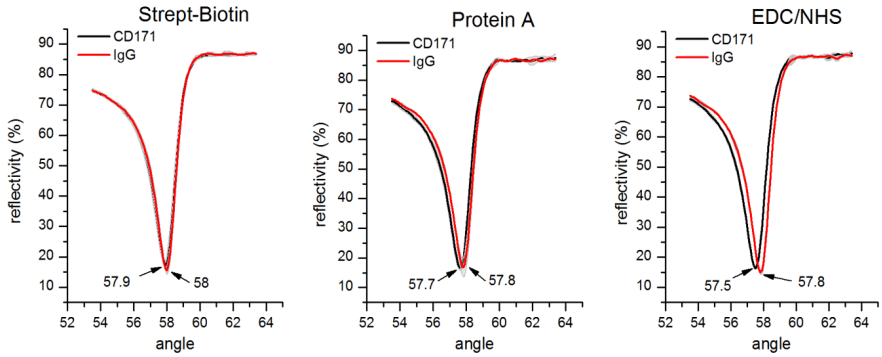

Figure S-3. Plasmonic curves related to the spots of anti CD171 and the negative control (IgG) conjugated on the chip by streptavidin-biotin chemistry, protein A and direct conjugation (EDC/NHS), just after the antibody immobilization. The bigger shift between the anti-CD171 spots and the negative control present in the EDC/NHS chip respect to the others is indicative of the higher amount of antibody immobilized on the surface.

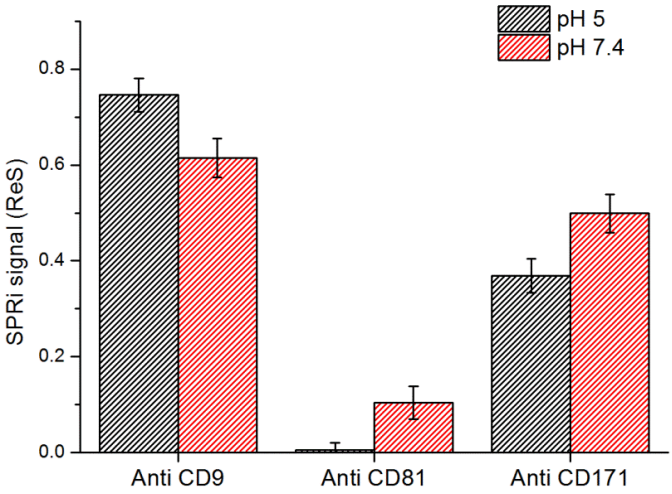

Figure S-4. Intensities of SPRi signals at the end of exosomes injection (340µl of 15 µg/ml protein content, 10µl/min) measured for the families of anti-CD9, anti-CD81 and anti-CD171 spotted on the surface with different pH: pH 5 or 7.4 (error bars indicate standard deviation of four spots on the same chip).

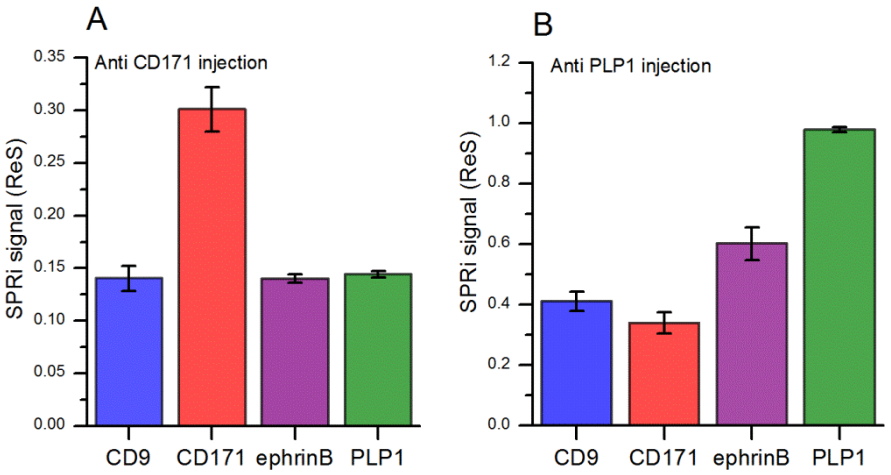

Figure S-5. SPRi intensities related to the injections of 200 µl of anti-CD171 (A) and 200 µl anti-PLP1 (B) in sequence, normalized for the amount of EXOs previously detected on the chip according to the expression on their membranes of CD9, CD171, ephrinB and PLP1. Anti-CD171 and Anti-PLP1 interact with a good specificity with CD171-positive exosomes and PLP1-positive exosomes, respectively. Error bars indicate standard deviations of four spots on the same chip.

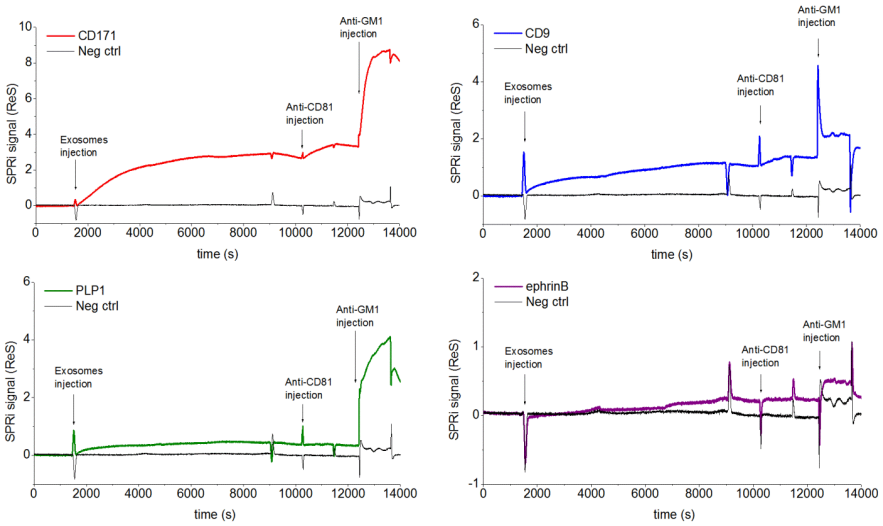

Figure S-6. Sensograms of the injection of 20 µg/ml of exosomes (500 µl), anti-CD81 (200 µl) and anti-GM1 (200 µl) in sequence on a SPRi chip with four different families of antibodies able to recognize exosomes from a specific cellular origin. The signal of each family is the average of four spots after the subtraction of the signals from the negative control (IgG) spotted in parallel on the same chip. The SPRi signal on a second family of the same IgG is shown in black.

2.6 References

(1) Théry, C.; Zitvogel, L.; Amigorena, S. Nat. Rev. Immunol. 2002, 2, 569−579.

(2) Raposo, G.; Stoorvogel, W. J. Cell Biol. 2013, 200, 373−383.

(3) Willms, E.; Johansson, H. J.; Mäger, I.; Lee, Y.; Blomberg, K. E. M.; Sadik, M.; Alaarg, A.; Smith, C. I. E.; Lehtiö, J.; El Andaloussi, S.; Wood, M. J.; Vader, P. Sci. Rep. 2016, 6, 22519.

(4) Gualerzi, A.; Niada, S.; Giannasi, C.; Picciolini, S.; Morasso, C.; Vanna, R.; Rossella, V.; Masserini, M.; Bedoni, M.; Ciceri, F.; Bernardo, M. E.; Brini, A. T.; Gramatica, F. Sci. Rep. 2017, 7, 9820.

(5) Camussi, G.; Deregibus, M. C.; Bruno, S.; Cantaluppi, V.; Biancone, L. Kidney Int. 2010, 78, 838−848.

(6) Tkach, M.; Théry, C. Cell 2016, 164, 1226−1232.

(7) Yang, C.; Robbins, P. D. Clin. Dev. Immunol. 2011, 2011, 842849.

(8) Tickner, J. A.; Urquhart, A. J.; Stephenson, S.-A.; Richard, D. J.; O'Byrne, K. J. Front. Oncol. 2014, 4, 127.

(9) Quek, C.; Hill, A. F. Biochem. Biophys. Res. Commun. 2017, 483, 1178−1186.

(10) Lim, Y.-J.; Lee, S.-J. Acta Neuropathol. Commun. 2017, 5, 64.

(11) Soria, F. N.; Pampliega, O.; Bourdenx, M.; Meissner, W. G.; Bezard, E.; Dehay, B. Front. Neurosci. 2017, 11, 26.

(12) György, B.; Szabó, T. G.; Pásztói, M.; Pál, Z.; Misják, P.; Aradi, B.; László, V.; Pállinger, E.; Pap, E.; Kittel, A.; Nagy, G.; Falus, A.; Buzás, E. I. Cell. Mol. Life Sci. 2011, 68, 2667−2688.

(13) Cobelli, N. J.; Leong, D. J.; Sun, H. B. Ann. N. Y. Acad. Sci. 2017, 1410, 57−67.

(14) Zhang, S.; Chuah, S. J.; Lai, R. C.; Hui, J. H. P.; Lim, S. K.; Toh, W. S. Biomaterials 2018, 156, 16−27.

(15) Ha, D.; Yang, N.; Nadithe, V. Acta Pharm. Sin. B 2016, 6, 287−296.

(16) Jarmalavičiūtė, A.; Pivoriūnas, A. Pharmacol. Res. 2016, 113, 816−822.

(17) García-Romero, N.; Carrión-Navarro, J.; Esteban-Rubio, S.; Lázaro-Ibáñez, E.; Peris-Celda, M.; Alonso, M. M.; Guzmán-De-Villoria, J.; Fernández-Carballal, C.; de Mendivil, A. O.; García- Duque, S.; Escobedo-Lucea, C.; Prat-Acín, R.; Belda-Iniesta, C.; Ayuso-Sacido, A. Oncotarget 2017, 8, 1416−1428.

(18) Aryani, A.; Denecke, B. Mol. Neurobiol. 2016, 53, 818−834.

(19) Grey, M.; Dunning, C. J.; Gaspar, R.; Grey, C.; Brundin, P.; Sparr, E.; Linse, S. J. Biol. Chem. 2015, 290, 2969−2982.

(20) Rajendran, L.; Honsho, M.; Zahn, T. R.; Keller, P.; Geiger, K. D.; Verkade, P.; Simons, K. Proc. Natl. Acad. Sci. U. S. A. 2006, 103, 11172−11177.

(21) Fiandaca, M. S.; Kapogiannis, D.; Mapstone, M.; Boxer, A.; Eitan, E.; Schwartz, J. B.; Abner, E. L.; Petersen, R. C.; Federoff, H. J.; Miller, B. L.; Goetzl, E. J. Alzheimer's Dementia 2015, 11, 600−607.e1.

(22) Sáenz-Cuesta, M.; Osorio-Querejeta, I.; Otaegui, D. Front. Cell. Neurosci. 2014, 8, 100.

(23) Witwer, K. W.; Buzás, E. I.; Bemis, L. T.; Bora, A.; Lässer, C.; Lötvall, J.; Nolte-‘t Hoen, E. N.; Piper, M. G.; Sivaraman, S.;

Skog, J.; Théry, C.; Wauben, M. H.; Hochberg, F. J. Extracell. Vesicles 2013, 2, 20360.

(24) Tang, Y.-T.; Huang, Y.-Y.; Zheng, L.; Qin, S.-H.; Xu, X.-P.; An, T.-X.; Xu, Y.; Wu, Y.-S.; Hu, X.-M.; Ping, B.-H.; Wang, Q. Int. J. Mol. Med. 2017, 40, 834−844.

(25) Zhu, L.; Wang, K.; Cui, J.; Liu, H.; Bu, X.; Ma, H.; Wang, W.; Gong, H.; Lausted, C.; Hood, L.; Yang, G.; Hu, Z. Anal. Chem. 2014, 86, 8857−8864.

(26) Sina, A. A. I.; Vaidyanathan, R.; Dey, S.; Carrascosa, L. G.; Shiddiky, M. J. A.; Trau, M. Sci. Rep. 2016, 6, 30460.

(27) Grasso, L.; Wyss, R.; Weidenauer, L.; Thampi, A.; Demurtas, D.; Prudent, M.; Lion, N.; Vogel, H. Anal. Bioanal. Chem. 2015, 407, 5425−5432.

(28) Di Noto, G.; Bugatti, A.; Zendrini, A.; Mazzoldi, E. L.; Montanelli, A.; Caimi, L.; Rusnati, M.; Ricotta, D.; Bergese, P. Biosens. Bioelectron. 2016, 77, 518−524.

(29) Im, H.; Shao, H.; Park, Y. I.; Peterson, V. M.; Castro, C. M.; Weissleder, R.; Lee, H. Nat. Biotechnol. 2014, 32, 490−495.

(30) Hosseinkhani, B.; van den Akker, N.; D'Haen, J.; Gagliardi, M.; Struys, T.; Lambrichts, I.; Waltenberger, J.; Nelissen, I.; Hooyberghs, J.; Molin, D. G. M.; Michiels, L. Nanomedicine 2017, 13, 1663−1671.

(31) van der Pol, E.; Coumans, F.; Varga, Z.; Krumrey, M.; Nieuwland, R. J. Thromb. Haemostasis 2013, 11 (Suppl 1), 36−45.

(32) van der Pol, E.; van Gemert, M. J. C.; Sturk, A.; Nieuwland, R.; van Leeuwen, T. G. J. Thromb. Haemostasis 2012, 10, 919−930.

(33) Welton, J. L.; Webber, J. P.; Botos, L.-A.; Jones, M.; Clayton, A. J. Extracell. Vesicles 2015, 4, 27269.

(34) Mol, E. A.; Goumans, M.-J.; Doevendans, P. A.; Sluijter, J. P. G.; Vader, P. Nanomedicine 2017, 13, 2061−2065.

(35) Baranyai, T.; Herczeg, K.; Onódi, Z.; Voszka, I.; Módos, K.; Marton, N.; Nagy, G.; Mäger, I.; Wood, M. J.; El Andaloussi, S.; Pálinkás, Z.; Kumar, V.; Nagy, P.; Buzás, E. I.; Ferdinandy, P.; Giricz, Z.; Kittel, Á. PLoS One 2015, 10, No. e0145686.

(36) EV-TRACK Consortium. Nat. Methods 2017, 14 (3), 228−232.

(37) Gámez-Valero, A.; Monguió-Tortajada, M.; Carreras-Planella, L.; Franquesa, M.; Beyer, K.; Borràs, F. E. Sci. Rep. 2016, 6, 33641.

(38) Nakai, W.; Yoshida, T.; Diez, D.; Miyatake, Y.; Nishibu, T.; Imawaka, N.; Naruse, K.; Sadamura, Y.; Hanayama, R. Sci. Rep. 2016, 6, 33935.

(39) Lötvall, J.; Hill, A. F.; Hochberg, F.; Buzás, E. I.; Di Vizio, D.; Gardiner, C.; Gho, Y. S.; Kurochkin, I. V.; Mathivanan, S.; Quesenberry, P.; Sahoo, S.; Tahara, H.; Wauben, M. H.; Witwer, K. W.; Théry, C. J. Extracell. Vesicles 2014, 3, 26913.

(40) Stranska, R.; Gysbrechts, L.; Wouters, J.; Vermeersch, P.; Bloch, K.; Dierickx, D.; Andrei, G.; Snoeck, R. J. Transl. Med. 2018, 16, 1.

(41) Altadill, T.; Campoy, I.; Lanau, L.; Gill, K.; Rigau, M.; Gil-Moreno, A.; Reventos, J.; Byers, S.; Colas, E.; Cheema, A. K. PLoS One 2016, 11, No. e0151339.

(42) Maiolo, D.; Paolini, L.; Di Noto, G.; Zendrini, A.; Berti, D.; Bergese, P.; Ricotta, D. Anal. Chem. 2015, 87, 4168−4176.

(43) Mustapic, M.; Eitan, E.; Werner, J. K.; Berkowitz, S. T.; Lazaropoulos, M. P.; Tran, J.; Goetzl, E. J.; Kapogiannis, D. Front. Neurosci. 2017, 11, 278.

(44) Gong, J.; Körner, R.; Gaitanos, L.; Klein, R. J. Cell Biol. 2016, 214, 35−44.

(45) Pasquale, E. B. J. Cell Biol. 2016, 214, 5−7.

(46) Krämer-Albers, E.-M.; Bretz, N.; Tenzer, S.; Winterstein, C.; Möbius, W.; Berger, H.; Nave, K.-A.; Schild, H.; Trotter, J. Proteomics: Clin. Appl. 2007, 1, 1446−1461.

(47) Exosome Quantitation, System Biosciences. https://www.systembio.com/products/exosome-research/exosome-quantitation/ (accessed February 5, 2018).

(48) Yoshioka, Y.; Konishi, Y.; Kosaka, N.; Katsuda, T.; Kato, T.; Ochiya, T. J. Extracell. Vesicles 2013, 2, 20424.

(49) Shi, M.; Liu, C.; Cook, T. J.; Bullock, K. M.; Zhao, Y.; Ginghina, C.; Li, Y.; Aro, P.; Dator, R.; He, C.; Hipp, M. J.; Zabetian, C. P.; Peskind, E. R.; Hu, S. C.; Quinn, J. F.; Galasko, D. R.; Banks, W. A.; Zhang, J. Acta Neuropathol. 2014, 128, 639−650.

(50) Debiec, H.; Christensen, E. I.; Ronco, P. M. J. Cell Biol. 1998, 143, 2067−2079.

(51) Pancook, J. D.; Reisfeld, R. A.; Varki, N.; Vitiello, A.; Fox, R. I.; Montgomery, A. M. J. Immunol. 1997, 158, 4413−4421.

(52) Inaguma, S.; Wang, Z.; Lasota, J. P.; Miettinen, M. M. Oncotarget 2016, 7, 55276−55289.

(53) Talebian, A.; Britton, R.; Ammanuel, S.; Bepari, A.; Sprouse, F.; Birnbaum, S. G.; Szabó, G.; Tamamaki, N.; Gibson, J.; Henkemeyer, M. Dev. Biol. 2017, 431, 179−193.

(54) Verdier, Y.; Zarándi, M.; Penke, B. J. Pept. Sci. 2004, 10, 229−248.

(55) Rushworth, J. V.; Hooper, N. M. Int. J. Alzheimer's Dis. 2010, 2011, 603052.

(56) Yanagisawa, K.; Odaka, A.; Suzuki, N.; Ihara, Y. Nat. Med. 1995, 1, 1062−1066.

(57) van Echten-Deckert, G.; Walter, J. Prog. Lipid Res. 2012, 51, 378−393.

(58) Marconi, S.; De Toni, L.; Lovato, L.; Tedeschi, E.; Gaetti, L.; Acler, M.; Bonetti, B. J. Neuroimmunol. 2005, 170, 115−121.

CHAPTER 3

A simple and universal enzyme-free approach for the detection of multiple microRNAs using a single nanostructured enhancer of surface plasmon resonance imaging

Andrea Sguassero, Álvaro Artiga, Carlo Morasso, Rafael Ramirez Jimenez, Rafael Martín Rapún, Roberta Mancuso, Simone Agostini, Ambra Hernis, Arturs Abols, Aija Linē, Alice Gualerzi, Silvia Picciolini, Marzia Bedoni, Marco Rovaris, Furio Gramatica, Jesus M. de la Fuente, Renzo Vanna

Analytical and Bioanalytical Chemistry, 2018
Doi: 10.1007/s00216-018-1331-0

Abstract

Here we describe a simple approach for the simultaneous detection of multiple microRNAs (miRNAs) using a single nanostructured reagent as surface plasmon resonance imaging (SPRi) enhancer and without using enzymatic reactions, sequence specific enhancers or multiple enhancing steps as normally reported in similar studies. The strategy involves the preparation and optimisation of neutravidin-coated gold nanospheres (nGNSs) functionalised with a previously biotinylated antibody (Ab) against DNA/RNA hybrids. The Ab guarantees the recognition of any miRNA sequence adsorbed on a surface properly functionalised with different DNA probes; at the same time, gold nanoparticles permit to detect this interaction, thus producing enough SPRi signal even at a low ligand concentration. After a careful optimisation of the nanoenhancer and after its characterisation, the final assay allowed the simultaneous detection of four miRNAs with a limit of detection (LOD) of up to 0.5 pM (equal to 275 attomoles in 500 μL) by performing a single enhancing injection. The proposed strategy shows good signal specificity and permits to discriminate wild-type, single- and triple-mutated sequences much better than non-enhanced SPRi. Finally, the method works properly in complex samples (total RNA extracted from blood) as demonstrated by the detection of four miRNAs potentially related to multiple sclerosis used as case study. This proof-of-concept study confirms that the approach provides the possibility to detect a theoretically unlimited number of miRNAs using a simple protocol and an easily prepared enhancing reagent, and may further facilitate the development of affordable multiplexing miRNA screening for clinical purposes.

Abbreviations

Ab	Antibody
C12E5	Pentaethylene glycol monododecyl ether
CCD	Charge-coupled device
DEPC	Diethyl pyrocarbonate
EDC	1-Ethyl-3-(3-dimethylaminopropyl)carbodiimide
GNSs	Gold nanospheres
ICP-AES	Inductively coupled plasma atomic emission spectroscopy
LOD	Limit of detection
miRNA	MicroRNA
MS	Multiple sclerosis
nGNSs	Neutravidin-coated gold nanospheres
NHS	N-Hydroxysuccinimide
NP	Nanoparticle
OD	Optical density
RT-PCR	Real-time PCR
SAM	Self-assembled monolayer
SPR	Surface plasmon resonance
SPRi	Surface plasmon resonance imaging
SSC3	Saline-sodium citrate
TCEP	Tris(2-carboxyethyl) phosphine

3.1 Introduction

The small size, low concentrations, various abundances and sequence similarity of microRNAs (miRNAs) make them challenging to detect and mean that, unlike the quantification of mRNA (i.e. gene expression measurements) for which existing analytical approaches satisfy most standard analytical and practical requirements, the methods of profiling and quantifying miRNAs are still to be improved[1]. The currently used platforms, most of which are based on quantitative polymerase chain reaction (PCR), deep sequencing and microarrays, do not always combine good analytical performance (sensitivity, specificity and multiplexing capacity) with sufficient usability (high-throughput power, simplified workflows and cost-effectiveness)[2,3]. This is one reason why, despite the potential use of miRNAs as circulating stable diagnostic markers or predictive markers of disease progression, they have not yet been screened in large patient cohorts thus probably delaying their introduction into clinical practice. There is therefore a need to develop new and technologically improved analytical approaches.

Much has recently been done in this direction and, among the promising new approaches based on optical, electrochemical and nanotechnological strategies (reviewed in [4–6]), surface plasmon resonance (SPR) has made a large contribution to the field of miRNA detection[7–9]. The relevance of SPR to DNA and RNA detection is mainly based on the direct capture of label-free signals arising from the simple adsorption of target molecules onto complementary probes, but the low molecular weight of miRNAs and their very small concentration in clinical samples require SPR enhancements. The

pioneering SPR-based method of miRNA detection using a signal enhancer was described by Corn et al., who demonstrated the detection of miRNA after coupling gold nanoparticles (NPs) and enzymatic reactions[10]. One type of further coming enhancement strategies developed with the aim of improving and simplifying miRNA detection is based on sequencesandwich (or super-sandwich) approaches to couple miRNA targets with enhancers based on Au NPs[11,12], grapheme oxide-Au NPs[13], streptavidin[14] ormultiple amplification steps using both Au and Ag NPs[15]. Even if these strategies may permit high sensitivity, some sequence-sandwich approaches imply the partial hybridisation of the miRNA target with a first semi-probe immobilised on the SPR chip, thus potentially reducing hybridisation efficiency and specificity given the shortness of miRNA (and DNA probes) sequences. In addition, sequence-sandwich strategies may require the use of as many sequence-specific regents as the number of miRNAs to be detected, or may require multiple enhancing steps, thus reducing multianalyte determination and practicality. Alternative solutions are enhancers able to recognise the presence of miRNA targets onto an array in a sequencesandwich-free manner. For example, anti-DNA/RNA hybrid antibodies[16] and protein p19[17] have been used as SPR signal enhancers reporting sensitivity above pM. Alternatively, the use of hairpin structure may be also a convenient approach[15,18]. Other strategies are those based on specific enzymes (such as ligase[19], polymerase[10] and nuclease[20]) able to discriminate the presence of miRNA molecules in order to produce a detectable signal cascade. But enzymatic reactions coupled with SPR approaches may be limited by specific enzymatic reaction

conditions, long reaction time, reproducibility biases and elevated costs.

The aim of this study is to develop a single universal SPR enhancer capable of simultaneously detecting multiple miRNAs with sensitivity below pM and without the use of enzymatic reactions, sandwich strategies, partial sequences hybridisation steps, multiple reagents or multiple enhancing steps. To this end, and as shown in Fig. 1, we combined (1) the universal sequence-independent recognition of miRNA thanks to the use of an Ab against all DNA/RNA hybrids, (2) the SPR-enhancing properties of gold NPs properly functionalised with the mentioned Ab and (3) the use of a SPR imaging (SPRi) instrumentation (reviewed by Scarano et al.[8]) that offers the capability to simultaneously detect in real-time multiple (potentially hundreds) molecular interactions in a multiarray format. The commercially available Ab used here recognises DNA/RNA hybrids without sequence specificity and is similar to the S9.6 Ab previously used for microarray-based[21], SPR-based[16] and graphene/ composite electrode-based methods of miRNA detection[22]. As far as we know, anti-DNA/RNA Abs have never been conjugated with gold nanospheres (GNSs) for enhanced SPR based strategies. Passing through careful protocol optimization and deep characterisation steps, anti-DNA/RNA Abs were conjugated with GNS using simple biotin/avidin strategy and the new nanoenhancer was tested by means of commercial, high-throughput and fully automated SPRi.

Multiple sclerosis (MS), a highly heterogeneous, chronic and immune-mediated demyelinating disease[23], was used as case study. On the basis of the most recent guidelines, a clinical evaluation and magnetic

resonance imaging (MRI) are still the only available means of staging and monitoring MS[24]. Some blood MS biomarkers have been proposed, but none of them has been clinically implemented for diagnostic, sub-typing or staging purposes[25]. Some miRNAs have been also reported as promising MS markers according to what reported by several studies[26–30] and by relevant reviews[31,32], but these still need to be validated in large patient cohorts, and further MS-related miRNAs may be discovered by means of multiple miRNA studies. MS is therefore a paradigmatic example of diseases for which the development of efficient and versatile multiplexing miRNA detection methods may help patient care. On the basis of these premises, we tested our enzyme-free universal SPRi enhancer to detect multiple MS-related miRNAs on total RNA extracted from blood, which is the standard sample used for miRNA detection.

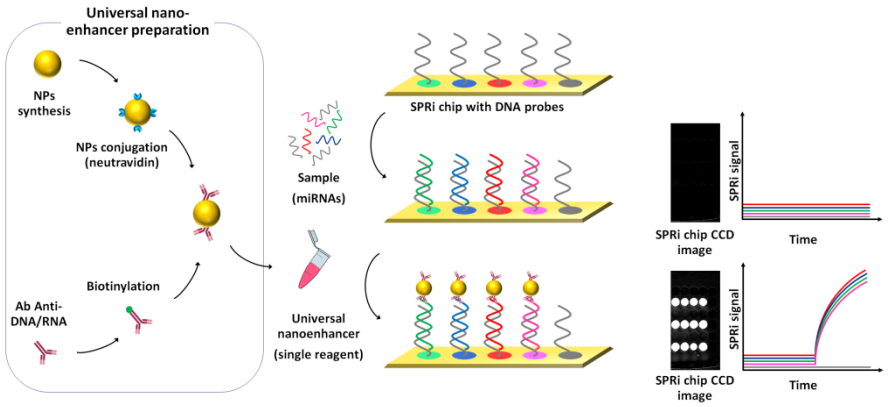

Fig. 1 Schematic representation of the strategy used for the simple and simultaneous detection of multiple miRNAs using the same nanoenhancer

3.2 Materials and methods

Materials

The reagents used in this study were purchased from Merck KGaA, Darmstadt, Germany, unless otherwise specified. Diethyl pyrocarbonate (DEPC)-treated RNase- and DNasefree water was used to prepare the thiol-modified DNA and RNA solutions. The oligonucleotide sequences (Eurofins Genomics, Germany) were purified by means of highperformance liquid chromatography (HPLC) by the manufacturer and the thiol-modified sequences were reduced with tris(2-carboxyethyl) phosphine (TCEP) before use (see details in the Electronic Supplementary Material (ESM)). All of the oligonucleotide sequences are shown in Table S1 (see ESM). The iodine-125 radionuclide was purchased from PerkinElmer, Spain.

GNS synthesis and conjugation with neutravidin

GNSs of 14 nm with maximum optical density (OD) at 520 nm were synthesised using the citrate-based approach as previously described excepting for the order of the addition of reagents which is here inverted[33] (ESM Fig. S1). Three hundred millilitres of ultrapure water was brought to the boil, after which 12 mL of sodium citrate 50 mM was added and stirred for 15 min; subsequently, 2.5 mL of tetrachloroauric acid ($HAuCl_4*3H_2O$) 20 mM was added and the solution was stirred under boiling conditions for ~ 1 h in order to obtain monodispersed GNS characterised by an intense red colour.

Finally, the solution was slowly cooled to room temperature under stirring for 2 h. Bare GNSs were coated with alpha-(11-mercapto-undecanoylamido)-omega-carboxy dodeca(ethylene glycol) (HS-FA-

PEG-COOH) (818 Da) using a protocol previously reported[34]. Briefly, 10 nM (see "nGNS characterization" below for GNS quantification) of GNSs were mixed with 0.028% sodium dodecyl sulphate and 20 μM HSFA-PEG-COOH. NaOH was further added to a final concentration of 25 mMand the mixture was incubated in agitation for 16 h at room temperature. The excess PEG chains were removed by centrifugation at 14,000×g for 30 min at 4 °C and the supernatant was discarded. This washing process was repeated three times and the pellet with GNSs was resuspended in ultrapure water and stored at 4 °C. The bare GNSs were then stored at 4 °C, a temperature at which they remain stable for several months if protected from direct light. Before beginning the conjugation with neutravidin, the GNSs were concentrated by centrifuging 1 mL of GNS (0.5 OD) at 14,000×g for 20 min and resuspended in 250 μL of water. A mixture of 60 μL 1-ethyl-3-(3-dimethylaminopropyl)carbodiimide (EDC 10 mM), 12 μL sulfo-N-hydroxysuccinimide (sulfo-NHS 10 mM) and 48 μL of water was added to the vial containing the 250 μL of GNS immediately after its preparation, and the suspension was gently stirred for 15 min. The GNSs were then centrifuged at 14,000×g for 20 min and resuspended in 880 μL of phosphate buffer, pH 5.2 (1 mM). Thereafter, different amounts (0, 2, 4, 6, 10, 15, 20 μL) of neutravidin (Thermo Fisher Scientific, Waltham, MA, USA, product nr. 31000) solution 280 μg mL^{-1} were added to different GNS solutions (reaching final neutravidin concentration from 0 to 104 nM) in order to screen the best amount of neutravidin, finally defined as 6 Ml (32 nM) (see ESM Fig. S1A). Each suspension was then gently stirred for 20 min. Subsequently, 160 μL of taurine 100 mM in sodium borate buffer (100

mM, pH 9) was added, and the suspension was gently stirred for 10 min. The neutravidin GNSs (nGNSs) were centrifuged at 12,000×g for 20 min and resuspended in 10 mM phosphate buffer saline (PBS) 10 mM pH 7.4. The conjugation of the GNS and neutravidin was followed by gel electrophoresis and also verified by means of ultraviolet-visible (UV-vis) spectroscopy. For gel electrophoresis experiments, nGNSs were resuspended in 20 μL of sucrose 20 mg mL^{-1}, instead of buffer, loaded onto 0.6% agarose gel, and the electrophoretic run was held for 30 min at 225V in TBE 0.5X, pH 8.

nGNS characterisation

The transmission electron microscopy (TEM) images for nGNS characterisation were collected using an FEI Tecnai T20 (FEI Europe, Eindhoven, The Netherlands) working at 200 kV. ImageJ software was used to measure the mean diameter of the nGNSs. For elemental analysis, the samples were evaluated by means of inductively coupled plasma atomic emission spectroscopy (ICP-AES) using an Optima 8300 (PerkinElmer, MA, USA). By correlating the absorbance at 450 nm revealed by means of UV-vis spectroscopy with the Au concentration measured by means of the ICP-AES analysis, it was possible to obtain a conversion factor (ε) of 12.6 mL mg mL^{-1} cm^{-1} for GNSs at 450 nm. The use of absorbance at 450 nm, instead of the maximum adsorption wavelength, for GNS quantification, permits to obtain more reproducible results. Assuming that the GNSs were spherical and using the diameter measured by means of TEM, the density of Au fcc (19.3 g cm^3), the Avogadro number and the theoretical molecular weight (MW) of GNSs was calculated (1.67 ×

10^7 g mol^{-1}). These data were used to calculate the protein: GNS molecular ratio and for radiolabelling experiments.

nGNS functionalisation with anti-DNA/RNA hybrid Ab

The monoclonal anti-DNA/RNA hybrid Ab (Ab; Covalab, mab0105-P, clone D5H6) was dialysed in PBS for using a Slide-A-Lyzed mini-dialysis unit with a 3.5 kDa MW cut-off limit (Thermo Fisher Scientific,Waltham, MA, USA, product nr. 69550) in order to remove the Tris, sucrose and glycin used as storage additives. The Ab was then diluted in PBS (0.5 mg mL^{-1}, 3.33 μM) and mixed with freshly prepared NHS-PEG4-biotin (EZ-Link™, Thermo Fisher Sci., 21330). Different amounts of the NHS-PEG4-biotin stock solution (1mM) were added to the Ab in order to obtain solutions with 5, 25, 50 and 75 biotin:Ab molar ratios. After 1 h of incubation at room temperature, the mixture was dialysed twice in PBS pH 7.4 in order to remove the unreacted biotinylation reagent, and the biotinylated Ab was stored at 4 °C until use. The neutravidin-coated GNSs (nGNSs) were functionalised with the biotinylated antibodies before each enhancement experiment by diluting them in PBS Tween 0.01% (0.25 OD measured at 524 nm) and mixing them with the biotinylated Ab in order to obtain a final Ab concentration of 5 nM. The mixture was incubated by means of gentle shaking for at least 30 min before use.

Radiolabelling protein quantification

A previously described, radiolabelling protein quantification method[35] was used with minor modifications (see details in ESM).

SPRi chip preparation

Bare gold SPRi biochips (HORIBA Scientific SAS, Palaiseau, France) were cleaned with piranha solution for 20 min at room temperature and washed with ultrapure water before use. They were then microspotted by means of contact printing (SPRi-Arrayer, HORIBA Scientific SAS, Palaiseau, France) using Xtend metal-ceramic capillary pins with a 700-µm spot diameter. Spotting was optimised by dissolving the thiol-modified (5′ thiohexyl (C6)) DNA oligonucleotides in different spotting solutions (PBS, pH 7.4; KH_2PO_4, pH 3.8: acetate 0.1M, pH 6; or saline-sodium citrate 3×) containing different surfactants (Tween-20 0.05%, sucrose monolaurate 0.05%, Triton X-100 0.05%, pentaethylene glycol monododecyl ether (C12E5) 0.05% or glycerol 0.05%) in order to obtain a final DNA concentration of 30 µM. The optimal spotting solution was PBS, pH 7.4, and Tween-20 0.05%. At least three spots were made for each probe, and negative control (reference) probes (PolyA DNAc 5-S) were spotted in parallel in order to minimise spikes related to differences in the position of the response and reference spots. The spotting procedure was performed at about 70% relative humidity and 20 °C. Before the spotting of each probe, at least three pre-spots were made on a separate chip in order to prepare the pins for definitive spotting. The printing pins were automatically washed with EtOH 10% and dried by air at least four times between the spotting of different samples. The spotted SPRi biochip was then incubated overnight at 20 °C with a relative humidity of 75% controlled using a saturated salt solution of sodium chloride, after which it was briefly washed with ultrapure water and then blocked

using PolyA DNA 5-S (10 μM) in water for 4 h at room temperature with gentle shaking. Finally, the chip was washed in water for 12 h to carefully remove unbound molecules, dried and immediately used or stored at 4 °C.

SPRi experiments

The SPRi experiments were carried out using XelPleX (HORIBA Scientific SAS, Palaiseau, France), a fully automated high-throughput SPRi system based on acquisitions at incident angles selected during the preparation phase on the basis of the best resonance condition for each spotted probe (a maximum of ten angles simultaneously). No more than three incident angles were simultaneously monitored. Before each experiment, the system and the SPRi chip were conditioned with the running buffer (PBS and Tween 0.01%) for more than 20 min and by means of two injections of NaOH 50 mM (100 μL) with a flow of 100 μL min^{-1} in order to stabilise the chip surface. Then, the array configuration and the spot regions to be read by the CCD were defined. The relevant region usually corresponds to the central part of the spots (i.e. around 80% of spot surface, equal to around 500 μm diameter). The CCD response of each spot was then calibrated and normalised by injecting 200 μL of sucrose 3 mg mL^{-1}. The flow rates used to inject the miRNAs, antibodies and nGNS were 10 or 50 μL min^{-1} depending on the type of experiments. The surface of the SPRi chip was regenerated by injecting one or twice 100 μL of NaOH 50mM. The calibration curve was calculated by performing a linear fitting of data after plotting them using a log-log scale. For each miRNA, the LOD signal was calculated as the average of three SPRi-enhanced signals obtained after the injection of running buffer

summed to three times the corresponding standard deviation (i.e. average of background signal + 3 SD). The miRNA concentration corresponding to each LOD signal was calculated using the fitting equations reported in Table S2 (see ESM).

Scanning electron microscopy

Scanning electron microscopy (SEM) images of the SPR chips were acquired using a field emission SEM Inspect F50 with an EDX INCA PentaFET×3 system (FEI Company, Eindhoven, The Netherlands) in an energy range of between 0 and 30 keV.

Tests on complex samples

The tests on complex samples were performed using blood from three healthy control subjects enrolled at IRCCS Fondazione Don Carlo Gnocchi. The subjects included in this study gave written informed consent in accordance with the protocols approved by the ethics committee of the same institution and according to the principles of the Declaration of Helsinki. Peripheral blood was collected in BD Vacutainer® SST™II Advance Tubes (Becton Dickinson, Franklin Lakes, NJ, USA). At the end of clotting time (60 min), serum was obtained by centrifugation at 1800g for 10 min at room temperature.

The clear supernatant was aliquoted into RNase/DNase-free tubes and stored at − 80 °C until use. Serum was then thawed on ice, centrifuged at 16,000×g for 5 min in a 4 °C, and then total RNAwas extracted from 200 μL of serum using spin-column chromatography (miRNeasy Serum/Plasma, Qiagen GmbH, Hilden, Germany) according to protocol suggested by the manufacturer. RNA was eluted by adding 15 μL of RNase-free water for each column. A total of 60 μL of RNA

obtained from 800 μL of serum was then resuspended in 550 μL (final volume) and analysed by SPRi. For the RT-PCR analysis see ESM.

3.3 Results and discussion

Spotting optimisation

Contact spotting procedures for depositing thiolated oligonucleotides on a chip's surface are practical and cost-effective, but the spotting needs to be suitably optimised. Before starting the enhancement experiments, a number of tests were carried out in order to select the spotting buffer that guaranteed the strongest SPRi signal and the greatest reproducibility.

We first studied the effects of various surfactants typically used for printing and spotting, including some reported in literature[36]: Tween-20, sucrose monolaurate, Triton X-100, pentaethylene glycol monododecyl ether (C12E5) and 0.05% glycerol were tested in PBS pH 7.4, and compared with pure water and PBS without any surfactant. As can be seen in Fig. 2a, the choice of surfactant affected both the shape of the spots and the final SPRi signal, whereas pure water and PBS alone did not produce good spots and led to very poor signals. Glycerol was completely inefficient; C12E5 led to relatively good signals but irregular spots with coffee-ring features and poor reproducibility; and only Triton X-100, sucrose monolaurate and Tween-20 all produced spots with regular boundaries and good homogeneity. Of the last three surfactants, Tween-20 was chosen as the best surfactant because this guaranteed the highest SPRi signals, which normally are collected from the central part of the spot. Besides, Triton X-100 produced too large spots that sometimes caused spots to merge (data not shown). In addition, Triton X-100 spots produced higher intensity mainly on boundaries (normally excluded by the CCD detection), thus reducing the overall signal intensity.

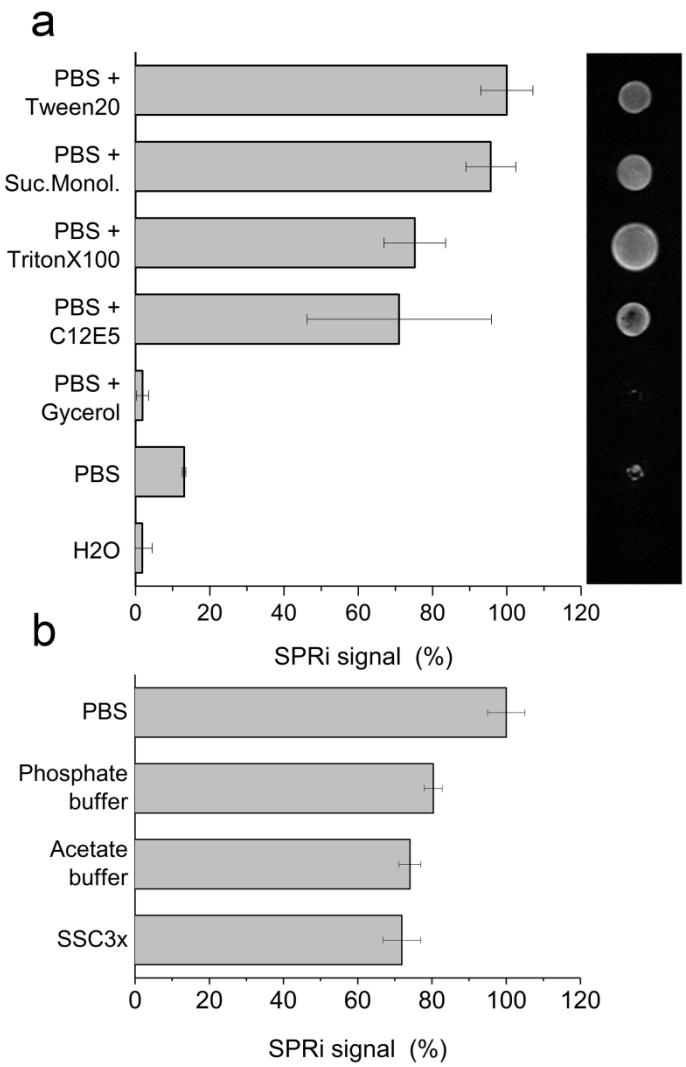

Fig. 2 Spotting optimisation. **a** SPRi signals detected in correspondence of thiolated DNA probes dissolved in solutions containing different surfactants. The CCD differential image (reflectivity variation) acquired during the measurement (association phase at equilibrium) is shown beside the bar plot. **b** SPRi signals detected in correspondence with the thiolated DNA probes dissolved in different buffers, all mixed with Tween-20 0.05%as the best surfactant. **a** and **b** both show the SPRi signal related to the injection of miR-223 (500 nM, signal at equilibrium) flowed onto a chip spotted with the same complementary thiolated DNA probe previously dissolved in different solutions. Each bar corresponds to the average signal obtained from three parallel spots and the subsequent average of two consecutive and identically administered injections (500 µL, 50 µL min^{-1})

Subsequently, various buffer solutions selected from the literature[37,38], as being among the most used for microarray spotting (i.e. PBS, pH 7.4; phosphate buffer 0.2 M, pH 3.8; acetate buffer 0.1 M, pH 6; and saline-sodium citrate 3×(SSC3×), pH 7.4), were mixed with Tween-20 0.05% in order to establish the best combination of buffer and surfactant, which proved to be PBS pH 7.4 + Tween-20 0.05% (Fig. 2b).

Universal nanoenhancer production: neutravidin GNS synthesis and functionalisation with anti-DNA/RNA hybrid Ab

The proposed SPRi enhancing strategy is based on the use of neutravidin GNS (nGNS) functionalised using anti-DNA/RNA hybrid Ab as previously described (Fig. 1). GNSs with a diameter of around 14 nm were prepared using citrate as the reducing agent and stabilised using a carboxylated selfassembled monolayer (SAM). The coated nanoparticles showed excellent stability and did not show any sign of aggregation for a few months. In order to define the best approach to guarantee a good neutravidin conjugation but also to prevent a loss in the stability of the nGNS leading to the higher unspecific adsorption of the surface of the SPRi chip, we optimised the protocol in order to define the best amount of neutravidin required to functionalise all the GNS. Neutravidin was conjugated onto the SAM layer using EDC/sulfo-NHS coupling and the neutravidin conjugation was followed by gel electrophoresis, UV-vis spectroscopy and TEM measurements (ESM Fig. S1). Among these approaches, gel electrophoresis was mainly used to visually select 32 nM as final optimal neutravidin concentration corresponding to the minimum

amount of neutravidin to obtain the functionalisation of all GNS (i.e. no residual bands related to non-conjugated GNS were visible). Coupling data acquired by means of ICP-AES and by radiolabelling protein determination using iodine-125 radionuclide made possible to quantify the number of neutravidin molecules attached to each nanoparticles when using this protocol. Radiolabelling allows the precise quantification of very low protein levels and is one of the few methods that can be used to measure the amount of protein linked and not linked to the nanoparticles at the same time[35]. The results showed that a mean 2.58 ± 0.19 neutravidin molecules were conjugated per GNS in the case of EDC/NHS covalent coupling and 1.6 ± 0.25 in the case of non-covalent adsorption (see ESM Table S3 for details), thus demonstrating that utility of covalent conjugation.

Considering the importance of using a robust and controlled procedure for the production of the nanoenhancer[39], before functionalising the nGNS with the biotinylated anti-DNA/RNA Abs, we tested various Ab:biotin molar ratios (1:5, 1:25, 1:50 and 1:75) taking in account a biotinylation reaction yield of around 10% according to protocol suggested by the manufacturer. This test was done in order to compare the activity of the original Ab and with that of the differently biotinylated Abs injected immediately after the injection of a high concentration of miRNA (500nM) and determine signals at equilibrium binding conditions (Fig. 3a–c). As expected, increasing the biotinylation molar ratio led to a progressive reduction in Ab activity due to the chemical modification of the antigen-binding site (Fig. 3a). On the other hand, Fig. 3b–d and ESM Fig. S2 show the results when the different Abs were mixed with nGNSs and injected

after the injection of a low concentration of miRNA (1 nM) with the aim of selecting the optimal Ab:biotin molar ratio and verifying the best conditions for SPRi enhancement. The biotinylated Abs mixed with nGNS greatly enhanced SPRi, thus confirming nGNS functionalization and Ab coupling. The SPRi signal progressively increased when moving from the non-biotinylated Ab (Ab:biotin molar ratio 1:0) to a ratio of 1:25 biotinylated antibodies, which led to approximately 900-fold enhancement (compared to non-enhanced SPRi miRNA detection), and began to decrease when the higher ratios of 1:50 and 1:75 were used. Taken together, these findings show that the 1:25 ratio offered the best compromise between Ab activity and the number of Abs linked to the nGNS. As shown in Fig. 3d and ESM Fig. S2, the nGNS alone did not show any significant signal arising from aspecific interactions between the nGNSs and the SPRi chip surface, and the original nonbiotinylated Abs used alone showed similar enhancement to that observed when the nGNSs were mixed with nonbiotinylated Abs (19-fold and 17-fold, respectively). This suggests that the non-biotinylated Abs do not spontaneously bind nGNS and that their combination does not lead to any significant additional signal due to aspecific interactions. It is finally worth noting that in these experiments and all of the further experiments involving model or real samples, the mixture of nGNS/Ab used as only enhancing reagent was stable for days without any further purification if stored at 4 °C.

Radiolabelling experiments were also used to determine the number of Abs effectively linked to the nGNS and clarify the importance of Ab biotinylation (Fig. 3e). Using the theoretical molecular weight of the

nGNS (1.67×10^7 $gmol^{-1}$), the molecular weight of the antibodies (about 150 kDa), and the gamma emissions produced by functionalised nGNSs after the reaction, the number of linked can be easily calculated (see more details in "Materials and methods" and ESM Table S4). The result confirmed that, under our experimental conditions and considering all the biotinylation ratios tested, the number of biotinylated Abs linked to each nGNS is between 0.7 and 4.1 and this is compatible with the number of biotin-binding sites provided neutravidin molecules immobilised on the nanoparticles (i.e. 2.58 neutravidin molecules/GNS multiplied by maximum four neutravidin binding sites = a maximum of ~ 10 Abs/nGNS). More in details, nGNSs conjugated with 1:5 biotinylated antibodies were linked with less than one Ab (0.73); the most active nGNSs (i.e. those conjugated with an Ab:biotin ratio of 1:25) were linked with an average of 1.9 Abs, whereas the less active nGNSs conjugated with more biotinylated Abs (i.e. at molar ratios of 1:50 and 1:75) were linked with respectively 2.4 and 4.1 Abs. These numbers are also close to the number of biotins supposed to be covalently bound to each Ab considering the biotinylation reaction yield of around 10% as claimed by manufacturer (i.e. 0.5, 2.5, 5 and 7.5 biotin/Ab for 1:5, 1:25, 1:50 and 1:75 M ratio respectively). As the enhancement factor did not linearly correlate with Ab activity or the number of immobilised Abs (see Fig. 3b), different biotinylation ratios may not only affect Ab activity and functionalisation efficiency but also the orientation of the immobilised Abs. All these data confirmed that the nGNSs linked with more Abs were less active due to Ab damage, wrong Ab orientation or steric hindrance, and that the preparation of

active nanoparticle-Ab conjugates require proper screening and optimisation steps[40].

Analytical performance. The specificity of the signal produced by the Ab + nGNS can be seen in the sensogram (Fig. 3a) and the chip CCD differential image (Fig. 4a), neither of which shows any significant signal related to the chip surface or negative control spots. The interaction between the Ab + nGNS and the SPRi chip was investigated by SEM at the end of an enhancement experiment that was without the regeneration steps normally used to remove interacting/adsorbed molecules. As shown in Fig. 4b, c, the positive spots are covered by nanoparticles of the expected size and probably clustered in correspondence with the presence of SH-DNA/miRNAs hybrids; the negative spots do not show any significant interactions.
In order to evaluate the enhancing properties and dynamic range of the proposed method, two synthetic miRNAs (miR- 422 and miR-223) injected in a wide range of concentrations were detected without enhancement, using only the Ab or using the Ab + nGNS. Figure 5a shows all of the calibration curves, which demonstrate the improvement in detection when using the two enhancing strategies.

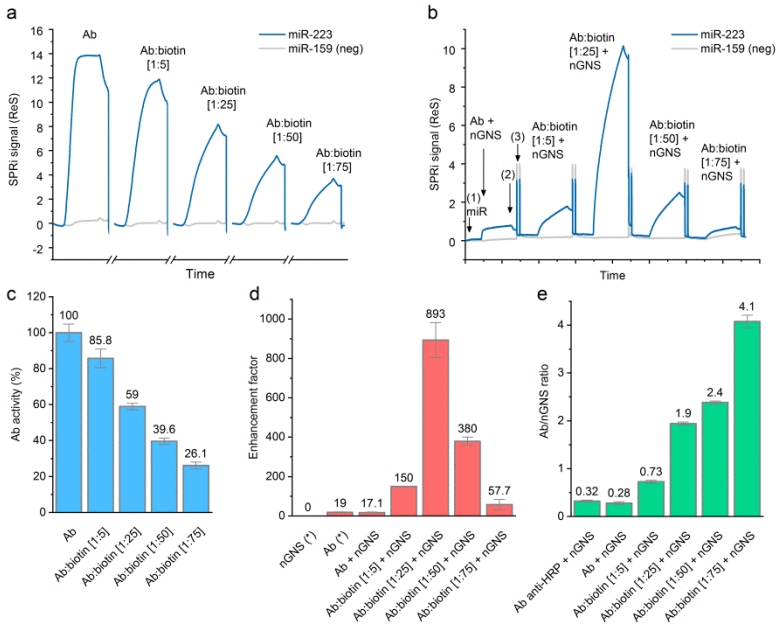

Fig. 3 nGNS functionalisation tests. **a** Ab activity tests. The sensograms relate to the activity of the original Ab and the differently biotinylated antibodies (Ab:biotin molar ratios 1:5, 1:25, 1:50 and 1:75) injected (5 nM, 500 µL, 10 µL mL^{-1}) after the injection of miR-223 (500 nM, 500 µL, 10 µLmin^{-1}) (not shown). **b** Enhancement test (see ESM Fig. S2 for larger graphs). The sensogram relates the injection of nGNS (0.25 O.D. at Abs. λ 524 nm) mixed with 5 nM of the original Ab and the differently biotinylated antibodies (Ab:biotin molar ratios 1:5, 1:25, 1:50, 1:75) (800 µL, 10 µL min^{-1}) after the injection of 1 nM of miRNA 223 "(1)" (500 µL, 50 µLmin^{-1}). Each Ab + GNS injection was followed by a dissociation phase (running buffer "(2)") and chip regeneration phase (double injection of NaOH 50 mM "(3)"). The signal in **a** and **b** are the average of three spots after the subtraction of the signals from the negative references (PolyA sequences) spotted in parallel on the same chip. Both sensograms also show the signal related to miR-159 (not injected). **c** Activity of Abs functionalised with increasing amounts of biotin; the SPRi signals shown in a were normalised using a non-biotinylated Ab as the reference (100%). **d** SPRi enhancement induced by the original Ab, the nGNS and the nGNS conjugated with differently biotinylated Abs; enhancement was calculated by dividing the SPRi signals (see **b**) produced by the Ab + nGNS by those produced by 1 nM of miR-223 alone injected before the Ab + nGNS. (*) See the sensograms in ESM Fig. S2 for the enhancement produced by the nGNS and the original Ab alone. **e** Results of the radiolabelling experiments; the values refer to the average number of Abs linked to each nGNS (see ESM Table S4 for details). Anti- HRP (horseradish peroxidase) was used as additional control

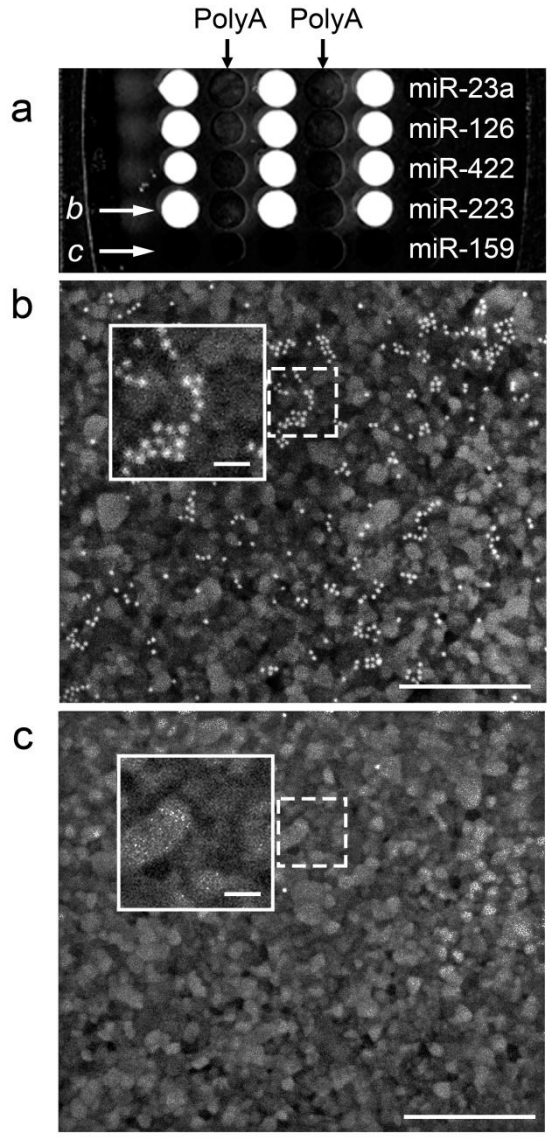

Fig. 4 SPRi chip images. **a** CCD differential image (reflectivity variation) of the SPRi chip acquired during Ab + nGNS-enhanced detection of four different miRNAs [100 pM]; the PolyA spots were used as references for each miRNA family, and miR-159 was used as negative control. The two letters indicate the chip positions visualised by means of SEM (panels below). **b** SEM image of the positive spot showing nGNS adsorbed on miR-223:DNA probe hybrids. **c** SEM image of one negative spot relating to miR-159, which was not injected in this experiment. Scale bar = 400 nm (× 200,000). The two regions indicated by the dashed lines are magnified in the boxes enclosed by the solid lines (scale bar = 50 nm (× 450,000).

The dynamic ranges of the three approaches were from about 1 to > 500 nM for direct detection (× 1), from about 50 pMto 100 nM (around × 20 enhancement) for Ab-enhanced detection and from about 0.5 pM to 1 nM (around × 1000–2000 enhancement) for Ab + nGNS enhanced detection. The sensitivity and the multiplexing capacities of the proposed method were tested by the simultaneous detection of four miRNAs that have been suggested as potential MS biomarkers (miR-422, miR-223, miR-126 and miR-23a)[26,27,29,41]. These miRNAs were mixed, serially diluted (1:2.5) in running buffer from 0.16 to 100 pM, injected in the SPRi instrument and then detected using Ab + nGNSs as a single enhancing reagent. As shown in Fig. S3 (see ESM), the SPRi chip surface was completely regenerated between injections. Most of the binding curves (Fig. 5b and ESM Fig. S4) were clearly separated from noise and their maximum values were plotted using a log-log scale for each miRNA (Fig. 5c).

The data can be interpolated linearly through most of the tested concentrations, and the linear equation was used to calculate the limit of detection (LOD: the average of three replicated blank injections + 3 SD) for each miRNA: 0.55 pM for miR 422, 0.88 pM for miR-223, 1.19 pM for miR-126 and 1.79 pM for miR-23a. The amounts of detectable miRNA given the 500 μL of injected volume are therefore between 275 and 890 attomoles. These data show that our universal enhancement strategy does not seem to be much affected by different sequences as the four calibration curves reside in similar SPRi signal intensity ranges. This is in line with the findings of a previous fluorescence microarray-based study that used an anti-DNA/RNA Ab to analyse small RNA expression[21].

In parallel, the sequence selectivity, necessary in case of mutated miRNA or miRNA isomers detection, was tested by comparing the SPRi signal obtained after injecting wild-type (WT) miR-23a and miR-23a carrying one or three mutations (Fig. 5d, ESM Table S1) in three different experiments comparing the selectivity of non-enhanced SPRi (miRNA injected at 100 nM), Ab-enhanced SPRi (miRNA injected at 1 nM) and Ab + nGNS-enhanced SPRi (miRNA injected at 100 pM). These experiments were conducted using different analyte concentrations according to the sensitivity range of the three different signal detection approaches. As shown in Fig. 5d, the use of both Ab and Ab + GNS increased the selectivity of the SPRi biosensor. When detecting a target with three mutated bases, the Ab + GNS enhancer produced only the 13% of signal if compared with the signal related to the WT target. In the case of the miR-23a carrying a single mutation, SPRi alone was unable to distinguish it (i.e. 96% of response signal in comparison with the wild-type sequence), and Ab still produced 77%of the signal but the use of Ab + nGNS reduced the sensor response to 52%. This demonstrates that Ab, but especially Ab + nGNS enhancement, easily allows to recognise the mutated sequence probably because of the three-dimensional changes arising from the base-base mismatch.

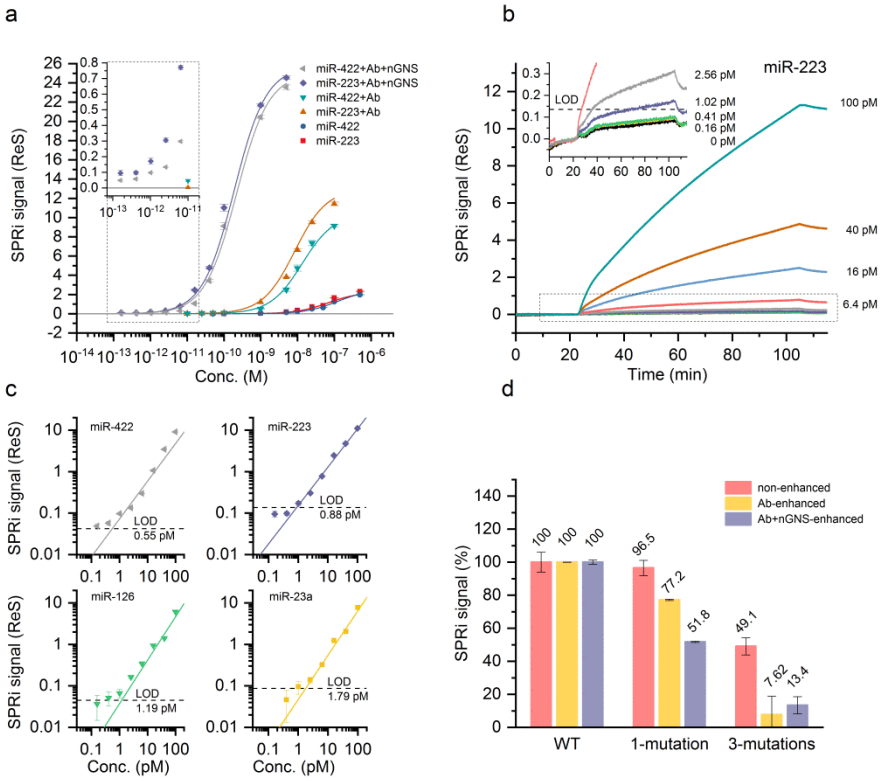

Fig. 5 Sensitivity and sequence selectivity. **a** The calibration curves of the detection of miR-422 and miR-223 by means of standard SPRi (blue and red), Ab-enhanced SPRi (jade and orange) and Ab + GNS-enhanced SPRi (grey and violet). **b** SPRi sensograms showing the Ab + nGNSenhanced detection of miR-223 within the low concentration range of 0–100 pM that was used to plot the calibration curves in **a** and **c** (see ESM Fig. S4 for the sensograms of all of the miRNAs). **c** Calibration curves of all of the studied miRNA families plotted using a log-log scale and fitted linearly (see equations in ESM Table S2). The LOD values shown in **b** and **c** were calculated as the blank (0 pM signal + 3 SDs). **d** Sequence selectivity. The bars represent the SPRi signals corresponding to the detection of non-mutated (WT) (100%)miR-23a, andmiR-23a carrying one and three mutations. The three variants were detected by means of nonenhanced SPRi (after injecting miR-23a 100 nM), Ab-enhanced SPRi (after injecting miR-23a 1 nM) and Ab + nGNS-enhanced SPRi (after injecting miR-23a 100 pM) in separate experiments.

Test on complex samples

In order to test our approach in a clinical relevant environment, we used total RNA extracted from serum samples taken from three healthy control subjects, which were processed as is usually done in pre-clinical research laboratories before RT-PCR quantification[29,30]. Total RNA samples were isolated from serum using a commercial extraction kit, diluted in 550 µL of running buffer and directly injected into the instrument, followed by the Ab + nGNS. All three samples were automatically and consecutively injected onto the SPRi chip, which had been previously used to define the calibration curves. The four studied miRNAs (miR-422, miR-223, miR-126 and miR-23a), selected because they have previously associated with MS[26,27,29,41], were then detected and quantified (Fig. 6a). These data show the varied contents of miRNAs in different samples, as expected and reported in literature, and show that, at least for these four selected miRNAs, the proposed approach is adequate for the realistic dynamic range for clinical purposes. A parallel quantification by RT-PCR was carried out, thus demonstrating a good agreement between the data obtained by the proposed SPRi approach and demonstrating that the total RNA complex sample does not interfere the SPRi measurement (Fig. 6b).Worthy of note, also RT-PCR was not able to detect miR-422 in Sample 1, probably because at a very low concentration in the real sample. It is obviously beyond the scope of this study to provide clinical evidence concerning significant differences in miRNA expression between subjects. On the other hand, our experiments aim to confirm that multiple miRNAs can be detected starting from

complex samples and passing through standard sample preparation followed by a very simple detection approach.

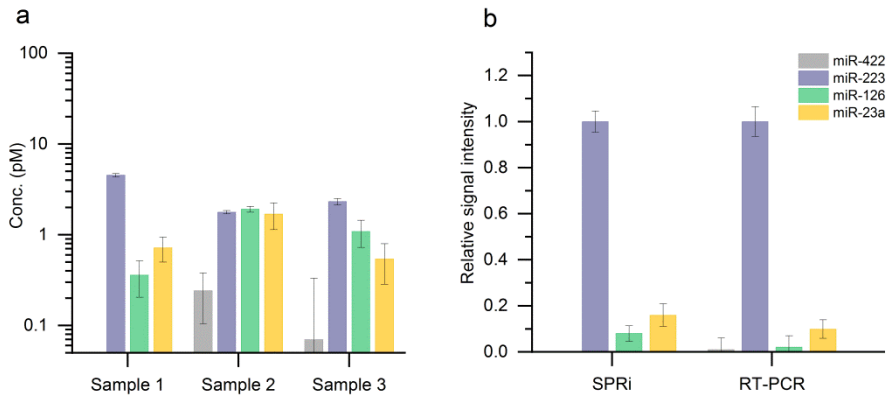

Fig. 6 Tests on complex samples. **a** Total RNAs extracted from serum samples taken from three healthy control subjects were analysed by SPRi. The concentrations of four different miRNAs (miR-223, miR-126, miR- 23a and miR-422) were calculated on the basis of the calibration curves shown in Fig. 5 and were corrected (1:0.687 dilution factor) considering that the RNA extracted from 800 µL of serum was then suspended in a final volume of 550 µL; 500 µL of those was injected (10 µL min^{-1}) followed by 800 µL Ab + nGNS (10 µL min^{-1}). **b** Comparison between the new proposed method and miRNA quantification by RT-PCR. The same sample of total RNA extracted from serum (Sample 1) was used as starting material for both quantifications. The relative signal intensity was based on the expression ratio between the four miRNAs and miR-223. For SPRi results were used the quantities and the standard deviation reported in a. For the RT-PCR results relative expression fold between each miRNA and miR-223 were used.

3.4 Conclusion

This paper describes a new and practical approach for the subpicomolar simultaneous and multianalyte detection of miRNAs without the use of enzymes or multistep enhancing protocols. The major advantage is that just one, stable and easy-to-prepare reagent consisting of gold nanoparticles functionalised using a commercially available Ab is sufficient for the detection of a theoretically unlimited number of miRNAs. To better understand the advantage of this approach, we report in Table S5 (see ESM) a brief overview of some recently reported SPR-based approaches for miRNA detection. Among these studies, higher sensitivity values were achieved by using enzymatic reactions[10,20], sequence dependent strategies[11] or multiple enhancing steps[15] which may reduce the simplicity and practicality; features that, according to a recent review by Kalogianni et al., may be required to their introduction in clinics[6]. A very recent article by Qian et al. reported an interesting and simple sequence-independent enhancing strategy by using boronic acid functionalised Au NPs able to recognise cis-diol groups of miRNA targets, but still not tested for multianalyte detection. Among recent studies, only Vaisocherova et al.[11] tested the simultaneous detection of four miRNAs by the same SPR-based biosensor as we here reported.

These advantages derive by the coupling of an Ab able to recognise RNA/DNA regardless of sequence with the very good enhancing properties of gold nanoparticles. Our protocol also allows specific interactions (without GNS adsorption on the chip surface or on negative spots) and better sequence selectivity than the intrinsically low sequence selectivity obtained by means oligonucleotide

hybridisation on a bare SPRi chip. Most of these benefits are due to the optimisation of GNS synthesis and functionalisation: the nanostructured enhancer was thoroughly characterised, including the absolute radiolabelling quantification of the average number of neutravidin molecules and antibodies immobilised on each single nanoparticle. As proof-of-concept, we tested our method by simultaneously detecting four miRNAs related to MS in real samples from human subjects instead of detecting miRNAs in spiked samples.
Further studies have been planned in order to increase the sensitivity of our system by (1) improving the Ab immobilization (i.e. by using oriented and biotin-free immobilization approaches), thus avoiding to reduce binding properties of the Ab, and by (2) screening other anti-DNA/RNA antibodies (e.g. the S9.6 Ab used by Sipova et al.[16]) that we could not use here due to its deactivation after biotinylation reactions (data not shown). We suppose that all the reported features could be also compatible with a direct detection of miRNAs in whole serum or plasma samples, without passing through a pre-purification step. On the other hand, we firstly wanted to test our approach using sample preparation protocols identical to those utilised in RT-PCR or microarray analyses. Further studies have been planned in order to test this approach on whole serum. Furthermore, we planned to carefully validate the method by increasing the number of real samples and the number of miRNAs that can be detected on the same chip, which is only limited by the number of spots that can be deposited on the chip surface. This should allow the development of more feasible and affordable methods of screening and validation of miRNAs related to the diagnosis, subtyping and progression of MS. At the same time, this

approach can obviously also be used to detect miRNAs related to any other disease or process of clinical or research interest.

ASSOCIATED CONTENTS

Electronic supplementary material

Electronic supplementary material The online version of this article (https://doi.org/10.1007/s00216-018-1331-0) contains supplementary material, which is available to authorized users.

ACKNOWLEDGEMENTS

The authors thank Dr. Domenico Caputo for subjects'recruitment and for his support for clinical aspects. They also thank Nicholas Corneli for his support for spotting and buffer optimisation. The authors gratefully acknowledge "TheAdvancedMicroscopy Laboratory" (INA-Universidad de Zaragoza) for access to their instrumentation and expertise. They also thank J.C. Raposo of the Servicio Central de Análisis de Bizkaia from SGIker of Universidad del País Vasco (EHU) for the ICP technical support and J. Puertas of the Radioisotope Service of Universidad de Zaragoza for the radiolabelling technical support.

FUNDING INFORMATION

Research funding was provided by the Italian Ministry of Health within the framework of the European EuroNanoMedII Project (Call 2015) entitled "NanoPlasmiRNA"; DGA-FSE (Diputación General de Aragón–Fondo Social Europeo); Ministerio de Educación, Cultura y Deportes of Spanish Government, FPU grant (FPU014/06249).

COMPLIANCE WITH ETHICAL STANDARDS

Healthy control subjects were involved in the study. Three subjects have been enrolled at IRCCS Fondazione Don Carlo Gnocchi. These subjects gave written informed consent in accordance with the protocols approved by the ethics committee of the same institution and according to the principles of the Declaration of Helsinki.

3.5 References

(1) Kappel A, Keller A. miRNA assays in the clinical laboratory: workflow, detection technologies and automation aspects. Clin Chem Lab Med. 2016; https://doi.org/10.1515/cclm-2016-0467.

(2) Pritchard CC, Cheng HH, Tewari M. MicroRNA profiling: approaches and considerations. Nat Rev Genet. 2012;13:358–69. https://doi.org/10.1038/nrg3198.

(3) Graybill RM, Bailey RC. Emerging biosensing approaches for microRNA analysis. Anal Chem. 2016;88:431–50. https://doi.org/ 10.1021/acs.analchem.5b04679.

(4) Degliangeli F, Kshirsagar P, Brunetti V, Pompa PP, Fiammengo R. Absolute and direct microRNA quantification using DNA–gold nanoparticle probes. J Am Chem Soc. 2014;136:2264–7. https:// doi.org/10.1021/ja412152x.

(5) Chamorro-Garcia A, Merkoçi A. Nanobiosensors in diagnostics. Nanobiomedicine. 2016;3:1849543516663574. https://doi.org/10. 1177/1849543516663574.

(6) Kalogianni DP, Kalligosfyri PM, Kyriakou IK, Christopoulos TK. Advances in microRNA analysis. Anal Bioanal Chem. 2018;410:695–713. https://doi.org/10.1007/s00216-017-0632-z.

(7) Carrascosa LG, Huertas CS, Lechuga LM. Prospects of optical biosensors for emerging label-free RNA analysis. TrAC Trends Anal Chem. 2016;80:177–89. https://doi.org/10.1016/j.trac.2016. 02.018.

(8) Scarano S, Mascini M, Turner APF, Minunni M. Surface plasmon resonance imaging for affinity-based biosensors.

Biosens Bioelectron. 2010;25:957–66. https://doi.org/10.1016/j.bios.2009. 08.039.

(9) Szunerits S, Spadavecchia J, Boukherroub R. Surface plasmon resonance: signal amplification using colloidal gold nanoparticles for enhanced sensitivity. Rev Anal Chem. 2014;33:153–64. https://doi. org/10.1515/revac-2014-0011.

(10) Fang S, Lee HJ, Wark AW, Corn RM. Attomole microarray detection of microRNAs by nanoparticle-amplified SPR imaging measurements of surface polyadenylation reactions. J Am Chem Soc. 2006;128:14044–6. https://doi.org/10.1021/ja065223p.

(11) Vaisocherová H, Šípová H, Víšová I, Bocková M, Špringer T, Ermini ML, et al. Rapid and sensitive detection of multiple microRNAs in cell lysate by low-fouling surface plasmon resonance biosensor. Biosens Bioelectron. 2015;70:226–31. https:// doi.org/10.1016/j.bios.2015.03.038.

(12) Wang Q, Liu R, Yang X, Wang K, Zhu J, He L, et al. Surface plasmon resonance biosensor for enzyme-free amplified microRNA detection based on gold nanoparticles and DNA supersandwich. Sensors Actuators B Chem. 2016;223:613–20. https://doi.org/10.1016/j.snb.2015.09.152.

(13) Wang Q, Li Q, Yang X, Wang K, Du S, Zhang H, et al. Graphene oxide–gold nanoparticles hybrids-based surface plasmon resonance for sensitive detection of microRNA. Biosens Bioelectron. 2016;77:1001–7. https://doi.org/10.1016/j.bios.2015.10.091.

(14) Zhang D,Yan Y, ChengW, ZhangW, Li Y, JuH, et al. Streptavidinenhanced surface plasmon resonance biosensor for highly sensitive and specific detection of microRNA. Microchim Acta. 2013;180: 397–403. https://doi.org/10.1007/s00604-013-0945-3.

(15) Liu R, Wang Q, Li Q, Yang X, Wang K, Nie W. Surface plasmon resonance biosensor for sensitive detection of microRNA and cancer cell using multiple signal amplification strategy. Biosens Bioelectron. 2017;87:433–8. https://doi.org/10.1016/j.bios.2016.08.090.

(16) Šípová H, Zhang S, Dudley AM, Galas D, Wang K, Homola J. Surface plasmon resonance biosensor for rapid label-free detection of microribonucleic acid at subfemtomole level. Anal Chem. 2010;82:10110–5. https://doi.org/10.1021/ac102131s.

(17) Nasheri N, Cheng J, Singaravelu R,Wu P, McDermottMT, Pezacki JP. An enzyme-linked assay for the rapid quantification of microRNAs based on the viral suppressor of RNA silencing protein p19. Anal Biochem. 2011;412:165–72. https://doi.org/10.1016/j. ab.2011.01.030.

(18) Ding X, Yan Y, Li S, Zhang Y, Cheng W, Cheng Q, et al. Surface plasmon resonance biosensor for highly sensitive detection of microRNA based on DNA super-sandwich assemblies and streptavidin signal amplification. Anal Chim Acta. 2015;874:59– 65. https://doi.org/10.1016/j.aca.2015.03.021.

(19) Zhou W-J, Chen Y, Corn RM. Ultrasensitive microarray detection of short RNA sequences with enzymaticallymodified

nanoparticles and surface plasmon resonance imaging measurements. Anal Chem. 2011;83:3897–902. https://doi.org/10.1021/ac200422u.

(20) Qiu X, Liu X, Zhang W, Zhang H, Jiang T, Fan D, et al. Dynamic monitoring of microRNA-DNA hybridization using DNAasetriggered signal amplification. Anal Chem. 2015;87:6303–10. https://doi.org/10.1021/acs.analchem.5b01159.

(21) Hu Z, Zhang A, Storz G, Gottesman S, Leppla SH. An antibodybased microarray assay for small RNA detection. Nucleic Acids Res. 2006;34:e52. https://doi.org/10.1093/nar/gkl142.

(22) Tran HV, Piro B, Reisberg S, Duc HT, Pham MC. Antibodies directed to RNA/DNA hybrids: an electrochemical immunosensor for microRNAs detection using graphene-composite electrodes. Anal Chem. 2013;85:8469–74. https://doi.org/10.1021/ac402154z.

(23) Goldenberg MM. Multiple sclerosis review. Pharmacol Ther.2012;37:175–84.

(24) Lublin FD, Reingold SC, Cohen JA, Cutter GR, Sørensen PS, Thompson AJ, et al. Defining the clinical course of multiple sclerosis. Neurology. 2014;83:278–86. https://doi.org/10.1212/WNL. 0000000000000560.

(25) Teunissen CE,Malekzadeh A, Leurs C, Bridel C, Killestein J. Body fluid biomarkers for multiple sclerosis—the long road to clinical application. Nat Rev Neurol. 2015;11:585–96. https://doi.org/10. 1038/nrneurol.2015.173.

(26) Keller A. Multiple sclerosis: microRNA expression profiles accurately differentiate patients with relapsing-remitting disease from healthy controls. PLoS One. 2009;4:e7440. https://doi.org/10. 1371/journal.pone.0007440.

(27) Cox MB, Cairns MJ, Gandhi KS, Carroll AP, Moscovis S, Stewart GJ, et al.MicroRNAs miR-17 and miR-20a inhibit Tcell activation genes and are under-expressed in MS whole blood. PLoS One. 2010;5:e12132. https://doi.org/10.1371/journal.pone.0012132.

(28) De Santis G, Ferracin M, Biondani A, Caniatti L, Rosaria Tola M, Castellazzi M, et al. Altered miRNA expression in T regulatory cells in course of multiple sclerosis. J Neuroimmunol. 2010;226:165–71. https://doi.org/10.1016/j.jneuroim.2010.06.009.

(29) Fenoglio C, Ridolfi E, Cantoni C, De Riz M, Bonsi R, Serpente M, et al. Decreased circulating miRNA levels in patients with primary progressive multiple sclerosis. Mult Scler Houndmills Basingstoke Engl. 2013;19:1938–42. https://doi.org/10.1177/1352458513485654.

(30) Mancuso R, Hernis A, Agostini S, RovarisM, Caputo D, Clerici M. MicroRNA-572 expression in multiple sclerosis patients with different patterns of clinical progression. J Transl Med. 2015;13:148. https://doi.org/10.1186/s12967-015-0504-2.

(31) Guerau-de-ArellanoM, Alder H, Ozer HG, Lovett-Racke A, Racke MK. miRNA profiling for biomarker discovery in multiple sclerosis: from microarray to deep sequencing. J

Neuroimmunol. 2012;248:32–9. https://doi.org/10.1016/j.jneuroim.2011.10.006.

(32) Junker A, Hohlfeld R, Meinl E. The emerging role of microRNAs in multiple sclerosis. Nat Rev Neurol. 2011;7:56–9. https://doi.org/ 10.1038/nrneurol.2010.179.

(33) Ojea-Jiménez I, Bastús NG, Puntes V. Influence of the sequence of the reagents addition in the citrate-mediated synthesis of gold nanoparticles. J Phys Chem C. 2011;115:15752–7. https://doi.org/10. 1021/jp2017242.

(34) Conde J, Ambrosone A, Sanz V, Hernandez Y,Marchesano V, Tian F, et al. Design of multifunctional gold nanoparticles for in vitro and in vivo gene silencing. ACS Nano. 2012;6:8316–24. https://doi.org/10.1021/nn3030223.

(35) Puertas S, de GraciaVilla M,Mendoza E, Jiménez-Jorquera C, de la Fuente JM, Fernández-Sánchez C, et al. Improving immunosensor performance through oriented immobilization of antibodies on carbon nanotube composite surfaces. Biosens Bioelectron. 2013;43: 274–80. https://doi.org/10.1016/j.bios.2012.12.010.

(36) Sola L, Damin F, Cretich M, Chiari M. Novel polymeric coatings with tailored hydrophobicity to control spot size and morphology in DNA microarray. Sensors Actuators B Chem. 2016;231:412–22. https://doi.org/10.1016/j.snb.2016.03.049.

(37) Ermini ML, Mariani S, Scarano S, Minunni M. Direct detection of genomic DNA by surface plasmon resonance imaging: an optimized approach. Biosens Bioelectron. 2013;40:193–9. https://doi. org/10.1016/j.bios.2012.07.018.

(38) Simon L, Lautner G, Gyurcsányi RE. Reliable microspotting methodology for peptide-nucleic acid layers with high hybridization efficiency on gold SPR imaging chips. Anal Methods. 2015;7: 6077–82. https://doi.org/10.1039/C5AY01239B.

(39) Fernández F, Sánchez-Baeza F, Marco M-P. Nanogold probe enhanced surface plasmon resonance immunosensor for improved detection of antibiotic residues. Biosens Bioelectron. 2012;34: 151–8. https://doi.org/10.1016/j.bios.2012.01.036.

(40) Špringer T, Chadtová S, Ermini ML, Lamačová J, Homola J.Functional gold nanoparticles for optical affinity biosensing. Anal Bioanal Chem. 2017;409:4087–97. https://doi.org/10.1007/s00216-017-0355-1.

(41) Junker A. MicroRNA profiling of multiple sclerosis lesionsidentifies modulators of the regulatory protein CD47. Brain. 2009;132:3342–52. https://doi.org/10.1093/brain/awp300.

CHAPTER 4

Raman spectroscopy uncovers biochemical tissue-related features of extracellular vesicles from mesenchymal stromal cells

Alice Gualerzi, Stefania Niada, Chiara Giannasi, Silvia Picciolini, Carlo Morasso, Renzo Vanna, Valeria Rossella, Massimo Masserini, Marzia Bedoni, Fabio Ciceri, Maria Ester Bernardo, Anna Teresa Brini, Furio Gramatica

Scientific Report, 2017; 7(1):9820.
Doi: 10.1038/s41598-017-10448-1

Abstract

Extracellular vesicles (EVs) from mesenchymal stromal cells (MSC) are emerging as valuable therapeutic agents for tissue regeneration and immunomodulation, but their clinical applications have so far been limited by the technical restraints of current isolation and characterisation procedures. This study

shows for the first time the successful application of Raman spectroscopy as label-free, sensitive and reproducible means of carrying out the routine bulk characterisation of MSC-derived vesicles before their use in vitro or in vivo, thus promoting the translation of EV research to clinical practice. The Raman spectra of the EVs of bone marrow and adipose tissue-derived MSCs were compared with human dermal fibroblast EVs in order to demonstrate the ability of the method to distinguish the vesicles of the three cytotypes automatically with an accuracy of 93.7%. Our data attribute a Raman fingerprint to EVs from undifferentiated and differentiated cells of diverse tissue origin, and provide insights into the biochemical characteristics of EVs from different sources and into the differential contribution of sphingomyelin, gangliosides and phosphatidilcholine to the Raman spectra themselves.

4.1 Introduction

Extracellular vesicles (EVs) are a heterogeneous group of membrane-bound vesicles that are constitutively released by cells of different tissue origins. Past controversies concerning nomenclature have now been resolved by the scientific community, which defines EVs as the group of particles made up of exosomes, microvesicles and apoptotic bodies1. Exosomes (30–100 nm) and microvesicles (up to 1000 nm) differ in size and cellular origin, but both mediate intercellular communication within a tissue and among organs thanks to body fluid transportation[1].

As is the case for most body cells, part of the secretome of mesenchymal stromal cells (MSCs) includes exosomes and microvesicles, which are currently being investigated because of their striking regenerative and immunomodulating potential. The bioactive molecules loaded onto/into EVs are involved in the paracrine effects of stem cells, and even the membrane constituents of vesicles seem to trigger intracellular protective/regenerative pathways in recipient cells[2]. It has been suggested that MSC-derived EVs may be sometimes even more therapeutically valuable than whole cells, because of their remarkable handling advantages, which can accelerate their clinical application in the so-called cell therapy without cells[3]. The possibility of overcoming the cell therapy drawbacks of having to administer living, replicating and difficult to control cells is currently one of the main challenges facing regenerative medicine, and EVs can be an effective means of stimulating the restoration of organ function through tissue regeneration and repair in the context of an integrated strategy of regenerative rehabilitation[4].

Over the last ten years, many studies have demonstrated the role that MSC-derived EVs can play in tissue repair and immunomodulation[5,6] and, in 2014, EVs ability to influence the activity of recipient cells and regulate immune responses was successfully exploited in a patient undergoing allogeneic hematopoietic stem cell transplantation who developed therapy-refractory graft-versus-host disease[7]. Their regenerative potential has also been assessed in in vitro and in vivo models of many diseases affecting heart[8–10], kidney[11–13], liver[14,15], bone and cartilage[16,17], muscle[18], skin[19], and central nervous system[20-23].

However, there are still concerns about the effect that the source of MSCs and cell culture conditions can have on EV production and characteristics as there is no standardised and optimised method for isolating and characterising EVs. Furthermore, the technical restraints of current techniques have limited their potential use in regenerative medicine[24,25] by preventing reproducible quality and safety assessments[26].

The aim of this study was to test Raman spectroscopy (RS) as a label-free, non-destructive, sensitive, rapid and automatable means of carrying out the bulk characterization of EVs. This technique provides a spectrum that qualitatively and quantitatively describes the chemical composition of a sample and thus avoids the need for specific protein biomarkers. It has been widely used in the pharmaceutical industry as a mean of verifying raw materials and quality controlling drug production, and we suggest it could help in purity and quality checking vesicle suspensions. It has already proved its value by characterising a wide range of cells and tissue samples for the

purposes of basic research, and as an innovative alternative to classic, time-consuming and operator-dependent diagnostic methods[27–34]. In the field of regenerative medicine, it has been used to analyse undifferentiated and differentiated human and murine embryonic stem cells[35–37] and to monitor MSCs stimulated towards osteogenic differentiation[38,39]. Efforts have also been made to develop Raman-based methods for the individual characterization of human vesicles[40,41], but although these have provided information at single-vesicle level, they are still far from being used diagnostically. What is required to allow the immediate transferability of EV research to clinical practice is a procedure that allows i) the rapid characterisation of a sample before its use in vitro or in vivo; ii) the identification of fingerprints of the EV populations used for regenerative purposes in order to determine the best experimental settings and compare results from different cell sources; and iii) the routine application of the analysis. The third point should be favoured by the current availability of portable Raman spectrometers that can automatically scan and analyse complex samples, which could bring Raman analysis easily in the reach of most laboratories. RS is much more suitable for achieving these goals than the widely used techniques of immunoblotting, cytofluorimetry and spectrometry because it can provide reproducible results quickly and in a label-free manner, and only requires tiny sample volumes in comparison with the large amounts needed by other methods, which cannot easily cope with the nanoscalar dimensions of exosomes.

This study provides the first Raman-based characterisation of the EVs of human MSCs isolated from bone-marrow (bone marrow

mesenchymal stromal cells, BM-MSCs) and subcutaneous adipose tissue (adipose tissue mesenchymal stromal cells, ASCs). The results were compared with those obtained using EVs released by dermal fibroblasts (DFs), in order to verify the ability of Raman analysis to distinguish vesicles from undifferentiated and differentiated cells, and gain insights into the biochemical features of EVs from different sources. Multivariate analysis was used to assess spectral differences and automatically distinguish the three groups. In addition, given the growing body of evidence concerning the pivotal role of lipids in mediating EV functions[42], we also evaluated the contribution of lipid membrane constituents to the Raman spectra. Our findings provide evidence supporting the use of RS for the routine characterisation of MSC-derived EVs before their in vitro/in vivo application.

4.2 Methods

All of the relevant experimental data have been submitted to the EV-TRACK knowledgebase (EV-TRACK ID: EV170012)[60].

Cell cultures. Human BM-MSCs were isolated from the residual bone marrow cells of healthy bone marrow (BM) transplantation donors (3 male donors, age range: 17–20 y/o) after approval by the Institutional Review Board of San Raffaele Hospital. Human ASCs and DFs were isolated from waste materials of abdominoplasty and liposuction procedures performed at IRCCS Galeazzi Orthopaedic Institute (subcutaneous adipose tissue of 4 female healthy donors - age range: 35–58 y/o - and de-epidermised dermis of 3 female healthy donors – age range: 26–46 y/o-, respectively). Tissues were collected following the procedure PQ 7.5.125 regarding waste materials to be used for research purposes, version 4 dated 22.01.2015, approved by the same institute. Written informed consent was obtained from all of the patients in accordance with the ethical principles of the Declaration of Helsinki. All of the samples were anonymised and no information or images that could lead to identification of a study participant might occur. All experiments were performed in accordance with the relevant guidelines and regulations of San Raffaele Hospital and IRCCS Galeazzi Orthopaedic Institute.

Cells were isolated following previously described protocols[61,63]. Briefly, mononuclear cells from BM aspirates were isolated by means of density gradient centrifugation (Ficoll 1.077 g/ml; Lympholyte, Cedarlane Laboratories Ltd., Burlington, Canada) and plated in non-coated 75–150 cm^2 tissue culture flasks (BD Falcon, Franklin Lakes,

NJ, USA) at a density of 160,000/cm^2 in complete culture medium: DMEM (Euroclone, Milan, Italy) supplemented with 10% ultracentrifuged foetal bovine serum (Gibco, Life Technologies LTD, Paisley, UK), penicillin 50 U/ml, 50 µg/ml streptomycin and 2 mM L-glutamine (L-Glu, Euroclone). Cultures were maintained at 37 °C in a humidified atmosphere, containing 5% CO_2. After 48-hour culture, non-adherent cells were removed. The ASCs were isolated from adipose tissue samples following digestion with 0.75 mg/ml type I Collagenase (250 U/mg, Worthington Biochemical Corporation, Lakewood, NJ, USA) and the filtering of the stromal vascular fraction. The DFs were obtained from de-epidermised dermis fragmented and digested with 0.1% collagenase type I. The ASCs and DFs (plating density: 10^5 cells/cm^2) were cultured (37 °C, 5% CO2) in complete culture medium. The medium was replaced every other day and, at 70–80% confluence, the cells were detached with 0.5% trypsin/0.2% EDTA, plated (BM-MSC plating density 4,000 cells/cm^2; ASC plating density 10,000 cells/cm^2; DF plating density 5,000 cells/cm^2) and expanded. Once at 80–90% confluence, cells at 3rd–4th passage were washed twice with DMEM, kept for one hour in serum-free DMEM (phenol-free DMEM supplemented with 2 mM L-glutamine, 50U/ml penicillin, 50 µg/ml streptomycin) and then cultured for 72 hours in serum-free DMEM.

Extracellular vesicle isolation. In order to avoid the presence of RS-visible isolation reagent residues in the EV suspension, the vesicles were isolated from cell-conditioned medium (CM) by means of differential centrifugation, as previously described[43]. Briefly, after 72 hours of starvation, the medium conditioned from approximately 6 ×

10^6 cells was centrifuged at 800 g for 10 min to remove non-adherent cells and then at 2,500 g for 15 min to remove potential apoptotic bodies. CM was then ultracentrifuged for 70 min at 100,000 g (L7–65; Rotor 55.2 Ti; Beckman Coulter, Brea, CA, USA) at 4 °C, and the pellet was re-suspended in sterile saline solution and ultracentrifuged again. The collected EV suspension (approximately 500 µl) was kept at 4 °C before making Raman and TEM analyses, and then frozen.

Western blotting. Immunoblotting was performed to characterise the EVs as suggested by ISEV minimal experimental requirements[44]. The EV pellets were re-suspended in SDS sample buffer with protease inhibitors64. Electrophoresis was performed under reducing conditions, and then proteins were transferred to nitrocellulose membrane. The antigens were probed with anti-flotillin-1 (BD Transduction Laboratories™, San Jose, CA, USA), anti-CD63 and anti-CD9 (System Biosciences, Palo Alto, CA, USA), and anti-calnexin (endoplasmic reticulum protein used as negative control, clone C5C9, Cell Signaling Technology, Danvers, MA, USA). As secondary antibodies goat anti-mouse (Thermo Fisher Scientific, Waltham, MA, USA) and goat anti-rabbit (System Biosciences) conjugated with HRP were used. Cell lysates were considered as the control for the specificity and working conditions of the considered antibodies.

Transmission electron microscopy and size measurement. For the TEM visualisation of EVs, 5 µl of purified exosomes were absorbed on Formvar carbon-coated grids for 10 min. The drops were then blotted with filter paper and negatively stained with 2% uranyl acetate

(5 µl) in aqueous suspension for 10 min. Excess of uranyl was removed by touching the grid to a filter paper. The grids were dried at room temperature and examined with a transmission electron microscope (Leo 812AB, Zeiss, Oberkochen, Germany) at 80 kV. The TEM images obtained in order to verify EV ultrastructure were used to assess vesicles' size using the particle analysis tool of ImageJ software (National Institutes of Health, Bethesda, MD, USA). At least 30 measurements per sample were done.

Raman spectroscopy. Freshly isolated EVs were analysed by means of Raman microspectroscopy (LabRAM Aramis, Horiba Jobin Yvon S.A.S, Lille, France) equipped with a diode-pumped solid-state laser operating at 532 nm and a Peltier-cooled CCD detector. 5–10 µl drops of EV suspension were deposited on a calcium fluoride slide and allowed to air dry. All of the measurements were performed with 50× objective (NA 0.75, Olympus, Tokyo, Japan), 1800 grooves/mm diffraction grating, 400 µm entrance slit, and confocal mode (600 µm pinhole) in the spectral ranges 500–1800 cm^{-1} and 2600–3200 cm^{-1}. Accumulation times were 2 × 10 s per spectrum.

The Raman shift was calibrated automatically using LabSpec 6 software (Horiba) using zero order line and Si line of a Si reference sample. In order to capture the spectra randomly, maps of about 150 μm^2 (with lateral steps of 20–30 µm) were acquired in the centre and at the borders of the air-dried drops. Before analysing the data, a two-class hierarchical clustering analysis (HCA) of the Raman maps was made in order to distinguish the spectra relating to vesicles from those related to background. At least 10 independent replicates of the

Raman spectra were obtained for every donor of the different cell types.

Data analysis. Baseline correction was made using LabSpec 6 processing tool by fitting all spectra with a sixth order polynomial curve in order to remove autofluorescence and background before unit vector normalisation. Post-acquisition calibration was carried out on normalised spectra, in order to compensate for possible thermal drifts. Principal component analysis (PCA) of the normalised and aligned spectra was made in order to reduce the dimension of the data and describe their major trends. The provided principal components (PCs) represent differences in the spectra of vesicles from the three cytotypes and therefore in their chemical composition. The first 25 PC scores were used in a supervised classification model, linear discriminant analysis (LDA), in order to discriminate and classify the data by maximizing the variance between groups. Data reduction by PCA before LDA was essential because LDA requires that the number of variables is smaller than the number of observations. The smallest number of PC scores was selected for the LDA to prevent data overfitting. A decreased number of PCs reduced the accuracy of the method in distinguishing the EVs, whereas an increased number did not improve the classification, but progressively decreased accuracy. Leave-one-out cross-validation was used to test the classification sensitivity, specificity, and accuracy of the LDA model. One-way ANOVA was performed on PC scores to verify that the means of each group were significantly different, despite within-group variance.
Data manipulations and statistical analysis were performed using Origin2017 (v. 9.4, OriginLab, Northampton, MA, USA).

CLS fitting. Reference molecules of some of the major known constituents of EV membrane were used to investigate the lipid content of vesicles. Cholesterol (Chol), ceramide (N-stearoyl-D-erythro-sphingosine; Cer), sphingomyelin (SM), phosphatidylcholine (16:0/22:6; PCh), L-α-phosphatidylethanolamine (PE), phosphatidic acid (PA), and monosialotetrahexosylganglioside (GM1) were purchased from Avanti Polar Lipids (Alabaster, AL, USA) and used to acquire reference spectra using the same acquisition settings as those used for the EV analysis.

Labspec 6 was used for the Classical Least-Squares (CLS) fitting of the PC1 and PC2 spectra, which allows to calculate the contribution of the reference chemicals to the PC spectra by evaluating any similarities. The resulting coefficients described the relationships between the PC spectra and the reference molecules.

4.3 Results

EV characterisation. EVs were isolated from BM-MSCs, ASCs and DFs following a multi-step ultracentrifugation protocol[43] and characterised by immunoblotting and transmission electron microscopy (TEM) to verify their peculiar features as suggested by the International Society for Extracellular Vesicles (ISEV)[44].
Immunoblotting confirmed the presence of EVs carrying flotillin-1, CD63 and CD9, and a significant reduction in calnexin-positive vesicles (Fig. 1A). The TEM images (Fig. 1B–D) confirmed the typical morphology of the EVs, whose ultrastructure and size were consistent with published data[45]. The vesicles in all of the samples were round (Fig. 1B–D) and their general mean diameter as calculated on the TEM images was 46.5 nm (±15.8 nm) with slight differences among cell groups. Supplementary Figure S1 shows a box plot with all of the recorded measurements.

Raman spectroscopy biochemical overview of EVs. Freshly isolated EVs were analysed by RS in the spectral ranges of 500–1800 cm^{-1} and 2600–3200 cm^{-1}, the most significant regions of the Raman spectrum for biological specimens. The spectra were obtained from random spots of air-dried drops of EV suspension and, given the size of the laser beam, we speculate that every spectrum described the biochemical features of small clusters of aggregated EVs.

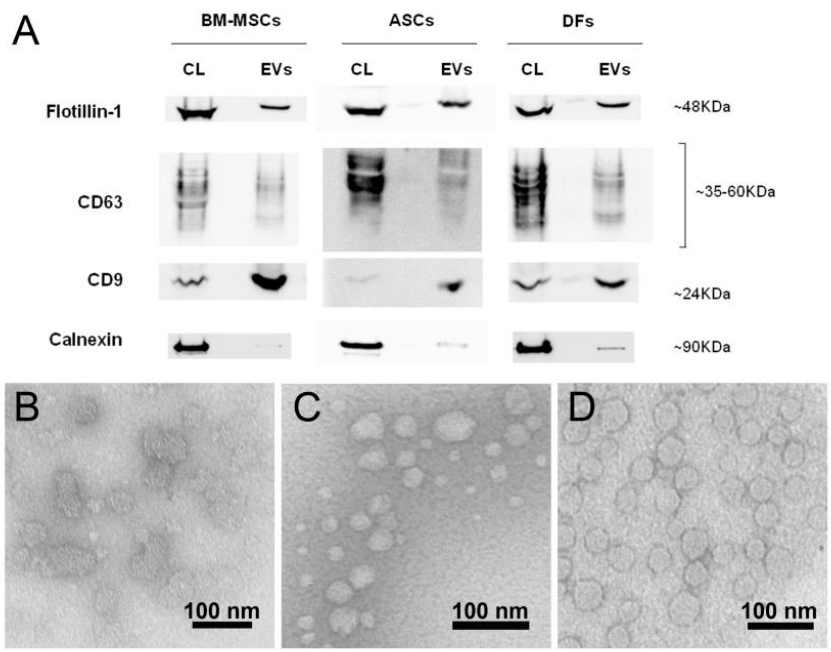

Figure 1. EV characterisation by means of Western blotting and transmission electron microscopy. (**A**) Western blot analysis of extracellular vesicles-enriched fractions (EVs) produced by BM-MSC, ASCs and DFs using the indicated antibodies. Flotillin-1, CD63 and CD9 are positive markers for EVs and Calnexin is considered a negative one. Corresponding cell lysate (CL) was used as control and depicts the specificity of the three antibodies. Western blots were cropped to improve clarity. All bands within the range of the molecular markers were retained and processing of the film was applied equally across the entire image. (**B**–**D**) Representative transmission electron photomicrographs of ultracentrifuged EVs from BM-MSCs (**B**), ASCs (**C**) and DFs (**D**) conditioned medium. The TEM images were used for size measurements. Bars = 100 nm.

Figure 2 shows representative mean Raman spectra (±1 standard deviation) of the vesicles isolated from the supernatants of BM-MSCs, ASCs and DFs. Each mean spectrum represents the average of 40–50 independent recordings obtained from all of the donors of the same cell type. The overall homogeneity in the spectra from the same tissue source underlines the reproducibility of the analytical method, which is not affected by the intrinsic inter-individual variability of donors.

The spectra showed characteristic Raman bands of nucleic acids (NAs, 720–820 cm^{-1}), phenylalanine (Phe, 1003 cm^{-1}), lipid and protein markers such as CH and CH2 groups (bands respectively centred at 1450 cm^{-1} and 2940 cm^{-1}) (Fig. 2 and Table 1). In particular, lipids made a large contribution, which is in line with previously reported spectroscopic evidence[40,41,46]. Lipid content was characterised by peaks attributable to cholesterol and cholesterol ester (537; 702; 1130; 1442 cm^{-1}) and peaks of varying intensity corresponding to the C-C stretch (around 1100 cm^{-1}) and CH, CH_2, and CH_3 bonds (in the spectral range 2600–3200 cm^{-1}). In addition, the areas usually assigned to NA bases (718; 748; 782 cm^{-1}) and phosphate backbone (785; ~1060 cm^{-1}) were variably prominent in the three average spectra. This is in line with many data demonstrating that EVs contain intact mRNA, long non-coding RNA, miRNA and other forms of RNA loaded into EVs[42]. The recurrent peaks attributable to proline/hydroxyproline (853; 920; 1206 cm^{-1}) and tryptophan (752–760; 1208; 1360; 1555 cm^{-1}) may be related to differences in cell metabolism and responses to serum-deprived culture conditions. Proline is known to be a signalling molecule and a sensor of cellular energy status when responding to metabolic stress[47], and the kynurenine pathway of tryptophan has been reported as being involved in the immunosuppressive effects of MSCs[48].

Comparison of the average spectra revealed many differences between the cytotypes (highlighted in bold characters in Table 1), suggesting discrepancies in the panel of protein biomarkers and lipid content of vesicles, although it is difficult to attribute divergences in peak intensity to specific molecules. The presence of a 1127 cm^{-1} peak

seemed to distinguish ASC spectra from those of both BM-MSC and DF EVs. The comparison of ASC and DF data highlighted minor divergences in the spectral range 2600–3200 cm^{-1}, which is greatly influenced by lipid molecules thus indicating similarities in the lipid content of ASC- and DF-derived vesicles.

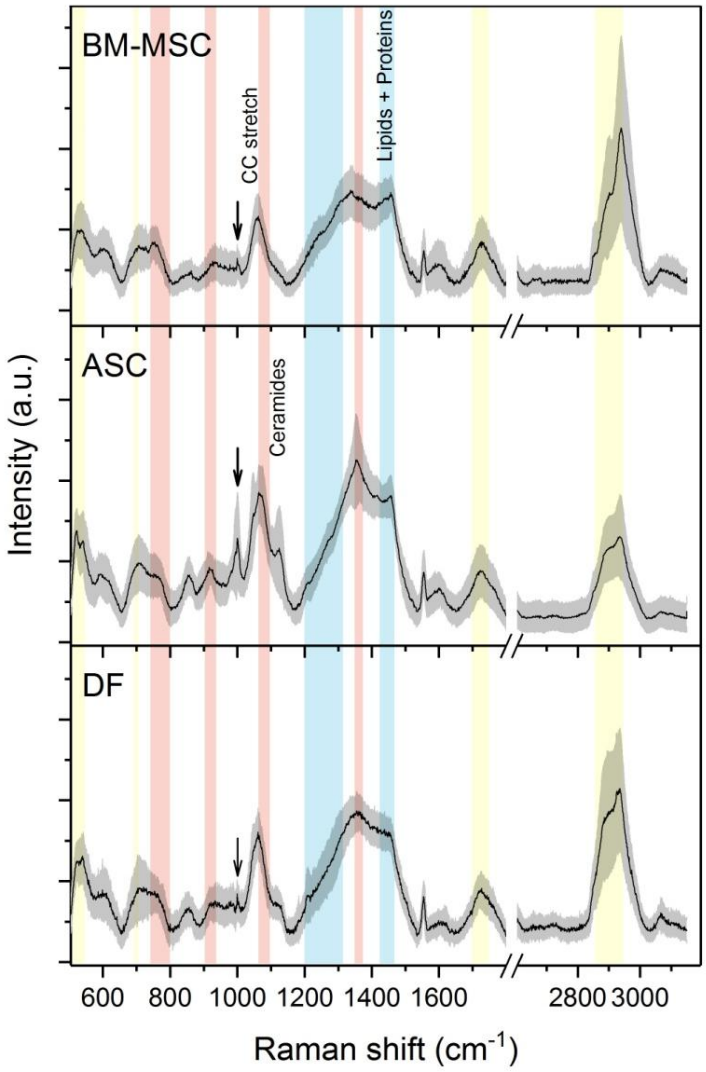

Figure 2. Raman fingerprint of BM-MSCs, ASCs, and DFs. Average Raman spectra obtained using an excitation wavelength of 532 nm and 10 seconds of exposure for 2 accumulations for each spectrum. The solid black line indicates the average of 40–50 spectra ± 1 standard deviation (shaded grey areas). The Raman bands corresponding to lipids are highlighted in yellow (500–540 cm^{-1}; the band centred at 700 cm^{-1}; 1700–1740 cm^{-1}; 2850–2950 cm^{-1}), those corresponding to proteins are in blue (1200–1300 cm^{-1}; the band centred at 1450 cm^{-1}), and those corresponding to nucleic acids are in red (720–820 cm^{-1}; the band centred at 915 cm^{-1}; 1060–1100 cm^{-1}; the band centred at 1360 cm^{-1}). The arrows indicate the 1003 cm^{-1} peak of Phenylalanine.

Position (cm^{-1})	Component
520	Phosphatidyinositol
524	Phosphatidylserine
537	**Cholesterol ester**
540	Glucose-saccharide band
596	Phosphatidylinositol
701-703	Cholesterol ester
720-820	Nucleic acids
752-760	**Tryptophan**
840-860	Polysaccharide structure
941	Polysaccharide structure
995	**C-O band of ribose**
1003	Phenylalanine
1048	Glycogen
1054	**C-O and C-N stretching of proteins**
1060-1095	C-C vibrations of lipids and carbohydrates PO_2^- stretching of nucleic acids
1120	C-O band of ribose; carotenoids
1127	**C-N stretching of proteins; ceramides**
1200-1300	Amide III *1230-1240 for β-sheets; 1260-1300 for α-helix*
1298	**Fatty acids**
1336	**CH3CH2 wagging mode of polynucleotide chain (purine bases)**
1337	**Tryptophan; Glycine backbone and Proline side chain**
1357; 1361	Guanine
1360	Tryptophan
1420-1480	CH functional groups of nucleic acids, proteins and lipids
1520-38	**Carotenoids**
1555-1558	Tryptophan
1716-1740	C=O group
2853-2881	CH_2 symmetric and asymmetric stretch of lipids
2910	**CH_3 stretching vibrations**
2940	**CH and CH_2 in lipids and proteins**

Table 1. Main Raman peak assignments from literature refs 65–67. The major divergent peaks are highlighted in bold characters.

Lipid membrane constituents account for spectral differences. Principal Component Analysis (PCA) was used to simplify the original data (n = 198) and all of the spectra were collectively represented by their principal components (PCs). Starting from PC1 (which accounted for 37.1% of total variance), the subsequent PCs describe differences in the Raman fingerprint that were progressively less prominent (Supplementary Table S1 and Supplementary Fig. S2). The first 2 PCs (Fig. 3A) were used to build the scatter plot shown in Fig. 3B. Combined analysis of the scatter plot and the PC1 and PC2 spectra revealed that the positive loadings in the PC1 spectrum mainly in PC2 represent BM-MSC vesicles rather than ASC or DF vesicles. One-way ANOVA performed on PC1 and PC2 scores demonstrated that the means of each group were significantly different (Prob > F < 0.05), despite within-group variance (Supplementary Table S2).

Based on the simple premise that a spectrum from a mixture of chemical ingredients is a mixture of the spectra from the pure ingredients, the PC1 and PC2 loadings were least squares fitted (classical least square (CLS) fitting) with specific reference spectra to investigate one possible cause of the observed spectral differences, following a previously reported procedure40. As we observed that the most variable spectral intervals in PC1 and PC2 were related to lipids, the membrane components cholesterol (Chol), ceramide (Cer), sphingomyelin (SM), phosphatidylcholine (PCh), phosphatidylethanolamine (PE), phosphatidic acid (PA), and monosialotetrahexosylganglioside (GM1, reference molecule for monosialoganglioside family) were used for CLS fitting.

Lipid reference molecules were preferred to protein markers because proteins spectra are dominated by backbone conformation signals, whereas lipids have more specific and defined peaks and can be more easily distinguished by RS. The resulting CLS fitting scores reported in Table 2 described the relative contribution of each standard molecule to PC1 and PC2 loadings, thus their contribution to the observed spectral differences between the three cytotypes. Figure 3C depicts the fitting coefficients in a bar graph, making apparent that SM and ganglioside (GM1) contribute to the shape of PC1 and PC2 loadings more than the other reference molecules. Similarly, PCh is the phospholipid which contributed most to fit the shape of PC1. In particular, the positive score attributed to SM after PC1 fitting demonstrated that it made a contribution to the spectrum of ASC-derived EVs, and this was further underlined by the negative SM score after PC2 fitting. On the contrary, GM1 and PCh were assigned a negative CLS fitting score in the case of PC1, suggesting their presence within the membrane of EVs from BM-MSCs and DFs rather than ASC-derived vesicles. After CLS fitting, the scores assigned to Chol, Cer, PE, and PA suggest their presence in the EVs from all three source cells, although they do not greatly contribute to the differences between EVs. It has to be noted that the considered lipids are only few of the constituents of vesicles, for this reason our results should be considered as hints for future studies aimed at verifying the exact membrane composition of vesicles.

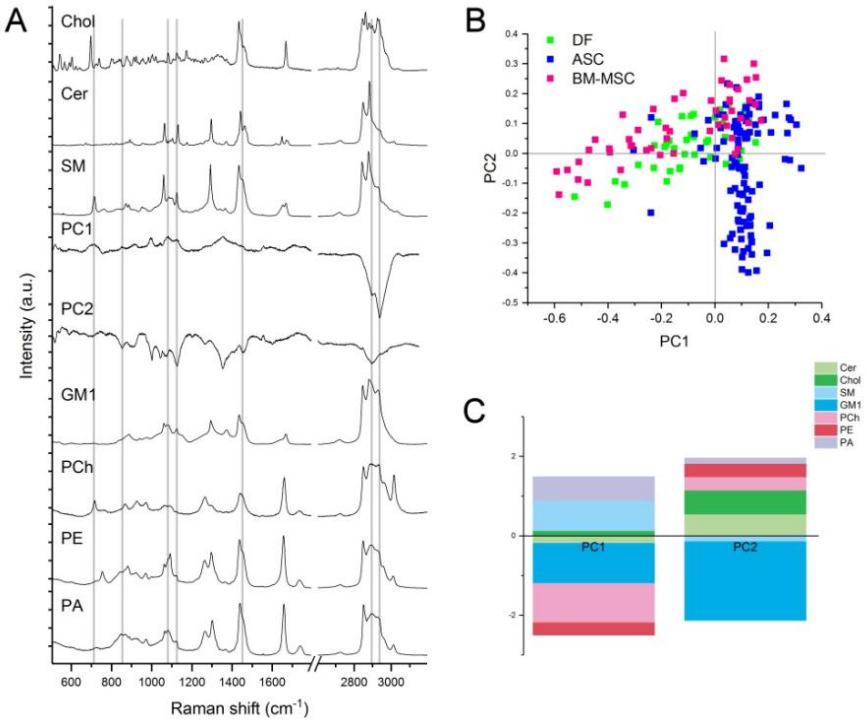

Figure 3. Multivariate analysis of the Raman spectra. (**A**) Raman spectra of reference lipid molecules, PC1 and PC2 that were considered for CLS fitting. The grey lines highlight the correspondences between the peaks of the standard lipids and the PC loadings. (**B**) Scatter plot of the PCA results showing the PC1 and PC2 scores assigned to each spectrum recorded from the EVs of BM-MSCs (pink), ASCs (blue) and DFs (green). Each square represents one spectrum. The scatter plot shows that a positive PC1 score described ASC-derived EVs better than those derived from DFs and BM-MSCs, whereas a positive PC2 score better described EVs derived from BM-MSC. (**C**) CLS scores obtained after fitting the spectra of Cer (light green), Chol (green), SM (light blue), GM1 (blue), PCh (pink), PE (red) and PA (violet) with the PC1 and PC2 loadings. The positive and negative scores obtained after CLS fitting are visualized as a bar graph and respectively indicate the contribution of each standard molecules to the positive or negative peaks visible in the PC1 and PC2 loadings. Cer: ceramide; Chol: cholesterol; SM: sphingomyelin; GM1: monosialotetrahexosylganglioside; PCh: phosphatidylcholine; PE: phosphatidylethanolamine; PA: phosphatidic acid.

	% variance	CLS fitting scores							% Error
		Chol	Cer	SM	GM1	PCh	PE	PA	
PC1	35.1	0.13	-0.19	**0.76**	**-1.01**	**-0.99**	-0.31	0.6	2.12
PC2	22.7	0.6	0.55	-0.15	**-1.98**	0.34	0.33	0.14	1.82

Table 2. Classical least-square (CLS) fitting. CLS fitting scores obtained after fitting the reference spectra of cholesterol (Chol), ceramide (Cer), sphingomyelin (SM), monosialotetrahexosylganglioside (GM1), phosphatidylcholine (PCh), phosphatidylethanolamine (PE), and phosphatidic acid (PA) to PC1 and PC2 loadings. The reported fitting scores are a measure of the contribution of each molecule to the considered PC loadings and provide hints to explain spectral differences between EV spectra. The percentage of total variance of PC1 and PC2 and the percentage of error obtained after CLS fitting are also reported.

		Predicted group			Total true	Sensitivity	Specificity	Accuracy
		BM-MSC	ASC	DF				
True group	BM-MSC	46	2	2	50	92%	98.7%	97.1%
	ASC	1	97	7	105	92.4%	91.8%	92.1%
	DF	1	7	35	43	81.4%	94.8%	92.1%
					198	**88.6%**	**95.1%**	**93.7%**

Table 3. PCA-LDA confusion matrix. Confusion matrix obtained from the results of the multivariate LDA of the first 25 PCA scores after leave-one-out crossvalidation. True positives, true negatives, false positives, and false negatives were used to calculate the sensitivity, specificity and accuracy of the method.

Raman spectroscopy can distinguish BM-MSC, ASC and DF EVs with 93.7% accuracy. The first 25 PCs were used for Linear Discriminant Analysis (LDA), which made possible to verify the ability of the method to identify between-group differences by maximising the variance among classes while minimizing intra-class variability. The results showed that RS clearly distinguished the biochemical fingerprints of the three groups. After leave-one-out cross-validation, the PCA-LDA model showed that the overall accuracy of the model was 93.7% and that its accuracy in distinguishing DFs from MSCs was 92% (Table 3). The LDA scatter plot (Fig. 4) revealed that the spectra of the ASC-derived EVs fell into a region that was clearly separated from those of the BM-MSC EVs. Although there was a limited overlap between the DF and ASC derived vesicles, RS distinguished their sources with a high degree of statistical confidence (Wilks' Lambda Test, $p < 0.001$). Details concerning the distribution of the individual donor spectra are shown in Supplementary Figure S3.

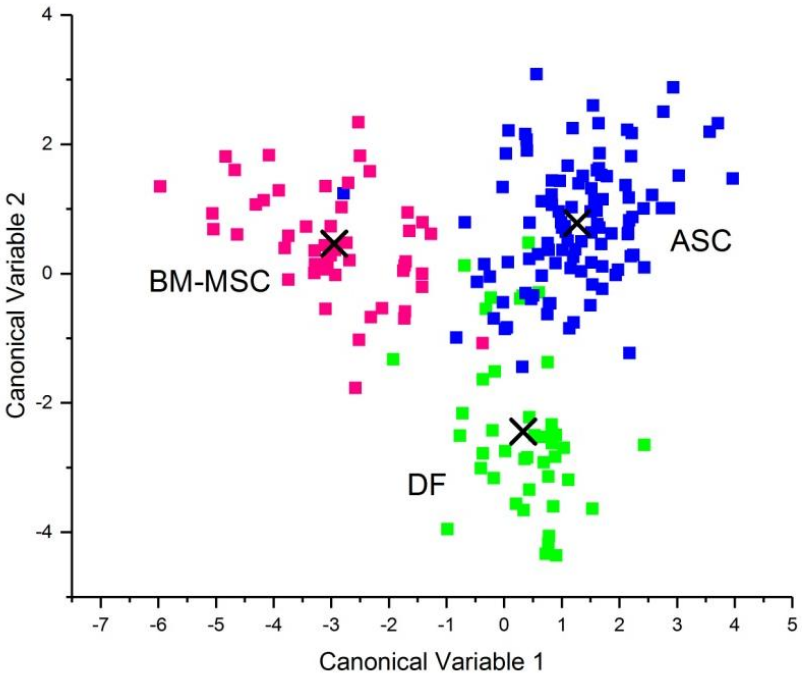

Figure 4. Linear discriminant analysis. The first 25 PC loadings calculated by means of PCA were used for the LDA. The scatter plot shows the LDA scores obtained for EVs from BM-MSCs (pink), ASCs (blue), and DFs (green). Each square represents a single spectrum. The crosses indicate the mean canonical observation score obtained for each group.

4.4 Discussion

The possibility of using regenerative medicine to treat diseased, damaged or aged tissues and restore organ function without side effects is one of the main challenges facing modern medical science, and so is no surprise that the discovery of the regenerative potential of EVs released by MSCs has aroused great interest. However, the main obstacle to the clinical use of vesicles is the lack of a robust and standardised method of characterising them[5].

In this study, we investigated the biochemical fingerprints of MSC-derived vesicles originating from different tissues and compared them with those of terminally differentiated dermal fibroblasts. Our findings demonstrate the ability of RS to identify tissue-related fingerprints for vesicles released by MSCs and fibroblasts without the use of any label. This is the first time that Raman analysis has been used to provide a biochemical overview of MSC-derived EVs from a limited volume of EV suspensions.

As previously reported in relation to other types of vesicles[40,41,49] our data on MSC-derived EVs confirm the ability of RS to reveal the presence of the main EV constituents in a single repeatable spectrum. Although we cannot exclude the possible presence of a limited amount of soluble factors other than vesicles in our suspension, the reproducibility of the results and the main peak attributions suggest the purity of the samples.

The main finding of this study is that RS can clearly distinguish not only vesicles from MSCs and terminally differentiated fibroblasts, but also vesicles of MSCs from bone marrow and adipose tissue. Although there are protein markers that define a stem cell phenotype

exist, a straightforward distinction between bone-marrow and adipose-tissue MSCs, based on biological and functional features, is still difficult to be obtained[50]. The ability of RS to highlight unique, tissue-specific features of vesicles should therefore assist scientists working with stem cells. Even if assessing the possible correlation between biochemistry and function goes beyond the scope of this study, the biochemical variations observed provide suggestions for further investigations into the functional differences of EVs from multiple MSC types and sources for which there is still not a definite marker[51,52].

Analysis of the spectra of MSC- and DF-derived EVs revealed that lipids made a substantial contribution to the Raman signals, as previously reported[40,41,49]. The prominence of membrane constituents in determining the fingerprints of vesicles is in line with the growing body of evidence demonstrating that lipids play a crucial role in the formation of EVs[1] and the fulfilment of their signalling functions[42]. It is known that a number of specific lipids are typically associated with lipid rafts and enriched in vesicles that inherit the plasma membrane composition of their cell of origin. In particular, cholesterol and sphingolipids are preferentially included in EV membranes and may be involved in the formation of vesicles and in their stability in the extracellular environment[42]. There is also evidence that lipids are involved in BM-MSC responses to a strongly pro-inflammatory environment[53]. Furthermore, it is possible that direct membrane interactions between vesicles and recipient cells is one of the mechanisms of action of EVs, as has already been demonstrated in the case of whole cells[2].

On the basis of CLS fitting results, we hypothesised that gangliosides, phosphatidylcholine and sphingomyelin directly contributed to the main spectral differences between the considered EVs. Our data are in agreement with those of a recent proteomic and lipidomic study demonstrating how sphingomyelins, ceramides, cholesterol and phosphatidylcoline were enriched in the exosomes of BM-MSCs in comparison with other cell types[54], but there is still a lack of data concerning the membrane composition of ASC-derived exosomes. Our observation that GM1 also contributes to the recorded spectra of BM-MSC vesicles is in line with the reported functional role of gangliosides in regulating the proliferation and neuronal differentiation of MSCs[55,56]. Similarly, it is known that ceramides and ceramide-containing lipids are involved in many of the pathways mediating immune responses, and that they modulate the adipogenic differentiation of MSCs[57]. Despite the reported functional significance of PA in the biogenesis and release of exosomes, our data did not reveal any significant difference of PA content in the EVs derived from the three cell types, as has also been noticed by Haraszti et al.[54] Further lipidomic studies are needed to verify the exact membrane composition of MSC-derived vesicles and to establish the role of lipid species in mediating vesicle function.

It is important to mention one limitation of our study related to the sex mismatch of our MSC donors. It is known that MSC activity and recipient responses are influenced by the sex of both donor and recipient because of circulating hormones[58], but, to the best of our knowledge, no specific study has been published concerning sex-related variations in the function of EVs derived from cultured cells.

Studies evaluating the efficacy of MSC-derived EVs in vitro and in vivo rarely refer to the sex of the donors, but this is very useful and should be always clearly indicated together with donor age[59]. Future in-depth analyses of larger donor cohorts should evaluate age and sex-related differences in EV function and chemical composition.

In conclusion, our findings demonstrate that RS can determine the chemical content of EVs in a label- and sample processing- free manner. The proposed method can be immediately transferred into laboratory practice as it allows the bulk characterisation of vesicle suspensions before their use in vitro or in vivo. As independent MSC-derived EV preparations can have different therapeutic potentials, the overall characterisation of vesicles offered by Raman spectroscopy might become a pivotal quality check for comparing data coming from different experiments or research labs, and thus hasten the clinical application of stem cell-derived products.

ASSOCIATED CONTENTS

Additional Information

Supplementary information accompanies this paper at doi:10.1038/s41598-017-10448-1

ACKNOWLEDGEMENTS

This study was supported by the Italian Ministry of Health (Ricerca Corrente 2015, IRCCS Fondazione Don Carlo Gnocchi ONLUS; Ricerca Corrente RC L1027, IRCCS Galeazzi Orthopaedic Institute) and by the Department of Biomedical, Surgical and Dental Sciences (University of Milan, grant no. 15-63017000-700).

4.5 References

(1) Raposo, G. & Stoorvogel, W. Journal of Cell Biology 200, 373–383, doi:10.1083/jcb.201211138 (2013).

(2) Xie, Y. C. et al. 32, 2397–2406, doi:10.1002/stem.1736 (2014).

(3) Teixeira, J. H., Silva, A. M., Almeida, M. I., Barbosa, M. A. & Santos, S. G. Transfusion and Apheresis Science 55, 53–61, doi:10.1016/j.transci.2016.07.015 (2016).

(4) Nurkovic, J., Grbovic, V., Nurkovic, S., Vucelj, S. & Dolicanin, Z. Osteoporosis International 27, S116–S116 (2016).

(5) Akyurekli, C. et al. Stem Cell Reviews and Reports 11, 150–160, doi:10.1007/s12015-014-9545-9 (2015).

(6) Phinney, D. G. & Pittenger, M. F. Stem Cells 35, 851–858, doi:10.1002/ stem.2575 (2017).

(7) Kordelas, L. et al. Leukemia 28, 970–973, doi:10.1038/leu.2014.41 (2014).

(8) Arslan, F. et al. Stem Cell Research 10, 301–312, doi:10.1016/j.scr.2013.01.002 (2013).

(9) Lai, R. C. et al. Stem Cell Research 4, 214–222, doi:10.1016/j.scr.2009.12.003 (2010).

(10) Suzuki, E., Fujita, D., Takahashi, M., Oba, S. & Nishimatsu, H. World Journal of Cardiology 7, 454–465, doi:10.4330/wjc.v7.i8.454 (2015).

(11) Zhou, Y. et al. Stem Cell Research & Therapy 4, doi:10.1186/scrt194 (2013).

(12) Eirin, A. et al. Kidney international, doi:10.1016/j.kint.2016.12.023 (2017).

(13) Ranghino, A. et al. Stem cell research & therapy 8, 24–24, doi:10.1186/s13287-017-0478-5 (2017).

(14) Li, T. F. et al. Stem Cells and Development 22, 845–854, doi:10.1089/scd.2012.0395 (2013).

(15) Haga, H., Yan, I. K., Takahashi, K., Matsuda, A. & Patel, T. Stem cells translational medicine, doi:10.1002/sctm.16-0226 (2017).

(16) Narayanan, R., Huang, C. C. & Ravindran, S. Hijacking. Stem Cells International, doi:10.1155/2016/3808674 (2016).

(17) Toh, W. S., Lai, R. C., Hui, J. H. P. & Lim, S. K. Seminars in cell & developmental biology, doi:10.1016/j.semcdb.2016.11.008 (2016).

(18) Nakamura, Y. et al. Febs Letters 589, 1257–1265, doi:10.1016/j.febslet.2015.03.031 (2015).

(19) Hu, L. et al. Scientific Reports 6, doi:10.1038/srep32993 (2016).

(20) Zhang, Y. L. et al. Journal of Neurosurgery 122, 856–867, doi:10.3171/2014.11.jns14770 (2015).

(21) Katsuda, T. et al. Scientific Reports 3, doi:10.1038/srep01197 (2013).

(22) Hu, B. et al. Cellular Physiology and Biochemistry 40, 155–162, doi:10.1159/000452533 (2016).

(23) Otero-Ortega, L. et al. Scientific reports 7, 44433–44433, doi:10.1038/srep44433 (2017).

(24) Marote, A., Teixeira, F. G., Mendes-Pinheiro, B. & Salgado, A. J. Frontiers in Pharmacology 7, doi:10.3389/fphar2016.00231 (2016).

(25) De Jong, O. G., Van Balkom, B. W. M., Schiffelere, R. M., Bouten, C. V. C. & Verhaar, M. C. Frontiers in Immunology 5, 1–13, doi:10.3389/fimmu.2014.00608 (2014).

(26) Lener, T. et al. Journal of Extracellular Vesicles 4, doi:10.3402/jev.v4.30087 (2015).

(27) Wachsmann-Hogiu, S., Weeks, T. & Huser, T. Current Opinion in Biotechnology 20, 63–73, doi:10.1016/j.copbio.2009.02.006 (2009).

(28) Smith, Z. J., Huser, T. R. & Wachsmann-Hogiu, S. Analytical Cellular Pathology 35, 145–163, doi:10.3233/acp-2011-0048 (2012).

(29) Krafft, C. & Popp, J. Analytical and Bioanalytical Chemistry 407, 699–717, doi:10.1007/s00216-014-8311-9 (2015).

(30) Moura, C. C., Tare, R. S., Oreffo, R. O. C. & Mahajan, S. Journal of the Royal Society Interface 13, doi:10.1098/rsif.2016.0182 (2016).

(31) Wu, Y. et al. Sci Rep 7, 38706, doi:10.1038/srep38706 (2017).

(32) Vanna, R. et al. Analyst 140, 1054–1064, doi:10.1039/c4an02127d (2015).

(33) Lui, H., Zhao, J. H., McLean, D. & Zeng, H. S. Cancer Research 72, 2491–2500, doi:10.1158/0008-5472.can-11-4061 (2012).

(34) Santos, I. P. et al. Analytical Chemistry 88, 7683–7688, doi:10.1021/acs.analchem.6b01592 (2016).

(35) Notingher, I. et al. Analytical Chemistry 76, 3185–3193, doi:10.1021/ac0498720 (2004).

(36) Chan, J. W., Lieu, D. K., Huser, T. & Li, R. Analytical Chemistry 81, 1324–1331, doi:10.1021/ac801665m (2009).

(37) Downes, A., Mouras, R., Bagnaninchi, P. & Elfick, A. Journal of Raman Spectroscopy 42, 1864–1870, doi:10.1002/jrs.2975 (2011).

(38) Azrad, E. et al. Journal of Raman Spectroscopy 37, 480–486, doi:10.1002/ jrs.1420 (2006).

(39) McManus, L. L. et al. Analyst 136, 2471–2481, doi:10.1039/c1an15167c (2011).

(40) Smith, Z. J. et al. Journal of Extracellular Vesicles 4, doi:10.3402/jev.v4.28533 (2015).

(41) Krafft, C. et al. Nanomedicine, doi:10.1016/j.nano.2016.11.016 (2016).

(42) Yanez-Mo, M. et al. Journal of Extracellular Vesicles 4, doi:10.3402/jev.v4.27066 (2015).

(43) Thery, C., Amigorena, S., Raposo, G. & Clayton, A. Current protocols in cell biology Chapter 3, Unit 3.22-Unit 23.22, doi:10.1002/0471143030.cb0322s30 (2006).

(44) Lotvall, J. et al. Journal of extracellular vesicles 3, 26913–26913, doi:10.3402/jev.v3.26913 (2014).

(45) Colombo, M., Raposo, G. & Thery, C. Annual Review of Cell and Developmental Biology, Vol 30 30, 255–289, doi:10.1146/annurev-cellbio-101512-122326 (2014).

(46) Lavialle, F. et al. International Journal of Pharmaceutics 380, 206–215, doi:10.1016/j.ijpharm.2009.06.039 (2009).

(47) Phang, J. M., Liu, W. & Zabirnyk, O. Annual Review of Nutrition, Vol 30 30, 441–463, doi:10.1146/annurev.nutr.012809.104638 (2010).

(48) Jones, S. P., Guillemin, G. J. & Brew, B. J. International journal of tryptophan researc: IJTR 6, 57–66, doi:10.4137/ijtr.s12626 (2013).

(49) Tatischeff, I., Larquet, E., Falcon-Perez, J. M., Turpin, P.-Y. & Kruglik, S. G. Journal of extracellular vesicles 1, doi:10.3402/jev.v1i0.19179 (2012).

(50) Dominici, M. et al. The International Society for Cellular Therapy position statement. Cytotherapy 8, 315–317, doi:10.1080/14653240600855905 (2006).

(51) Collins, E. et al. Journal of Immunology 193, 4381–4390, doi:10.4049/jimmunol.1401636 (2014).

(52) Rasmussen, J. G. et al. Cell Transplantation 23, 195–206, doi:10.3727/096368912x659871 (2014).

(53) Campos, A. M. et al. Journal of Cellular Physiology 231, 1024–1032, doi:10.1002/jcp.25191 (2016).

(54) Haraszti, R. A. et al. Journal of Extracellular Vesicles 5, doi:10.3402/jev.v5.32570 (2016).

(55) Freund, D., Fonseca, A. V., Janich, P., Bornhauser, M. & Corbeil, D. Cytotherapy 12, 131–142, doi:10.3109/14653240903476438 (2010).

(56) Moussavou, G. et al. Bmb Reports 46, 527–532, doi:10.5483/BMBRep.2013.46.11.179 (2013).

(57) Xu, F., Yang, C. C., Gomillion, C. & Burg, K. J. L. Applied Biochemistry and Biotechnology 160, 197–212, doi:10.1007/s12010-008-8505-8 (2010).

(58) Sammour, I. et al. Plos One 11, 10, doi:10.1371/journal.pone.0164269 (2016).

(59) Shah, K., McCormack, C. E. & Bradbury, N. A. American Journal of Physiology 306, C3–C18, doi:10.1152/ajpcell.00281.2013 (2014).

(60) Van Deun, J. et al. EV-TRACK: transparent reporting and centralizing knowledge in extracellular vesicle research. Nature methods 14, 228–32, doi:10.1038/nmeth.4185 (2017).

(61) Conforti, A. et al. Plos One 8, 11, doi:10.1371/journal.pone.0076989 (2013).

(62) Brini, A. T. et al. Journal of Craniofacial Surgery 27, 656–661, doi:10.1097/scs.0000000000002540 (2016).

(63) Niada, S. et al. Differentiation 92, 291–297, doi:10.1016/j.diff.2016.04.001 (2016).

(64) Gabrielli, M. et al. Embo Reports 16, 213–220 (2015).

(65) Czamara, K. et al. Journal of Raman Spectroscopy 46, 4–20, doi:10.1002/jrs.4607 (2015).

(66) Movasaghi, Z., Rehman, S. & Rehman, I. U. Applied Spectroscopy Reviews 42, 493–541, doi:10.1080/05704920701551530 (2007).

(67) Krafft, C., Neudert, L., Simat, T. & Salzer, R. Spectrochimica Acta Part a-Molecular and Biomolecular Spectroscopy 61, 1529–1535, doi:10.1016/j.saa.2004.11.017 (2005).

CHAPTER 5

Summary, conclusions and future perspectives

Extracellular vesicles (EVs) are naturally produced nanoscaled vesicles that physiologically mediate intercellular communication. The quantity of EVs released from cells and their composition was demonstrated to change according to the physio-pathological condition of the tissue of origin, mirroring their direct involvement in specific pathogenic mechanisms and thus being promising biomarkers of diseases. Besides, EVs are able to cross multiple physiological barriers including the blood-brain barrier and specific neural subpopulations of circulating EVs could reflect the composition of brain-derived EVs, thus offering the unique opportunity to study the complex and multifaceted biochemical processes inside the central nervous system from a biofluid easy to access as human blood.[1]

EVs have gained interest also as valid therapeutic platforms, exploiting their native biological effects, their functions as vehicles of bioactive molecules or their ability to carry and deliver other exogenous and synthetic therapeutics to a target site.

Nowadays, the emerging remarkable potential of EVs is investigated from a technical and biological point of view, but its translation to clinics is limited by the lack of effective and reproducible standardized methods for their detection and characterization from biological samples, that are still needed for their successful integration into daily practice.[2,3]

The aim of the present thesis was to develop innovative technological platforms for the detection and characterization of EVs cargo, taking advantage of methods borrowed from the nanotechnological and biophotonic field to overcome the current technical limitations that prevent the validation of EVs as biomarkers or therapeutic agents.

Surface Plasmon Resonance imaging (SPRi) and Raman spectroscopy are well-known photonic-based technologies that are experiencing recent progresses and increasing application in the biomedical research, thanks to their sensitivity, label-free and high-throughput features[4,5].

Thanks to these properties, we propose SPRi and Raman spectroscopy as innovative and valuable tools for the characterization of EVs with the specific aim to detect and characterize them as possible tools for diagnosis and monitoring of treatment efficacy in neurodegenerative diseases.

First, we developed an antibody SPRi-array in order to separate different neurally-derived EVs pre-isolated from human blood plasma by size-exclusion chromatography: those from neurons (CD171- or ephrinB- positive), oligodendrocytes (PLP1-positive), astrocytes (Glast-positive; data not published) and microglia (IB4-positive; data not published) were successfully identified with good sensitivity and specificity.

The analysis of the relative amount of proteins and lipids present on the EVs membrane of each subpopulation was concomitantly performed, demonstrating their heterogeneous composition and the potentiality of SPRi-based biosensor to study EVs interaction with molecules potentially involved in neurodegenerative processes.

For example, EVs can interact with extracellular amyloid-β (Aβ) species influencing the complex process of Aβ aggregation behind the mechanism of pathogenesis of Alzheimer's disease (AD)[6]. Specific surface molecules able to mediate the interaction between EVs and Aβ have been identified, such as ganglioside GM1 that can form a

complex with Aβ and act as a seed for its aggregation[7]. The SPRi-based biosensor has shown to have the ability to evaluate the presence and relative amount of GM1 on different neural EVs populations by using a sandwich approach injecting GM1 antibody on the EVs immobilized on the chip.

The efficacy of the SPRi biosensor was evaluated and verified by analyzing vesicles from a little and homogeneous cohort of healthy subjects, demonstrating the possibility to detect and identify GM1 on the EV subpopulations in all the samples.

The future activities will include the comparison of the vesicle components between patients with AD and healthy controls, in order to use this biosensor for the diagnosis and monitoring of the disease and possibly to identify EV-related biomarkers that can correlate with the progression of the disease. To implement this work, future analysis will be focused on studying other clinically relevant molecules present on or interacting with the EV membranes that could be involved in specific pathological processes. For example it is possible to study the effect of the interaction between EVs carrying GM1 and Aβ in order to clarify the role of EVs in the pathogenesis of AD and understand whether their promote or counteract the deleterious action of Aβ.

Besides, starting from the emerging hypothesis that neurological diseases share common pathological mechanisms that relate with EVs biochemical composition and rely on EVs for the spread of the disease[8,9], the SPRi platform will be used to characterize EVs in other neurological disorders.

From the technological point of view, the possibility to enhance the sensitivity of the SPRi-based biosensor is under investigation by

implementing the characterization procedure using gold nanoparticles (NPs) conjugated with specific antibodies/molecules expected to interact with the EV surface. To achieve reliable and reproducible results, there are some parameters that need to be optimized, such as (1) the features of NPs, in terms of size and shape; (2) the surface chemistry for the conjugation of NPs with antibodies and (3) the amount of molecule to be attached at NPs surface.

Secondly, the SPRi technology was used as an alternative approach for the detection of microRNAs (miRNAs) that represent good diagnostic, subtyping and prognostic potential biomarkers for several diseases. miRNAs are a group of small non-coding RNAs whose dysregulation has been associated to the onset and the development of several diseases. Currently both circulating and vesicular miRNAs are proposed as biomarkers for diseases, including nervous system disorders, diabetes, cardiovascular disorders and cancers[10].

In particular, our setting up of SPRi-based method was performed by analyzing miRNAs related to multiple sclerosis (MS). MS is an immunobased progressive neurological disorder that is currently lacking for biomarkers and the only two indicators of pathology are the clinical signs of the patients and magnetic resonance imaging. However, in recent years, some specific miRNAs are emerging as potential biomarkers in MS[11], but their quantitative analysis with conventional methods (PCR, microarray and next generation sequencing) are still challenging and have some limitations[12]. We have proposed to use SPRi as an alternative high sensitive approach for the detection of circulating miRNAs related to the progression of MS.

DNA sequences complementary to the miRNAs of interest were immobilized on the surface of an SPRi chip; conversely miRNAs were flowed on the gold surface for the DNA/RNA hybridization by complementary bond. Subsequently, a commercial antibody specific for the hybrid DNA/RNA conjugated to gold NPs, was used as an universal enhancer of the SPRi signal. In this way, the properties of SPRi technology (label free, real time measurements and minimal preparation of the sample) were combined with the high sensitivity due to the enhancement and plasmonic properties of NPs.

The specificity and the multiplexing capacity of this approach were verified by detecting seven different miRNAs and by recognizing single- and three-mutated sequences. The sensitivity was tested by measuring miRNAs at increasing known concentrations and the maximum achieved limit of detection was around 0.5 pM. This enhancing approach was furthermore validated in a clinical relevant environment by the detection of miRNAs in real human samples. The results of this study demonstrated that this universal and enzyme free strategy allows to detect multiple miRNAs independently by their sequence using a simple protocol assay and a single enhancing reagent.

Further studies will include the validation of this method by increasing the number of patient samples and the number of miRNAs that can be detected on the same chip, in order to develop a more feasible and affordable method for the screening of specific miRNAs related to the diagnosis and monitoring of MS or other diseases or processes of clinical interest.

Moreover, this approach can obviously be used to detect not only miRNAs circulating in the blood but also those present inside EVs, that are related to any pathological process.

Finally, a procedure for analysis of EVs based on Raman spectroscopy was optimized in order to obtain a snapshot of the EVs biochemical profile. To draw up and evaluate the feasibility of the method, ultracentrifuged EVs obtained from conditioned media of human mesenchymal stromal cells from bone marrow and adipose tissue and dermal fibroblast were analyzed by confocal Raman microspectroscopy with 532 nm laser sources in the spectral ranges 500-1800 cm^{-1} and 2600-3200 cm^{-1}.

Multivariate statistical analysis (PCA-LDA) and Classical Least Squares (CLS) fitting with reference lipid molecules (cholesterol, ceramide, phosphatidylcholine, phosphatidylethanolamine, phosphatidic acid, and GM1) were performed on the recordings obtained on air-dried drops of EV suspensions. When vesicles were irradiated, Raman bands of nucleic acids, proteins, and lipids (cholesterol, phospholipids) were visible in the spectra providing a biochemical fingerprint of the considered vesicles. CLS fitting allowed us to identify the main lipid families involved in the spectral differences between EVs from different cell sources.

Raman spectroscopy was proved to be able to clearly distinguish vesicles originated by different cell-types with good accuracy (around 93%) thanks to biochemical features typical of the cell/tissue of origin. Further lipidomic studies are still needed to verify the exact membrane composition of EVs and to establish the role of lipid species in mediating vesicle function.

Raman spectroscopy has thus demonstrated to be a valuable approach for EVs characterization prior to their use as therapeutic agents in complex disease models. In particular, requiring minimal amount of samples and no preliminary preparation, Raman analysis can be immediately transferred into laboratory practice and used as a routine quality check method for bulk characterization of EVs suspensions before in vitro or in vivo use, being also more informative compared to other complementary techniques. Considering the different therapeutic potentials of mesenchymal stem cells-derived EV preparation, the overall characterization by Raman spectroscopy might become a primary method for the comparison between data coming from different research studies. The use of this method has the potentiality to hasten the clinical application not only of stem cell-derived products but also of other kinds of vesicles used as therapeutic agents or drug delivery systems.

Besides, the optimized Raman method could also be translated to the study of EVs as circulating biomarkers of several diseases. Indeed, Raman spectroscopy could provide insights in the biochemical features of EVs circulating in the blood of neurological patients, that are known to be associated/loaded with atypical cargoes.

Considering the future applications of these biophotonics based approaches for the analysis of clinical samples, an important aspect that needs to be considered and evaluated is the definition of appropriate inclusion and exclusion criteria for the recruitment of the patients and the relative healthy controls who will be enrolled in the research study in order to create a large and representative cohort of subjects. The proper selection of subjects will help to identify and

evaluate how the specific molecular features are associated to physical and emotional symptoms of neurological diseases.

Collectively, the data obtained in the framework of the present thesis have demonstrated that SPRi is a very sensitive and useful technique for the characterization of circulating EVs with the perspective of investigating their possible use as peripherally-sourced clinical biomarkers of neurodegenerative diseases, enabling greater patient tolerability, integration with existing sample testing infrastructure, and the scalability and affordability necessary for population-level screening. Once validated, the SPRi-based biochemical profile of EVs and EV-related miRNA collected from any biological fluids (such as blood, urine and saliva) could be an indication of the presence or a state of a particular neurological disorder avoiding the invasive collection of cerebrospinal fluid.

At the same time, the combination of the SPRi platform with the Raman approach could provide new hints to support the role of EVs in pathogenesis of diseases, like neurodegenerative diseases (e.g., Parkinson's disease[13], Alzheimer's disease[14]), cardiovascular diseases (e.g., heart failure[15]), infectious diseases and cancers (e.g., cancer of lung[16], breast[17], prostate[18], gastrointestinal tract[19], skin[20]).

The combination of SPRi and Raman characterization methods of circulating EVs is an innovative approach with high potential of transferability to the clinical practice.

5.1 **References**

(1) Kanninen, K. M.; Bister, N.; Koistinaho, J.; Malm, T. Exosomes as New Diagnostic Tools in CNS Diseases. *Biochim. Biophys. Acta* **2016**, *1862* (3), 403–410.

(2) Szatanek, R.; Baj-Krzyworzeka, M.; Zimoch, J.; Lekka, M.; Siedlar, M.; Baran, J. The Methods of Choice for Extracellular Vesicles (EVs) Characterization. *Int. J. Mol. Sci.* **2017**, *18* (6).

(3) Momen-Heravi, F.; Balaj, L.; Alian, S.; Trachtenberg, A. J.; Hochberg, F. H.; Skog, J.; Kuo, W. P. Impact of Biofluid Viscosity on Size and Sedimentation Efficiency of the Isolated Microvesicles. *Front. Physiol.* **2012**, *3*, 162.

(4) Sina, A. A. I.; Vaidyanathan, R.; Dey, S.; Carrascosa, L. G.; Shiddiky, M. J. A.; Trau, M. Real Time and Label Free Profiling of Clinically Relevant Exosomes. *Sci. Rep.* **2016**, *6*, 30460.

(5) Yuyama, K.; Igarashi, Y. Exosomes as Carriers of Alzheimer's Amyloid-ß. *Front Neurosci* **2017**, *11*.

(6) Eitan, E.; Hutchison, E. R.; Marosi, K.; Comotto, J.; Mustapic, M.; Nigam, S. M.; Suire, C.; Maharana, C.; Jicha, G. A.; Liu, D.; et al. Extracellular Vesicle-Associated Aβ Mediates Trans-Neuronal Bioenergetic and Ca^{2+}-Handling Deficits in Alzheimer's Disease Models. *npj Aging and Mechanisms of Disease* **2016**, *2*, 16019.

(7) Krafft, C.; Popp, J. The Many Facets of Raman Spectroscopy for Biomedical Analysis. *Anal. Bioanal. Chem.* **2015**, *407* (3), 699–717.

(8) Candelario, K. M.; Steindler, D. A. The Role of Extracellular Vesicles in the Progression of Neurodegenerative Disease and Cancer. *Trends Mol. Med.* **2014**, *20* (7), 368–374.

(9) Rajendran, L.; Bali, J.; Barr, M. M.; Court, F. A.; Krämer-Albers, E.-M.; Picou, F.; Raposo, G.; van der Vos, K. E.; van Niel, G.; Wang, J.; et al. Emerging Roles of Extracellular Vesicles in the Nervous System. *J. Neurosci.* **2014**, *34* (46), 15482–15489.

(10) Wang, J.; Chen, J.; Sen, S. MicroRNA as Biomarkers and Diagnostics. *J. Cell. Physiol.* **2016**, *231* (1), 25–30.

(11) Cox, M. B.; Cairns, M. J.; Gandhi, K. S.; Carroll, A. P.; Moscovis, S.; Stewart, G. J.; Broadley, S.; Scott, R. J.; Booth, D. R.; Lechner-Scott, J.; et al. MicroRNAs MiR-17 and MiR-20a Inhibit T Cell Activation Genes and Are under-Expressed in MS Whole Blood. *PloS One* **2010**, *5* (8), e12132.

(12) Kappel, A.; Keller, A. MiRNA Assays in the Clinical Laboratory: Workflow, Detection Technologies and Automation Aspects. *Clin. Chem. Lab. Med.* **2017**, *55* (5), 636–647.

(13) Gui, Y.; Liu, H.; Zhang, L.; Lv, W.; Hu, X. Altered MicroRNA Profiles in Cerebrospinal Fluid Exosome in Parkinson Disease and Alzheimer Disease. *Oncotarget* **2015**, *6* (35), 37043–37053.

(14) Goetzl, E. J.; Abner, E. L.; Jicha, G. A.; Kapogiannis, D.; Schwartz, J. B. Declining Levels of Functionally Specialized Synaptic Proteins in Plasma Neuronal Exosomes with Progression of Alzheimer's Disease. *FASEB J. Off. Publ. Fed. Am. Soc. Exp. Biol.* **2018**, *32* (2), 888–893.

(15) Ye, W.; Tang, X.; Yang, Z.; Liu, C.; Zhang, X.; Jin, J.; Lyu, J. Plasma-Derived Exosomes Contribute to Inflammation via the TLR9-NF-KB Pathway in Chronic Heart Failure Patients. *Mol. Immunol.* **2017**, *87*, 114–121.

(16) Sandfeld-Paulsen, B.; Jakobsen, K. R.; Bæk, R.; Folkersen, B. H.; Rasmussen, T. R.; Meldgaard, P.; Varming, K.; Jørgensen, M. M.; Sorensen, B. S. Exosomal Proteins as Diagnostic Biomarkers in Lung Cancer. *J. Thorac. Oncol. Off. Publ. Int. Assoc. Study Lung Cancer* **2016**, *11* (10), 1701–1710.

(17) Khan, S.; Bennit, H. F.; Turay, D.; Perez, M.; Mirshahidi, S.; Yuan, Y.; Wall, N. R. Early Diagnostic Value of Survivin and Its Alternative Splice Variants in Breast Cancer. *BMC Cancer* **2014**, *14*, 176.

(18) Logozzi, M.; Angelini, D. F.; Iessi, E.; Mizzoni, D.; Di Raimo, R.; Federici, C.; Lugini, L.; Borsellino, G.; Gentilucci, A.; Pierella, F.; et al. Increased PSA Expression on Prostate Cancer Exosomes in in Vitro Condition and in Cancer Patients. *Cancer Lett.* **2017**, *403*, 318–329.

(19) Shiromizu, T.; Kume, H.; Ishida, M.; Adachi, J.; Kano, M.; Matsubara, H.; Tomonaga, T. Quantitation of Putative Colorectal Cancer Biomarker Candidates in Serum

Extracellular Vesicles by Targeted Proteomics. *Sci. Rep.* **2017**, *7* (1), 12782.

(20) Logozzi, M.; De Milito, A.; Lugini, L.; Borghi, M.; Calabrò, L.; Spada, M.; Perdicchio, M.; Marino, M. L.; Federici, C.; Iessi, E.; et al. High Levels of Exosomes Expressing CD63 and Caveolin-1 in Plasma of Melanoma Patients. *PloS One* **2009**, *4* (4), e5219.

PUBLICATIONS

Silvia Picciolini, Alice Gualerzi, Renzo Vanna, Andrea Sguassero, Furio Gramatica, Marzia Bedoni, Massimo Masserini, Carlo Morasso. *Detection and Characterization of Different Brain-Derived Subpopulations of Plasma Exosomes by Surface Plasmon Resonance Imaging*.
Analytical Chemistry, 2018; 90(15):8873-8880.
doi: 10.1021/acs.analchem.8b00941

Andrea Sguassero, Álvaro Artiga, Carlo Morasso, Rafael Ramirez Jimenez, Rafael Martín Rapún, Roberta Mancuso, Simone Agostini, Ambra Hernis, Arturs Abols, Aija Linē, Alice Gualerzi, **Silvia Picciolini**, Marzia Bedoni, Marco Rovaris, Furio Gramatica, Jesus M. de la Fuente, Renzo Vanna. *A simple and universal enzyme-free approach for the detection of multiple microRNAs using a single nanostructured enhancer of surface plasmon resonance imaging*. *Analytical and Bioanalytical Chemistry, 2018.*
doi: 10.1007/s00216-018-1331-0

Alice Gualerzi, Stefania Niada, Chiara Giannasi, **Silvia Picciolini**, Carlo Morasso, Renzo Vanna, Valeria Rossella, Massimo Masserini, Marzia Bedoni, Fabio Ciceri, Maria Ester Bernardo, Anna Teresa Brini, Furio Gramatica. *Raman spectroscopy uncovers biochemical tissue-related features of extracellular vesicles from mesenchymal stromal cells.*
Scientific Report, 2017; 7(1):9820. *doi: 10.1038/s41598-017-10448-1*

Silvia Picciolini, Dora Mehn, Isaac Ojea-Jiménez, Furio Gramatica, Carlo Morasso. *Hydroquinone Based Synthesis of Gold Nanorods*. *Journal of Visualized Experiments, 2016; (114). doi: 10.3791/54319*

Chiara Finetti, Laura Sola, Margherita Pezzullo, Davide Prosperi, Miriam Colombo, Benedetta Riva, Svetlana Avvakumova, Carlo Morasso, **Silvia Picciolini**, Marcella Chiari. *Click Chemistry Immobilization of Antibodies on Polymer Coated Gold Nanoparticles*. *Langmuir, 2016; 32(29):7435-41*.
doi: 10.1021/acs.langmuir.6b01142.

Carlo Morasso, **Silvia Picciolini**, Domitilla Schiumarini, Dora Mehn, Isaac Ojea-Jime´nez, Giuliano Zanchetta, Renzo Vanna, Marzia Bedoni, Davide Prosperi, Furio Gramatica. *Control of size and aspect ratio in hydroquinone-based synthesis of gold nanorods*.
Journal of Nanoparticle Research, 2015; 17:330. https://doi.org/10.1007/s11051-015-3136-9

Silvia Picciolini, Nicola Castagnetti, Renzo Vanna, Dora Mehn, Marzia Bedoni, Furio Gramatica, Marco Villani, Davide Calestani, Maura Pavesi, Laura Lazzarini, Andrea Zappettini, Carlo Morasso. *Branched gold nanoparticles on ZnO 3D architecture as biomedical SERS sensors*.
RSC Advance, 2015; 5, 93644-93651. doi: 10.1039/C5RA13280K

Renzo Vanna, Paola Ronchi, Aufried T. M. Lenferink, Cristina Tresoldi, Carlo Morasso, Dora Mehn, Marzia Bedoni, **Silvia Picciolini**, Leon W. M. M. Terstappen, Fabio Ciceri, Cees Otto, Furio Gramatica. *Label-free imaging and identification of typical cells of acute myeloid leukaemia and myelodysplastic syndrome by Raman microspectroscopy*.
Analyst, 2014; 140(4):1054-64. doi: 10.1039/c4an02127d.

Silvia Picciolini, Dora Mehn, Carlo Morasso, Renzo Vanna, Marzia Bedoni, Paola Pellacani, Gerardo. Marchesini, Andrea Valsesia, Davide Prosperi, Cristina Tresoldi, Fabio Ciceri, Furio Gramatica. *Polymer Nanopillar_Gold Arrays as Surface-Enhanced Raman Spectroscopy Substrate for the Simultaneous Detection of Multiple Genes.*
ACS Nano, 2014; 8(10):10496-506. *doi: 10.1021/nn503873d*.

ACKNOLEDGEMENT

I am really grateful to my tutor Prof. Massimo Masserini and my co-tutor Dott. Furio Gramatica for their support and for giving me the possibility to conduct this research activity. I want also to thank all the people of Labion for their collaboration and the help they provided to me. In particular, special thanks to Alice Gualerzi, Marzia Bedoni, Carlo Morasso and Renzo Vanna for their precious suggestions and for their passion they always communicate to me.

A huge thank to other colleagues and collaborators that I have met and worked with during these years: Francesca Re, Simona Mancini, Antonella Orlando, Silvia Sesana, Maria Gregori, Alysia Cox, Roberta Dal Magro, Beatrice Formicola, Andrea Sguassero, Cristiano Carlomagno, Agustin Enciso Martinez, Martina Gabrielli, Ilaria Prada, Amrita Sahu, Hikaru Mamiya, Zachary Clemens and Sunita Shinde. Thanks for your support, your teachings and your friendships.

I am also grateful to Dott. Claudia Verderio for her precious suggestions and mentoring activity, and to Fabrisia Ambrosio for the great opportunity to visit her lab in Pittsburgh sharing with me her enthusiasm for the world of scientific research.